Identification of Novel Endogenous Modulators of (Inflammatory) Lymphangiogenesis by Analyzing Mouse Strain-specific Differences

Doctoral thesis
for
the award of the doctoral degree
of the Faculty of Mathematics and Natural Sciences
of the University of Cologne

Submitted by

Niloofar Hatami

Accepted in the year 2026

Table of contents

Figures and tables

Figures

Tables

Abbreviations

Abbreviation	Explanation
AF 647	AlexaFluor 647
AF 488	AlexaFluor 488
AF 555	AlexaFluor 555
α-MSH	α-melanocyte-stimulating hormone
ANGPTL4	Angiopoietin-like 4
B2M	β2-macroglobulin
bEND3	Brain-derived Endothelial Cells, clone 3
cANGPTL4	C-terminal fragment of Angiopoietin-like 4
cAMP	Cyclic adenosine monophosphate
CBS	Cystathionine β-synthase
CD31	Cluster of Differentiation 31
CTH	Cystathionine-γ-lyase
C57BL/6	C57 black 6
cDNA	Complementary DNA
DOPA	levodopa and l-3,4-dihydroxyphenylalanine
d0	Day 0
d8	Day 8
d14	Day 14
DNA	Deoxyribonucleic acid
DPBS / PBS	Dulbecco´s phosphate-buffered saline
DPBS / PBS	Dulbecco´s phosphate-buffered saline
EGF	Epidermal growth factor
FACS	Fluorescence-activated cell sorting
FCS	Fetal calf serum
FGF-2	fibroblast growth factor-2
FITC	Fluorescein isothyocyanite
HDLECs	Human Dermal Lymphatic Endothelial Cells
HGF	Hepatocyte growth factor
HUVECs	Human umbilical vein endothelial cells
HDMVECs	human dermal microvascular endothelial cells
H2S	Hydrogen sulfide
IFN-γ	Interferon-γ
IL-6	Interleukin-6
IRS-1	Insulin Receptor Substrate 1

LYVE-1	Lymphatic vessel endothelial hyaluronan receptor 1
MCP-1	Monocyte Chemoattractant Protein-1
MPST	3-mercaptopyruvate sulfurtransferase
MT-MMP1	Membrane Type 1-Matrix Metalloproteinase
nANGPTL4	N-terminal fragment of Angiopoietin-like 4
NRP-1	Neuropilin-1
NP-2	Neuropilin-2
NC	Negative control
PAI-1	Plasminogen activator inhibitor-1
PCR	Polymerase chain reaction
PDGF	Platelet-derived growth factor
P21	Cyclin-dependent kinase inhibitor 1 (CDKN1A)
Prox1	Prospero Homeobox Protein 1
QTL	Quantitative trait locus
rh-EGF	Recombinant human epidermal growth factor
rh-VEGF-A 165	Recombinant human vascular endothelial growth factor A165
Rsp29	Ribosomal protein S29
RT-PCR	Real-Time PCR
Sema-3F	Semaphorin-3F
siRNA	Small interfering RNA
TGF-α	transforming growth factor-α
TGF-β	Transforming growth factor-β
TSP-1	Thrombospondin-1
VASH-1	Vasohibin-1
VEGF-A	Vascular Endothelial Growth Factor A
VEGF-C	Vascular Endothelial Growth Factor C
VEGF-D	Vascular Endothelial Growth Factor D
VEGFR-2	Vascular Endothelial Growth Factor receptor2
VEGFR-3	Vascular Endothelial Growth Factor receptor3
VIP	Vasoactive intestinal peptide

Abbreviation	**Unit/explanation**
°C	Celsius degree
Bp	Base pairs
g/mg/µg/ng	Gramm/Milligramm/Microgramm/Nanogramm

Hr	Hour
kDa	Kilo Dalton
l/ml/µl	Liter/Milliliter/Microliter
M/mM/µM	Molar/Millimolar/Micromolar
Rpm	Rounds per minute
S	Second
Xg	Force exerted on the centrifuge sample

Zusammenfassung

Diese Arbeit untersucht die Rolle neuartiger endogener Modulatoren in der inflammatorischen Lymphangiogenese und konzentriert sich auf die Analyse von stammspezifischen Unterschieden bei Mäusen. Das Verständnis der Lymphangiogenese ist entscheidend aufgrund ihrer Auswirkungen auf Immunantworten, den Flüssigkeitsausgleich und verschiedene pathologische Zustände, einschließlich Krebsmetastasen und entzündlichen Erkrankungen. Diese Studie zielt darauf ab, Einblicke in die molekularen Mechanismen zu geben, die die Lymphangiogenese regulieren, um therapeutische Strategien für Zustände zu informieren, die durch abnormale Bildung lymphatischer Gefäße gekennzeichnet sind.

In der Arbeit werden eine Kombination aus *in vitro* und *in vivo* experimentellen Ansätzen verwendet. Zur Untersuchung der Effekte der Cystathionin β-Synthase (CBS) und von Angiopoietin-like 4 (ANGPTL4) auf die Lymphangiogenese wurden humane dermale lymphatische Endothelzellen verwendet. Verschiedene Assays, darunter Proliferations-, Apoptose-, Migrations- und Tubeformierungsassays, wurden durchgeführt, um die Auswirkungen dieser Proteine auf die Lymphangiogenese zu untersuchen. Zur Analyse der Rolle von Angptl4 bei der Bildung lymphatischen Gefäße wurden Knockout-Mäuse verwendet. Darüber hinaus kamen *in-vivo*-Modelle mit verschiedenen Mauslinien (C57BL/6 und BALB/c) zum Einsatz, um die inflammatorische Lymphangiogenese mittels Naht-induziertes korneales Neovaskularisationsassay zu analysieren.

Um zusätzliche, neuartige Modulatoren der Lymphangiogenese zu identifizieren, wurden naive Augen von verschiedenen Collaborative Cross (CC) Linien gewonnen. Ganze Cornea-Präparate wurden mit LYVE-1 gefärbt, um die lymphatischen Gefäße zu visualisieren und zu quantifizieren. Zudem wurden 8- bis 12-wöchige männliche und weibliche BOON_HF und NUK_AC Mäuse für die Untersuchung der entzündungs-induzierten Neovaskularisation bei CC-Linien-Mäusen verwendet.

Die Studie identifizierte CBS und ANGPTL4 als bedeutende Regulatoren der Lymphangiogenese. Die Untersuchung von CBS zeigte, dass das Enzym die Proliferation und Migration von HDLECs beeinflusst und die Expression lymphangiogener Faktoren wie VEGFR-2 und VEGFR-3 moduliert. Darüber hinaus konnte nachgewiesen werden, dass Angptl4 die Bildung lymphatischer Gefäße

reguliert. Knockout-Tiere zeigten dabei eine erhöhte Lymphgefäßfläche im Vergleich zu den Wildtyp-Mäusen.

Die genetische Analyse innerhalb der CC-Linien offenbarte stammspezifische Unterschiede in den lymphangiogenen Reaktionen hervor und stellte eine Verbindung zwischen genetischem Hintergrund und lymphangiogenem Potential her.

Diese Untersuchung etabliert CBS und ANGPTL4 als neuartige Regulatoren der Lymphangiogenese und unterstreicht deren potenzielle Rolle bei der Modulation lymphatischer Reaktionen hervor. Darüber hinaus trägt die Studie zum Verständnis endogener Modulatoren der Lymphangiogenese bei und hebt das Potenzial des Collaborative Cross (CC)-Projekts hervor, zusätzliche neuartige Regulatoren zu identifizieren. Dadurch könnten künftig neuartige therapeutische Interventionen bei Erkrankungen ermöglicht werden, die mit abnormalem Wachstum lymphatischer Gefäße verbunden sind.

Abstract

This thesis investigates the role of novel endogenous modulators in lymphangiogenesis, with a focus on analysing mouse strain-specific differences. Understanding lymphangiogenesis is crucial due to its implications for immune responses, fluid balance, and various pathological conditions, including cancer metastasis and inflammatory diseases. This study aims to provide insights into the molecular mechanisms that regulate lymphangiogenesis, which could inform therapeutic strategies for conditions involving aberrant lymphatic vessel formation. The research employed a combination of *in vitro* and *in vivo* experimental approaches. Human dermal lymphatic endothelial cells (HDLECs) were utilized to assess the effects of cystathionine β-synthase (CBS) and angiopoietin-like 4 (ANGPTL4) on lymphangiogenesis. Various assays, including proliferation, apoptosis, migration, and tube formation assays, were conducted to evaluate the impact of these proteins on lymphangiogenesis. For the study of Angptl4, knockout mice were used to understand its role in lymphatic vessel formation. Additionally, *in vivo* models involving different mouse strains (C57BL/6 and BALB/c) were employed to analyze inflammatory lymphangiogenesis via suture-induced corneal neovascularization assays. To identify additional novel modulators of lymphangiogenesis, naïve eyes from different Collaborative Cross (CC) lines were obtained, and whole-mount cornea staining was performed using LYVE-1 to analyze lymphatic vessel formation. Furthermore, 8- to 12-week-old male and female BOON_HF and NUK_AC mice were used for the suture-induced inflammatory corneal neovascularization assay for CC line mice.

The study identified CBS and ANGPTL4 as significant regulators of lymphangiogenesis. Investigation of CBS revealed its impact on the proliferation and migration of HDLECs, as well as its influence on the expression of lymphangiogenic factors, including VEGFR-2 and VEGFR-3. Furthermore, ANGPTL4 has been shown to affect lymphatic vessel formation, with knockout models demonstrating an increased lymphatic surface area compared to their wild-type counterparts. Genetic analysis within the CC lines highlighted strain-dependent differences in lymphangiogenic responses, establishing a link between genetic background and lymphangiogenic potential.

This investigation establishes CBS and ANGPTL4 as novel regulators of lymphangiogenesis, highlighting their potential role in modulating lymphatic responses.

Furthermore, this research contributes to the understanding of endogenous modulators of lymphangiogenesis, highlighting the potential of the Collaborative Cross (CC) project in identifying additional novel regulators, thereby paving the way for therapeutic interventions in diseases associated with abnormal lymphatic vessel growth.

1.Introduction

1.1. Lymphatic system

The lymphatic system, a complex network of vessels found throughout the vertebrate bodies, plays a pivotal role in both the immune surveillance and the maintenance of circulatory homeostasis. Its primary function is to return lymphatic fluid, which contains white blood cells, cellular debris, and dietary fats, to the systemic blood circulation[1]. This lymphatic system is composed of lymphatic vessels, lymph nodes, lymphoid organs, and lymphoid tissues that together facilitate immune regulation and fluid transport[2, 3]. Additionally, the lymphatic system drains excess extracellular fluid from the interstitial spaces surrounding tissues and organs, maintaining fluid balance and preventing tissue swelling or edema[4].

Beyond fluid regulation, the lymphatic system plays a critical role in immune defense [5]. When antigens, such as bacteria, viruses, or other foreign substances, enter the body, they are captured by specialized antigen-presenting cells - particularly dendritic cells - in peripheral tissues[2, 6]. These cells migrate via lymphatic vessels to the draining lymph nodes, where they present processed antigens primarily to naïve T cells, initiating their activation[7]. Activated T helper cells subsequently provide essential signals for B cell activation, while B cells differentiate into plasma cells that produce antibodies to neutralize pathogens[8]. Macrophages further contribute to clearing pathogens and infected cells, thereby amplifying the immune response[8, 9]. Through this coordinated process of antigen capture, presentation, and lymphocyte activation, the lymphatic system ensures effective immune surveillance and initiates the protective responses[10-14]. Within lymph nodes, the interactions among dendritic cells, T cells, and B cells orchestrate a tightly regulated immune reaction that eliminates invading pathogens[15]. Acting in concert with other immune organs, such as the spleen and bone marrow, the lymphatic system maintains tissue homeostasis and protects the body against infections and disease[16-18].

Lymphatic vessels are extensively distributed throughout the body, with the notable exceptions of certain regions such as the central nervous system and the cornea. The formation of novel lymphatic vessels from pre-existing ones, a process known as lymphangiogenesis, plays essential roles in tumor metastasis, wound healing, tissue fluid balance, graft rejection, and immune response[12, 19, 20].

1. 2 . Anatomy of the eye and cornea

The eyeball is a complex organ composed of multiple specialized structures essential for vision and ocular movement. Injuries to any part of the eye can cause discomfort, vision impairment, or even blindness. Due to its exposed and delicate structures, the eye is susceptible to trauma, infections, and various pathological conditions, making a thorough understanding of its anatomy critical for healthcare professionals.

The adult eyeball measures approximately 2.5 cm in diameter, with only about one-sixth exposed to the external environment. It is composed of three layers: the fibrous tunic, the vascular tunic, and the retina. The fibrous tunic, the outermost layer, comprises the transparent cornea and the opaque sclera. The cornea, essential for refracting light, has a multi-layered structure and receives oxygen and nutrients primarily from the tear film and aqueous humor. In contrast, the sclera provides structural support and protection, maintaining the shape of the eye. The vascular tunic, or uvea, consists of the choroid, ciliary body, and iris (Figure 1). The choroid supplies nutrients to the retina and absorbs excess light. The ciliary body produces aqueous humor and adjusts the lens for focusing, while the iris regulates the amount of light entering the eye.

The innermost layer, the retina, is crucial for processing visual information. It contains a pigmented layer and a neural layer, the latter containing photoreceptor cells (rods and cones) that convert light into nerve impulses. Cones are responsible for colour vision, while rods enable vision in low light. Visual signals are processed through layers of retinal neurons before reaching the optic nerve. The lens, situated posterior to the pupil and iris, divides the eye's interior into the anterior and vitreous cavities. The anterior chamber contains aqueous humor, while the vitreous chamber is filled with the vitreous body, which helps maintain the eye's shape and secures the retina in place [14].

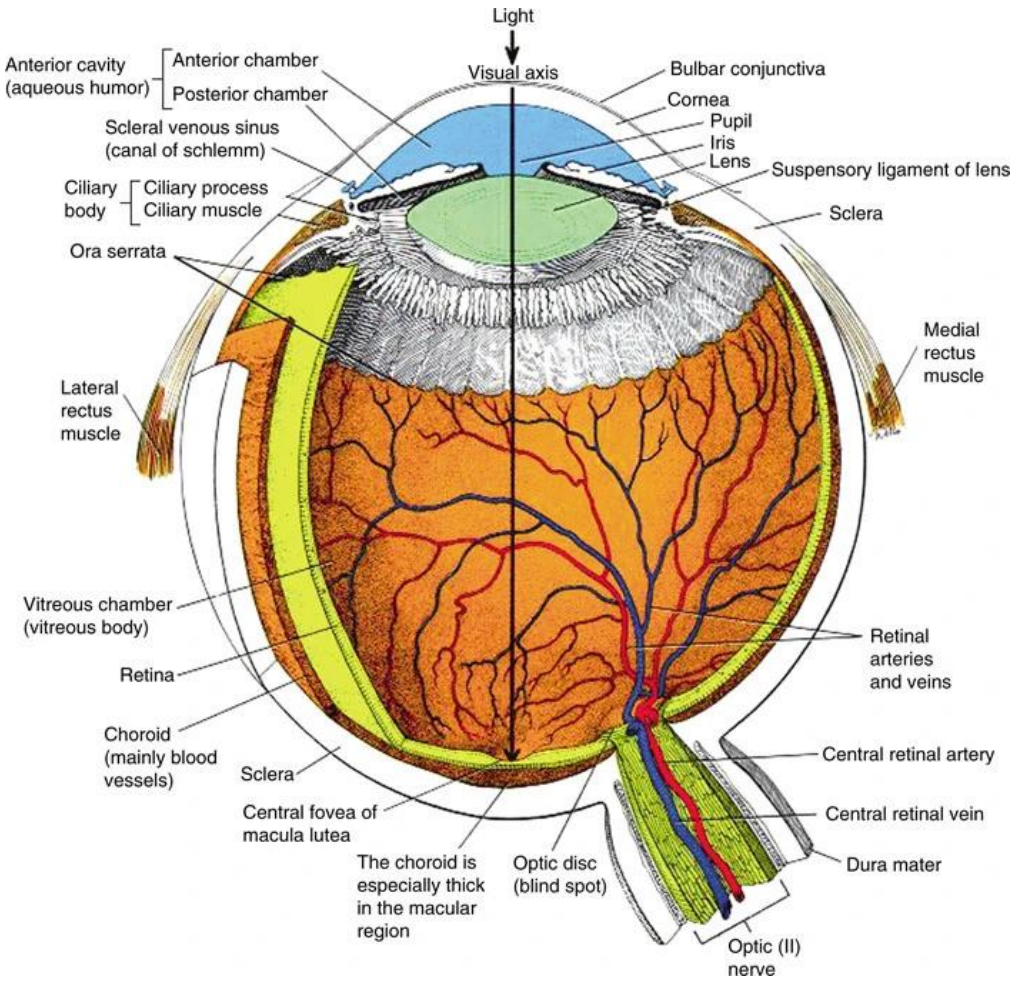

Figure 1. Schematic drawing of the human eye. The human eye's cross-sectional diagram illustrates key anatomical structures, including the cornea, sclera, iris, lens, retina, and optic nerve, which are vital for light processing and vision[15].

The cornea, often described as the transparent "windscreen" of the eye, serves as a protective outer layer covering the iris, pupil, and anterior chamber[21]. Its unique transparency and curved shape allow light to enter the eye, playing a crucial role in vision by contributing approximately two-thirds of the eye's total optical power through its refractive capabilities. The cornea's layered structure includes five layers: the epithelium, Bowman's layer, stroma, Descemet's membrane, and endothelium (Figure 2)[22, 23].

The transition from the cornea to the limbus is characterized by the termination of Bowman's layer anteriorly and Descemet's membrane posteriorly, defining the anatomical limbus, a ring-shaped area approximately 1.5 mm wide. The limbus contains several specialized structures, including the trabecular meshwork, scleral spur, Schlemm’s canal, limbal stroma, episcleral, conjunctival stroma, and conjunctival

epithelium. This transition zone is essential for maintaining a barrier between these tissues and supporting epithelial renewal[24]. Additionally, it facilitates immune surveillance through the presence of resident immune cells, contributing to ocular defense mechanisms[25]**.** Clinically, the limbus plays a vital role in corneal wound healing and serves as a key surgical landmark in procedures such as glaucoma surgeries and corneal transplantation. Dysfunction of the limbus can lead to conditions such as limbal stem cell deficiency or elevated intraocular pressure, underscoring its critical role in maintaining ocular health[26].

The palisades of Vogt, radial fibrovascular protrusions located on the anterior surface of the limbal stroma, create specialized niches for limbal epithelial stem cells, which are essential for the regeneration of the corneal epithelium. The limbus receives its blood supply primarily from the anterior ciliary arteries, with lymphatic vessels situated superficially, with episcleral vessels lying beneath them. Venous drainage occurs via the intrascleral venous plexus and branches of the anterior ciliary and circular limbal arteries. Age has been shown to influence the anatomy and reactivity of limbal lymphatic vessels; in older age individuals, inflammation-induced corneal lymphangiogenesis is reduced, which may potentially improve outcomes following corneal transplantation[24].

In summary, the cornea, through its structural integrity and clarity, works in concert with the anterior chamber and lens to refract and focus light, highlighting its critical role in vision and the importance of maintaining corneal health for optimal visual function [23, 24].

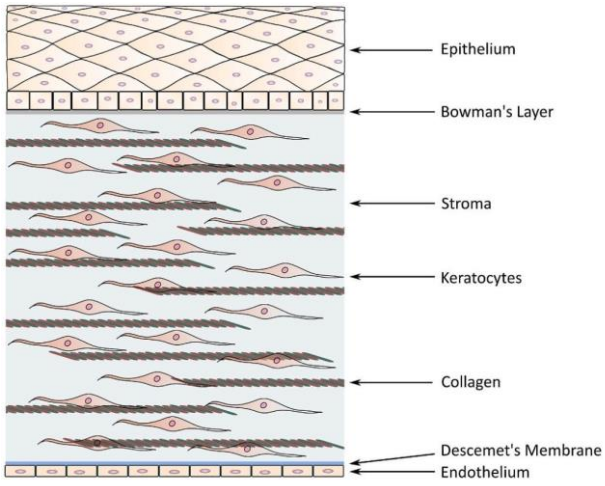

Figure 2. Anatomy of the cornea. Schematic representation of the cornea depicting its

distinct anatomical layers: the epithelium, Bowman's layer, stroma, Descemet's membrane, and endothelium[24].

1.3. Corneal (Lymph-)angiogenic privilege

The recent discovery of lymphatic vessels in ocular diseases represents a significant advancement in our understanding of the eye's vascular system. In the past, the eye was described as free of lymphatic vessels, a view that reinforced the concept of the eye's immune privilege[1, 27].

Over the past two decades, this perception has shifted with the discovery of lymphatic-like vessels in the eye[24]. The cornea, one of the few tissues typically free of blood and lymphatic vessels, can develop lymphatic vessels under inflammatory conditions. These newly formed vessels facilitate the transport of immune cells, contributing to corneal graft rejection and exacerbating other ocular surface pathologies. This has significant implications for corneal transparency and vision, as well as for immune responses and transplant survival[27, 28].

Under normal conditions, the absence of vascularization in the cornea limits access of immune cells to corneal antigens and prevents the trafficking of cells to regional lymph nodes. Blood and lymphatic vessels from the conjunctiva terminate at the limbus, marking the boundary between the densely vascularized conjunctiva and the avascular cornea[24, 27].

Recent studies have identified several molecular markers crucial for investigating corneal lymphangiogenesis. These markers, which exhibit strong lymphatic specificity, include Prospero Homeobox Protein 1 (Prox1), Vascular Endothelial Growth Factor receptor 3 (VEGFR-3), Vascular Endothelial Growth Factor C (VEGF-C), Lymphatic vessel endothelial hyaluronan receptor 1 (LYVE-1), and podoplanin[27]. Maintaining the limbal barrier and corneal avascularity requires a delicate balance between pro- and anti-lymphangiogenic of promoting and inhibit. Several growth factors and signaling molecules are crucial for lymphangiogenesis. Key members of the VEGF family, such as VEGF-A, VEGF-C, and VEGF-D, play a central role in the formation of lymphatic vessels[24, 29]. Other important factors include fibroblast growth factor (FGF-2)[30], which promotes the proliferation and migration of lymphatic endothelial cells, and platelet-derived growth factor (PDGF-BB)[31], which stabilizes new vessels

by recruiting pericytes. Angiopoietins[32] contribute to lymphatic vessel remodeling and stabilization, while hepatocyte growth factor (HGF)[33] and transforming growth factor-β (TGF-β)[31] modulate lymphangiogenesis in a context-dependent manner. Insulin-like growth factor (IGF-1)[34] enhances lymphatic endothelial cell survival and proliferation, and epidermal growth factor (EGF) stimulates lymphatic endothelial migration and proliferation, particularly in cancer. Additionally, tumor necrosis factor-α (TNF-α)[34], a pro-inflammatory cytokine, promotes lymphangiogenesis by upregulating VEGF-C and VEGF-D and recruiting immune cells. Together, these factors coordinate the complex process of lymphatic vessel formation and function. Various endogenous inhibitors counterbalance their activity, though only a few inhibitors have been identified to date[29, 34].

These markers have facilitated the study of lymphatic vessels in the eye, particularly in the cornea, which serves as an ideal model tissue for such research due to its avascularity and accessibility. This has led to novel insights into the roles of lymphatic vessels in various ocular diseases, including dry eye disease, ocular graft-versus-host disease, and pterygium, among others[24, 35, 36].

The corneal epithelium plays a crucial role in maintaining the avascular and alymphatic states of the cornea, partly due to the expression of VEGFR-3 on epithelial cells, which contributes to the regulation of lymphangiogenesis[37]. It expresses both soluble and membrane-bound forms of VEGF receptors 2 and 3, which act as decoy receptors to sequester VEGF-C and -D. Recent research has identified several novel endogenous modulators involved in lymphangiogenesis, including thrombospondin-1, vasohibin-1, membrane-type matrix metalloproteinase-1 (MT-MMP1), neuropilin-2 (NP-2), semaphorin-3F (Sema-3F), tyrosinase, vasoactive intestinal peptide (VIP), alpha-melanocyte-stimulating hormone (alpha-MSH), and insulin receptor substrate-1 (IRS-1)[38-44]. These modulators represent potential therapeutic targets for conditions associated with abnormal lymphangiogenesis, such as cancer metastasis, lymphedema, and inflammatory diseases. However, their clinical application remains to be established. Targeted therapeutic strategies under investigation include monoclonal antibodies, small-molecule inhibitors, and peptide-based agents to modulate the activity of these factors[42-44].

Various ocular diseases, including infections and corneal injuries, have the potential to disrupt the delicate balance between pro- and anti- (lymph)angiogenic factors, thereby

promoting the ingrowth of blood and lymphatic vessels. Such dysregulation increases the risk of rejection reactions in subsequent corneal transplants. Despite advances in the development of anti-hem- and anti-lymphangiogenic treatment strategies targeting the corneal VEGF pathway, clinical approaches to modulate lymphangiogenesis remain unavailable[27].

1.4. Cornea as a model for identifying novel endogenous modulators of lymphangiogenesis

The cornea provides a valuable *in vivo* model for the identification of new lymphangiogenesis modulators[43]. Differences in lymphangiogenic responses among various classical and wild-type inbred mouse strains suggest that genetic factors play a significant role in influencing this process. Phenotypic variations in lymphatic vessel formation are associated with changes in gene expression, indicating that underlying genetic differences contribute to the observed discrepancies in lymphangiogenic responses.

To determine strain-specific differences in limbal lymphatic vasculature, resting limbal lymphatic vasculature was analyzed in six mouse strains: five commonly used inbred strains (BALB/c, C57BL/6, SJL, 129S1/Sv, FVB) and one wild strain (Cast/Ei)[45]. The limbal lymphatic vascular area and the number of sprouts and vascular extensions from the main limbal lymphatic vessel into the avascular cornea were determined. The analysis revealed that both the resting limbal lymphatic vasculature and the number of physiological extensions varied among strains. BALB/c exhibited the lowest limbal lymphatic vasculature, whereas other strains demonstrated significant variability, with 129S1/Sv and C57BL/6 showing 1.4-fold and 1.8-fold increases, respectively, compared to BALB/c (Figure 3A). Additionally, C57BL/6 mice display 1.5-fold more sprouts into the avascular cornea, and both SJL and FVB strains had 1.6-fold more compared to BALB/c (Figure 3B).

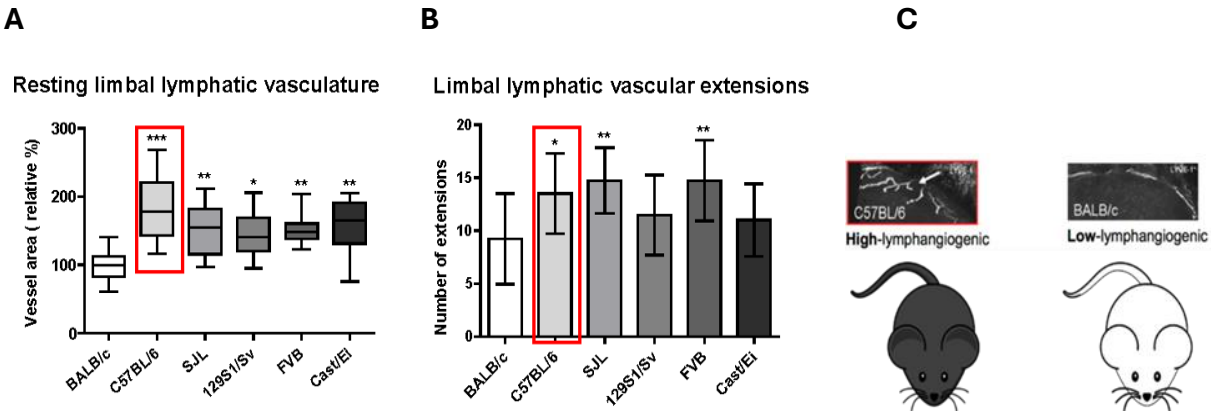

Figure 3. The extent of lymphovascularization in the limbal transition zone of naïve corneas differs significantly across various inbred and wild-type mouse strains. (A) (i.e., physiological extensions of conjunctival lymphatic vessels into the avascular cornea) varied 1.8-fold between Balb/cAnNCrl and C57BL/6NCrl, 1.5-fold between Balb/cAnNCrl and SJL/JCrl, 1.4-fold between Balb/cAnNCrl and 129S1/SvImJ, 1.5-fold between Balb/cAnNCrl and FVB/NCrl, and 1.6-fold between Balb/cAnNCrl and Cast/EiJ. Statistical evaluation was done by Kruskal-Wallis analysis with Dunn's multiple comparison posttest. *P < 0.05, **P < 0.01, ***P < 0.001. (B) The number of sprouts significantly differed between Balb/cAnNCrl and C57BL/6NCrl (1.5-fold), BALB/c and SJL/JCrl (1.6-fold), as well as between Balb/cAnNCrl and FVB/NCrl (1.6-fold). *P < 0.05, **P < 0.01. Statistical evaluation was done by analysis of variance with Bonferroni multiple comparison. (C) Comparison of lymphangiogenic responses in different mouse strains. Representative images showing corneal lymphatic vessels stained with LYVE-1. The C57BL/6 strain exhibits a high-lymphangiogenic response, while the BALB/c strain demonstrates a low-lymphangiogenic response[45].

Strain-dependent differences were also observed in lymphangiogenesis induced by sutures and VEGF-C. The lymphatic vascular surface area generated by the suture-induced corneal neovascularization model varied up to 1.7-fold among strains, and VEGF-C-induced lymphangiogenesis varied up to 1.9-fold compared to BALB/c, depending on the mouse strain (Figure 4)[45].

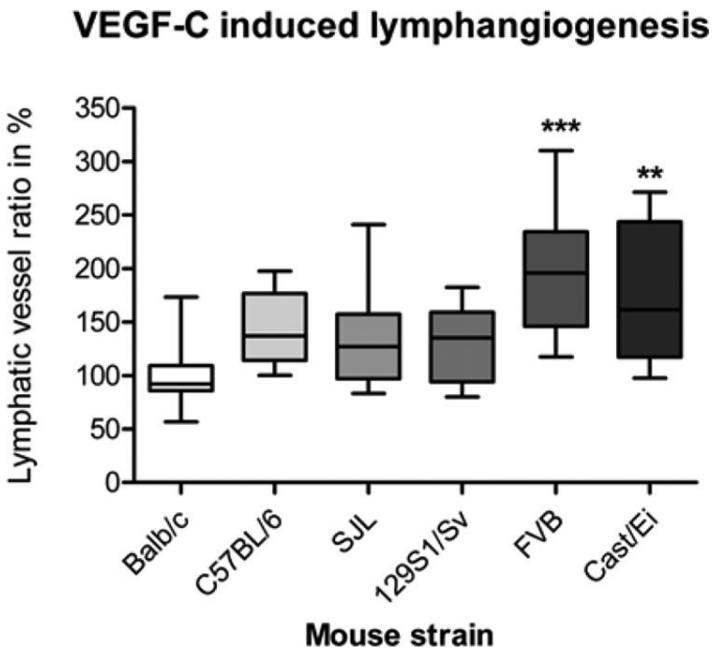

Figure 4. Strain-dependency of lymphangiogenesis induced by VEGF-C pellets in the murine corneal micropocket assay. Lymphangiogenesis induced by the lymphangiogenic growth factor (VEGF-C) differed significantly between Balb/cAnNCrl and FVB/NCrl ($P < 0.001$) and Balb/cAnNCrl and Cast/EiJ ($P < 0.01$). The mean lymphvascularized area induced by 200 ng VEGF-C for Balb/cAnNCrl was 100 ± 28% ($n = 15$), for C57BL/6NCrl 143 ± 35% ($n = 16$), for SJL/JCrl 132 ± 48% ($n = 11$), for 129S1/SvImJ 132 ± 35% ($n = 14$), FVB/NCrl 194 ± 55% ($n = 21$), and for Cast/EiJ 177 ± 63% ($n = 13$), respectively. VEGF-C-induced lymphangiogenesis varied up to 1.9-fold between different murine strains. The figure shows a boxplot where the box represents 50% of all values and the whiskers show the lowest and highest values. Statistical evaluation was done by Kruskal-Wallis analysis with Dunn's multiple comparison post-test. $^{**}P < 0.01$, $^{***}P < 0.001$[45].

Comparative studies involving different mouse strains have highlighted substantial genetic influences on lymphangiogenic responses. Further exploration of genetic variations among mouse strains could lead to the discovery of novel regulators of lymphangiogenesis[45].

Differences in lymphangiogenic responses among various classical and wild-type inbred mouse strains suggest that underlying genetic factors influence these responses, as phenotypic variations correlate with changes in gene expression[45]. Pathway-specific expression analysis of naïve corneas from highly lymphangiogenic C57BL/6 mice and low lymphangiogenic BALB/c and FVB mice revealed 13 genes with differential expression (at least a 2-fold change) in C57BL/6 mice compared to BALB/c and FVB mice[46]. Altered expression levels were also noted in genes known to affect lymphangiogenesis, such as TSP-1[47]. Furthermore, two novel candidate

genes potentially influencing lymphangiogenesis were identified: Tumor Necrosis Factor Superfamily (Tnfsf, Trail) and Tissue Plasminogen Activator (Plat/tPA). Both TRAIL and tPA were shown to inhibit the proliferation of lymphatic endothelial cells *in vitro.* These results demonstrate that analyzing naïve corneas of different mouse strains, which naturally show variations in limbal lymphatic architecture, is a valuable tool to discover novel endogenous regulators of lymphangiogenesis[46].

Lymphangiogenesis is a quantitative trait that can be precisely evaluated by measuring various morphometric parameters, such as vessel area, length, and branching, in the mouse cornea[48]. In a follow-up study to discover additional novel modulators, low-lymphangiogenic BALB/cN mice were crossed with high-lymphangiogenic C57BL/6N mice, up to the F2 generation. Subsequently, five morphometric parameters were determined in the naïve cornea: lymphatic vessel area, lymphatic vessel length, number of sprouts, number of endpoints, and number of branching points in the BALB/cN x C57BL/6N F2 intercross. The distribution of these traits in the F2 population extended beyond the ranges observed in the parental strains, suggesting a polygenic nature (Figure 5)[44].

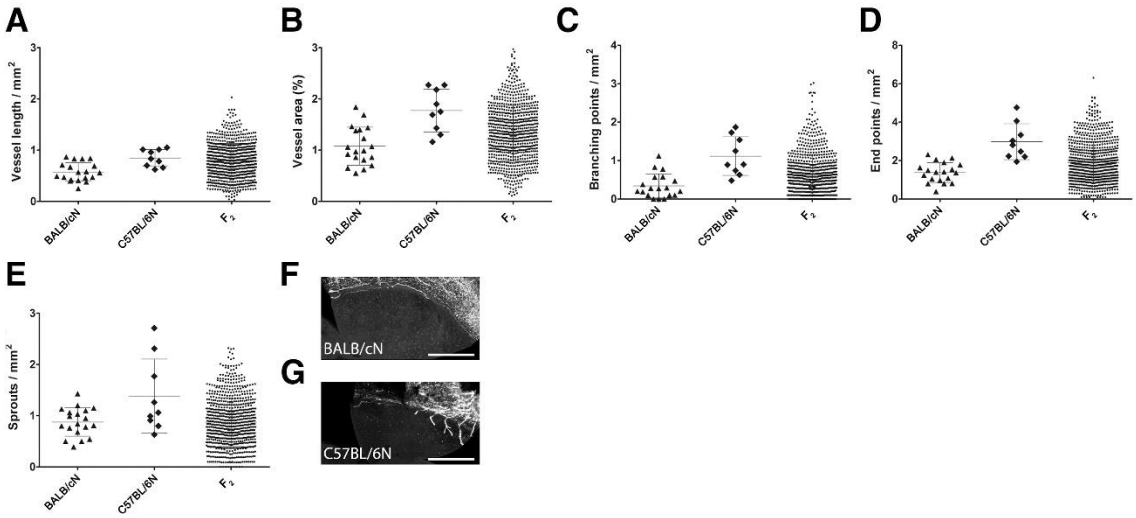

Figure 5. Phenotype of resting limbal lymphatic vasculature in parental strains BALB/cN and C57BL/6N and the F_2 population. Vessel length/mm^2 (A), vessel area (percentage; B), branching points/mm^2 (C), end points/mm^2 (D), and sprouts/mm^2 (E) of the parental strains BALB/cN and C57BL/6N and in F_2 animals. Representative whole mounts of the murine cornea of low-lymphangiogenic BALB/cN (F) and high-lymphangiogenic C57BL/6N (G) mice stained for LYVE-1. *n* = 19 (A–E, BALB/cN animals); *n* = 9 (A–E, C57BL/6N animals); *n* = 795 (A–E, F_2 animals). Scale bar = 1 mm (F and G). Original magnification, ×200 (F and G)[44].

Quantitative trait locus (QTL) analysis identified a genome-wide significant locus on chromosome 7 and a weaker locus on chromosome 17, both associated with variations in limbal lymphatic architecture between BALB/c and C57BL/6 mice (Figure 6)[44].

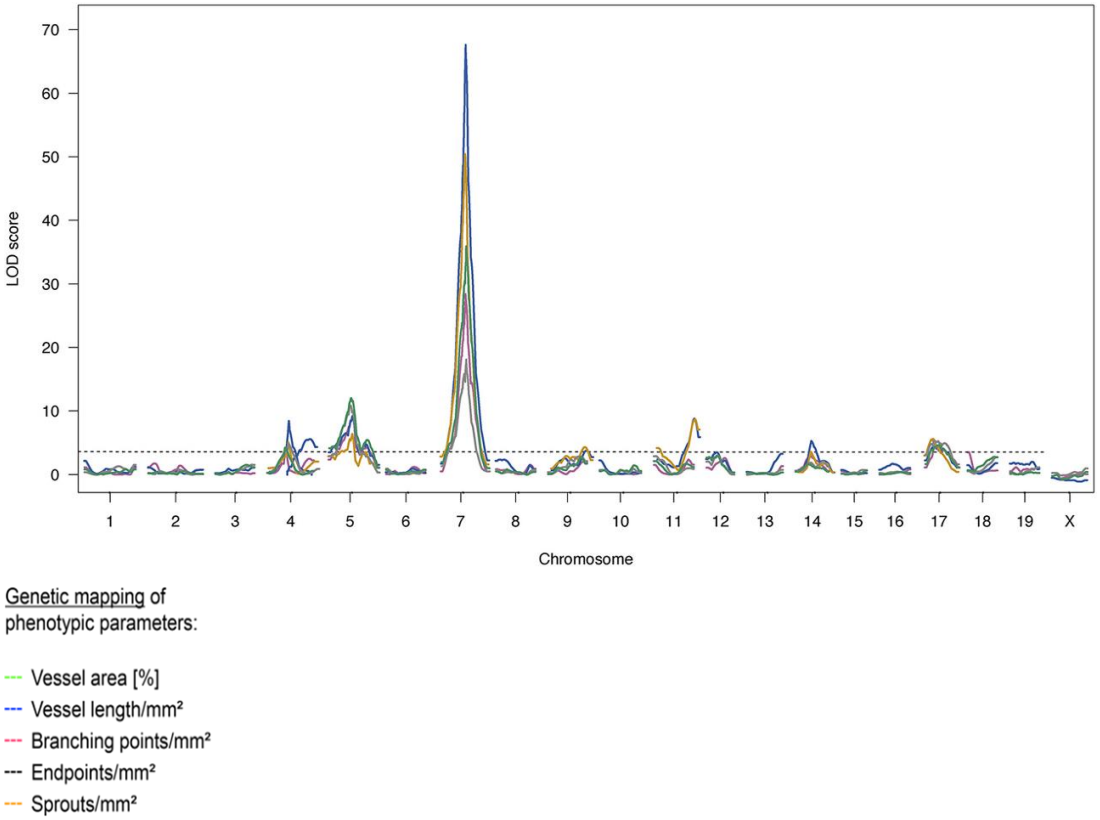

Figure 6. Genome-wide logarithm of the odds (LOD) score profiles showing quantitative trait loci (QTL) for five lymphangiogenesis-related phenotypes. Genome-wide QTL profiles for vessel length/mm^2 (green), vessel area (percentage; gray), branching points/mm^2 (orange), endpoints/mm^2 (blue), and sprouts/mm^2 (purple, all Box-Cox-Transform) mapped in 795 F2 animals using R/qtl's stepwise forward selection and backward elimination search for the best multilocus model based on Haley-Knott regression and penalized LOD scores. The threshold for genome-wide significance was determined empirically for each phenotype by 10,000 permutations (the maximal autosomal threshold for any phenotype LOD = 3.63 as dashed line). Genome-wide significant loci for all phenotypes have been identified on chromosomes 5, 7, and 17[44].

Importantly, *tyrosinase*, identified as a potential novel regulator of lymphangiogenesis, was located on chromosome 7. Traditionally known for its role in melanin biosynthesis [49], we were able to show that tyrosinase plays a significant inhibitory role in both developmental and inflammatory lymphangiogenesis. Using C57BL/6N mice and albino C57BL/6N (B6N-Tyr$^{c\text{-}Brd}$) mice, it was observed that the latter exhibited a larger lymphatic surface area in the resting limbal vasculature of the naïve cornea, as marked

by LYVE-1, without differences in blood vessel areas. The albino mice also displayed a greater number of branching and point endpoints in their lymphatic vessel networks, suggesting increased complexity. In a suture-induced corneal neovascularization assay, albino mice again showed higher lymphatic and blood vessel areas compared to tyrosinase-proficient control mice. These findings suggest that tyrosinase negatively regulates both basal and inflammation-induced lymphangiogenesis. In the cornea, tyrosinase has been shown to inhibit excessive lymphangiogenesis in physiological conditions and modulate inflammatory lymphangiogenesis during pathological responses. This dual role underscores its significance in both developmental and inflammatory lymphatic processes [44]. The combination of QTL analysis and molecular studies, exemplified by the discovery of tyrosinase's regulatory function, demonstrates the effectiveness of using genetic mapping to identify novel modulators of lymphangiogenesis. This approach provides valuable insights into the mechanisms underlying both normal and pathological lymphatic development[43, 44].

Fine mapping of the chromosome 17 locus and further prioritization using expression QTL (eQTL) analysis identified *cystathionine β-synthase* (*CBS*) and *angiopoietin-like 4* (*Angptl4*) as potential candidate genes influencing strain-dependent differences in the limbal lymphatic vasculature of naïve corneas between C57BL/6 N and BALB/cN. This finding suggests that CBS and Angptl4 may play important roles in modulating lymphangiogenesis and warrant further investigation to elucidate their specific molecular mechanisms. Overall, this comprehensive genetic and molecular analysis enables the identification of potential candidate genes regulating lymphangiogenesis, providing deeper insights into the genetic determinants of lymphatic vessel development and function.

1.5. The Collaborative Cross (CC)

Due to their genetic and physiological similarities to humans, relatively short generation time, and ease of handling in laboratory settings, mice serve as the primary mammalian model for biomedical and aging research. A wide array of genetic and experimental resources is available to support research using mice, catering to diverse scientific objectives. These include classical inbred lines, which have been bred for genetic homogeneity over many generations, allowing for consistent and reproducible results

across experiments[50]. Genetically modified mice, such as knockouts, transgenics, and humanized models, provide powerful tools for investigating the functions of specific genes and molecular pathways in health and disease[51].

Selective breeding programs have produced strains with defined traits or susceptibilities relevant to aging and disease, while congenic strains carry genomic segments from one strain introduced onto the background of another, allowing the study of individual genetic loci[52]. Recombinant inbred panels serve as a powerful resource for mapping complex traits through linkage analysis. The Collaborative Cross (CC), in particular, represents a major advance in the genetic analysis of complex traits. Outbred and heterogeneous stocks capture genetic diversity more closely resembling that of natural populations, facilitating studies on genetic interactions and population-based research[50]. Additionally, wild-derived strains, originating from natural mouse populations, provide insight into the genetic basis of phenotypic variation and adaptation[53].

Together, these mouse resources form a comprehensive toolkit for investigating diverse aspects of aging, disease pathogenesis, and therapeutic interventions, contributing to our understanding of human health and advancing biomedical research. However, these traditional resources alone may not fully capture the complexity of phenotypic effects resulting from random combinations of naturally occurring genetic variants, as seen in the heterogeneous human population[54].

To address this limitation, the Collaborative Cross (CC) was developed as a large panel of recombinant inbred (RI) strains specifically designed to model complex genetic interactions and to analyse phenotypes influenced by combinatorial allelic effects (Figure 7). As an established panel of multi-parental recombinant inbred mouse lines, the CC has become a new standard in modern QTL mapping. The allele frequency distribution of the CC mirrors that of human populations, where most variants are rare and only a few are common[55]. The eight parental inbred lines that contribute to the CC collectively cover over 90% of the known genetic variation present in all laboratory mouse strains, making the CC a powerful tool for identifying genes associated with complex traits, such as obesity[56, 57]. The CC, therefore, represents a well-designed and genetically diverse model system that supports both fundamental and translational research.

Beyond its basic genetic value, the CC has significant implications for understanding, diagnosis, and treatment of various common and chronic human diseases, including cancer, pulmonary and cardiovascular diseases, obesity, diabetes, behavioral disorders, and neurodegenerative diseases[58]. By providing a genetically diverse population with extensive genetic variation, the CC enables researchers to study complex traits and the interactions between multiple genetic factors that influence disease susceptibility, progression, and therapeutic response[56].

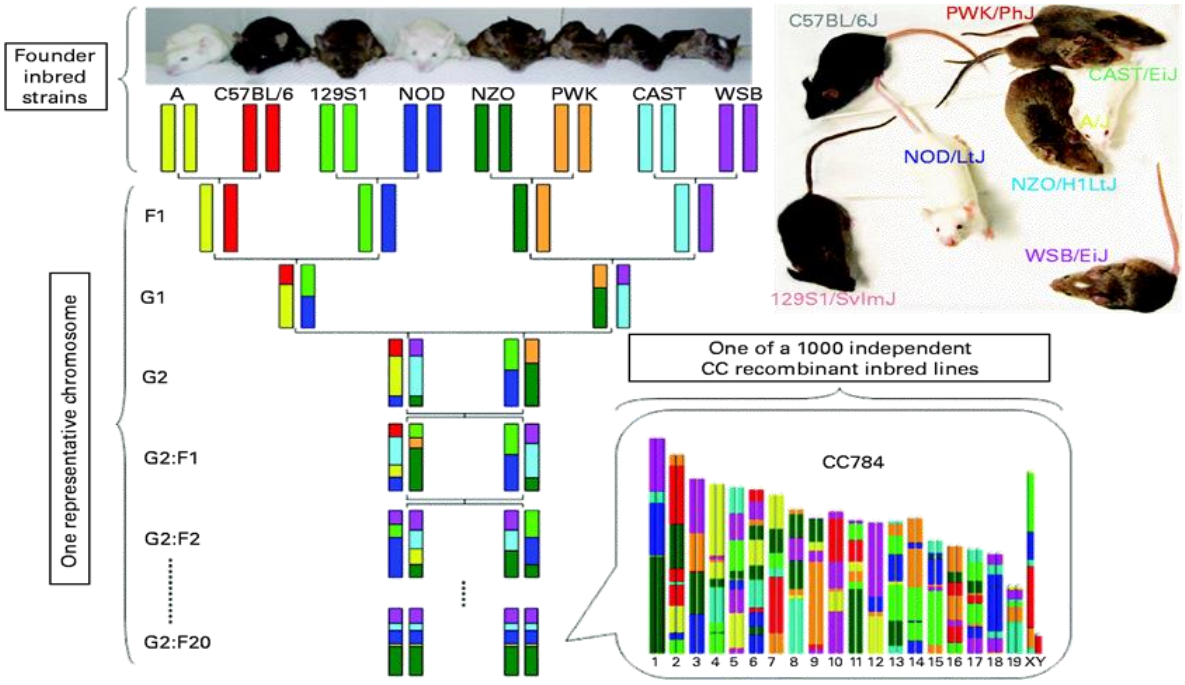

Figure 7. The Collaborative Cross (CC) is a large panel of recombinant inbred mouse lines designed to model human genetic diversity. Each individual line of the CC (one theoretical example depicted here) represents a genetic mosaic of the eight founder strains. Derived from the crossbreeding of five classic inbred lines (C57BL A/J, C57BL/6 J, 129S1/SvImJ, NOD/ltJ, and NZO/H1LtJ) and three wild-derived mouse lines (WSB/EiJ, CAST/EiJ, and PWK/PhJ), the CC captures more than 90% of the genetic diversity across the mouse genome. This diversity enables the CC to serve as a valuable tool for studying a wide range of complex human diseases and traits[57].

Given the extensive phenotypic variation observed in the CC population and its capability to elucidate the genetic basis of disease, it is conceivable that these mice could also facilitate the identification of novel modulators of lymphangiogenesis[56]. Since lymphangiogenesis plays a crucial role in various physiological and pathological

processes, including cancer metastasis, wound healing, and immune responses, understanding the genetic determinants of this process is of considerable interest. By utilizing the CC population in combinations with genetic mapping approaches focused on lymphangiogenesis-related phenotypes, researchers may uncover novel genetic loci and pathways involved in regulating lymphatic vessel growth and function. Such discoveries could lead to the identification of new therapeutic targets for diseases characterized by dysregulated lymphangiogenesis, such as cancer and inflammatory disorders.

In summary, the Collaborative Cross (CC) represents a collective scientific initiative aimed at generating an extensive repository of genetic and physiological data from a uniform, reproducible, and stable mouse population. Unlike traditional approaches relying on isolated and transient crosses, the CC provides a large, genetically defined, and permanent reference population that serves as a shared resource for the scientific community. This standardized population facilitates the accumulation and integration of data (Figure 8)[59], promoting a systems-level understanding of mammalian biology. Moreover, the application of the CC holds significant promise for advancing our understanding of complex biological processes, such as lymphangiogenesis, and may ultimately contribute to the development of novel therapeutic interventions for a broad spectrum of human diseases[56].

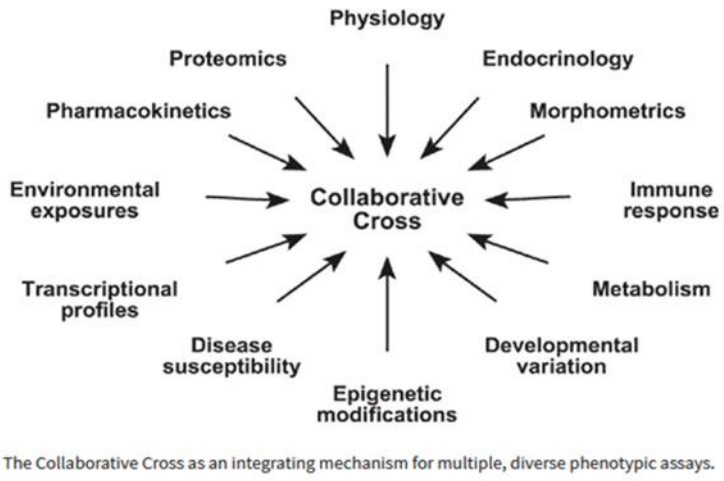

Figure 8. The Collaborative Cross is an integrating mechanism for multiple, diverse phenotypic assays[59].

1.6. AIM

Lymphatic vessels are found in almost all tissues of the body. The main functions of the lymphatic system are to maintain fluid balance in the tissue, absorb dietary fat and lipids, and play a crucial role in immune surveillance. On the other hand, lymphatic vessels also provide a route for tumor cells to metastasize and play a role in transplant rejection, lymphedema, and chronic inflammatory diseases. Given their involvement in both physiological and pathological processes, identifying new endogenous modulators of lymphangiogenesis is significant.

The cornea serves as an excellent model for studying the mechanism of lymphangiogenesis. By using the BALB/c x C57BL/6 intercross, two potential novel modulators of lymphangiogenesis were identified. The present study aimed to focus on analyzing the functional relevance and molecular mechanisms of Cystathionine β-synthase (CBS) and Angiopoietin-like 4 (Angptl-4) in the regulation of lymphangiogenesis.

As mentioned above, the genetic background strongly influences lymphangiogenesis. Differences in the limbal lymphatic architecture among inbred mouse strains provide a powerful tool to identify novel endogenous regulators of both developmental and inflammatory lymphangiogenesis. To identify additional loci that influence lymphangiogenic traits, we therefore aim to identify novel modulators of lymphangiogenesis and novel factors contributing to (lymph)angiogenic privilege by systematic genetic mapping in Collaborative Cross lines and mapping of expression QTLs of transcripts from the corneal transcriptome.

Discovering these novel regulators may provide valuable insights into the molecular mechanisms governing lymphatic vessel formation and offer new avenues for therapeutic interventions in diseases associated with abnormal lymphatic vessel development.

2. Method and Material

2.1. Material

Table 1: Primer and oligos

Name	Sequence (5' →3')	Product number
Human primers		
ANGPTL4-for	CCA CTT GGG ACC AGG ATC AC	
ANGPTL4-rv	CGG AAG TAC TGG CCG TTG AG	
β2-macroglobulin-for	AGG ACT GGTCTT TCT ATC TCT TG	
β2-macroglobulin-rv	CGG CAT CTT CAA ACC TCC AT	
CBS_for	TCA TCG TGA TGC CAG AGA AG	
CBS_rv	TTG GGG ATT TCG TTC TTC AG	
CTH-for	AGG ACT GGTCTT TCT ATC TCT TG	
CTH-rv	CGG CAT CTT CAA ACC TCC AT	
MPST-for	CAC GAG GAC ATC CTG GAG AAC T	
MPST-rv	GAA CGG GAT GTT TAC TGAGCCAG	
VEGF-C-for	GCC TGT GAA TGT ACA GAA AGT CC	
VEGF-C-rv	AATATG AAG GGA CAC AAC GAC AC	
VEGF-D-for	CCG CCA TCC ATA CTC AAT TAT C	
VEGF-D- rv	CCA TAG CAT GTC AAT AGG ACA GAG	
VEGF-R2-for	GCG ATG GCC TCT TCT GTA AG	
VEGF-R2-rv	ACAGA CTC CAT GTT GGT CA	
VEGF-R3-for	GGT ACA TGC CAA CGA CAC	
VEGF-R3-rv	AGCTC AAA GTC TCT CAC GAA CAC G	

Mice primers		
Rsp29-for	GAG CAG ACG CGG CAA	
Rsp29-rv	CCT TTC TCC TCGTTG GG C	
Vegf-a-for	CAT GGA TGT CTA CCA GCG AAG	
Vegf-a-rv	CAT GGT GAT GTT GCT CTC TGAC	
Vegf-c-for	AGA ACG TGT CCA AGA AAT CAG C	
Vegf-c-rv	ATG TGG CCT TTT CCA ATA CG	
Vegf-d-for	ATG GCG GCT AGG TGA TTC C	
Vegf-d-rv	CCC TTC CTT TCT GAG TGC TG	
Vegf-r2-for	ATT CTG GAC TCT CCC TGC CTA C	
Vegf-r2-rv	GCT CTT TCG CTT ACT GTT CTG G	
Vegf-r3-for	GTC CCT CTA CTT CCA ACT GCT TC	
Vegf-r3-rv	CACTCC TCC TCT GTG ACT TTG AG	
siRNA		
Hs-ANGPTL4-5	AGCTCGTTTAGTGAACCGTCAGATC	SI03057691
Hs-ANGPTL4-6	TCTGCGAGGGTACTAGTGAG	SI03065734
Hs-CBS-5	CGCAGAGTGGATTAAAGGCAA	SI02777159
Hs-CBS-6	TAGGATGAACACAGGCAATGA	SI02777166
Hs-CTH-6	CGGCTCTACCTGCGTGCTTTA	SI04207560
Hs-CTH-7	CATGTTATAATTACAGGTCAA	SI04235476
Hs-CTH-8	ACCAAGCTTGTTTGGATCGAA	SI05460399
Hs-MPST-7	CGCCGCTTTCTTCGACATCGA	SI03084571
Hs-MPST-6	AGAGAGTGTTTCTTCACTCAA	SI03042249
Hs-MPST-5	ACCAAGTGCTAAATCTTGTAA	SI03038308

Hs-MPST-2	CAGGATTCCGTTGACTTGTT	SI00129409

Table 2: Cell culture

Product	Company (+Headquarter)	Product number
Human dermal lymphatic endothelial cells (HDLECs)	Promocell, Heidelberg, Germany	-
Complete endothelial cell growth medium MV2	Promocell, Heidelberg, Germany	C-22022
Endothelial Cell Basal Medium MV2	Promocell, Heidelberg, Germany	C-22221
Dulbecco's Phosphate-Buffered Saline (DPBS)	Gibco	14190-094
Fetal calf serum (FCS)	Sigma-Aldrich	F9665
Matrigel® Basement Membrane Matrix	Corning, Kaiserslautern	354234
µ-Slide 15 Well 3D	Ibidi, Martinsried, Germany	81506
T25 cell culture flask	Greiner Bio One	690175
T75 cell culture flask	Greiner Bio One	658175
96-Well Cell Culture Plates	Thermo Scientific™	MIR6600
Trypan blue solution 0.4%	Sigma-Aldrich	260860
6-well Cell Culture Plates	Thermo Fisher Scientific (Waltham, Massachusetts, USA)	K497500
SuperFrost slides	Menzel-Glaser, Braunschweig, Germany	630-0950

Table 3: Antibodies

Target	Species	Company (+Headquarter)	Product number
CBS Antibody (B-4)	Mouse	Santa Cruz, Heidelberg, Germany	sc-133154
Anti-CDKN2A/p16INK4a antibody [EPR1473]	Rabbit	Abcam, Amsterdam, Netherlands	ab108349
Goat anti mouse Alexa Fluor 488	Mouse	(Invitrogen, Darmstadt, Germany)	MAC133
goat anti-rabbit-Cy3	Rabbit	(Dianova, Hamburg, German	111-165-045
rabbit anti-mouse LYVE-1 antibody	Rabbit	AngioBio Co., Del Mar, CA	11-034
CD31 Clone ER-MP12	Rat	OriGene Technologies GmbH, Herford, Germany)	BM4086
F4/80-AlexaFluor647	Rat	Biolegend, Koblenz, Germany	123122
Goat anti-rabbit AlexaFluor 488	Rabbit	Invitrogen, Darmstadt, Germany)	A11008
Goat anti-rat AlexaFluor 555	Rat	Invitrogen, Darmstadt, Germany	A21434

Table 4: Kits, reagents, and accessories

Product	Company (+ Headquarter)	Product number
RNeasy Mini Kit	Qiagen, Hilden, Germany	74104

RNeasy Micro Kit	Qiagen, Hilden, Germany	74004
RNase-free DNase Set	Qiagen, Hilden, Germany	79254
RevertAid First-Strand Synthesis cDNA Synthese Kit	ThermoScientific, Langenselbold, Germany	K1621
SsoFast EvaGreen Supermix kit	BioRad, Munich, Germany	1725201
PowerTrack SYBR Green Master Mix	ThermoScientific, Langenselbold, Germany	A46012
FITC Annexin V Apoptosis Detection Kit with 7-AAD	Biotium (Fremont, California, USA)	640922
Ketamine (Ketanest®S)	PFIZER PHARMA GmbH, Berlin	08509884
Xylazine (Rompun)		
HiPerFect Transfection Reagent	Qiagen	301705
Aminooxy acetic acid(AOAA)	Sigma Aldrich, Taufkirchen, Germany	15035-1G
Angiopoietin-related protein 4	R&D Systems, NE Minneapolis, USA	-
Recombinant Mouse Angiopoietin-like 4 Protein	R&D Systems, Wiesbaden, Germany	4880-AN-050
Bovine serum albumin (BSA)	VWR, Langenfeld, Germany	422351SP
Chemicals Paraformaldehyde, 4 % in PBS (PFA)	Alfa Aesar, Kandel, Germany	15424389
11-0 nylon sutures	Serag Wiessner, Naila, Germany	ZO010188

Table 5: Devices

Name (+Version)	Company (+Headquarter)	Function
Devices		
IncuCyteTM Zoom	Essen Biosciences, Hertfordshire, UK	Live cell imaging
Zeiss Primo Vert inverted microscope fitted with an AxioCam ERc5s camera	Carl Zeiss Microscopy GmbH, Jena, Germany	Imaging
BioRad CFX96	BioRad, Munich, Germany	Detection and quantification of nucleic acid
Bioscience FACSCanto II Flow Cytometer	BD Biosciences, Heidelberg, Germany	Cell sorting analysis
Fluorescence microscope	Olympus BX63	Imaging
NanoDrop 2000c	Thermo Fisher Scientific	DNA quantification
Applied Bioscience Quantstudio 6	ThermoScientific, Langenselbold, Germany)	Detection and quantification of nucleic acid

Table 6: Software

Software	Company (+Headquarter)	Function
IncuCyteTM software Version 2016B and 2018A	Essen Biosciences, Hertfordshire, UK	Live cell image analysis
FlowJo 8.7.3	Beckton Dickenson, Ashland, USA	Cell sorting analysis
FACS DIVA 8.0.2	Beckton Dickenson, Ashland,	Cell sorting analysis

	USA	
MATLAB R2021a	MathWorks Inc., Natick, USA	Image analysis
cell^F 3.4	Olympus Europe, Hamburg, Germany	Image analysis
NanoDrop 2000 (v.1.5)	Thermo Fisher Scientific	DNA quantification
GraphPad Prism software version 8	GraphPad Software, San Diego, CA	Statistical analysis
Image J (1.53K)	National group of Health, USA	Image analysis

Table 7: Animals

Mice	**Company (+Headquarter)**
C57BL/6 NCrl Mice	Charles River Germany, Sulzfeld, Germany
BALB/cAnNCrl Mice	Charles River Germany, Sulzfeld, Germany
Angptl4$^{-/-}$ Mice	Kind donation from Prof Sander Kersten Nutrition, Metabolism and Genomics Group, Wageningen University, Wageningen, The Netherlands
Angptl4-WT Mice	Kind donation from Prof Sander Kersten Nutrition, Metabolism and Genomics Group, Wageningen University, Wageningen, The Netherlands
CC008 (BOON_HF)	Jackson Laboratories, Bar Harbor, USA
CC010 (NUK_AC)	Jackson Laboratories, Bar Harbor, USA
PAT_CD	Kindly provided by Geniad Pty Ltd
BOON_HF	Kindly provided by Geniad Pty Ltd
LOT_EC	Kindly provided by Geniad Pty Ltd
ROGAN_CF	Kindly provided by Geniad Pty Ltd
LUF_AD	Kindly provided by Geniad Pty Ltd

FIV_AC	Kindly provided by Geniad Pty Ltd
CIS_AD	Kindly provided by Geniad Pty Ltd
LAT_AD	Kindly provided by Geniad Pty Ltd
NUK_AC	Kindly provided by Geniad Pty Ltd

2.2. Method

2.2.1. Cell Culture

Adult human dermal lymphatic endothelial cells (HDLECs; Promocell, Heidelberg, Germany) were used for all *in vitro* experiments in this study. Culturing was performed under consistent conditions using complete endothelial cell growth medium MV2 (Promocell, Heidelberg, Germany), which consists of Endothelial Cell Basal Medium MV2 supplemented with 5% fetal calf serum (FCS), 5 ng/ml recombinant human epidermal growth factor (rh-EGF), 10 ng/ml recombinant human basic fibroblast growth factor (rh-bFGF), 20 ng/ml insulin-like growth factor, 0.5 ng/ml recombinant human vascular endothelial growth factor A 165 (rh-VEGF-A 165), 1 µg/ml ascorbic acid, and 0.2 µg/ml hydrocortisone (full medium). Endothelial Cell Basal Medium MV2 without supplements (basal medium) was used as a control. All cells were cultured in a humidified incubator at 37°C with 5% CO2.

Determination of Transient Knockdown by siRNA Transfection Targeting Region for CBS, CTH, MPST, and ANGPTL4

HDLECs were seeded at a density of 1.25x10^5 cells per well in 2 ml of complete endothelial cell growth medium MV2 (PromoCell, Heidelberg, Germany) in 6-well plates and incubated overnight. The next day, HDLECs were transfected with siRNA to perform a knockdown of either CBS, CTH, MPST, or Angptl4. Therefore, 100 µl of basal medium was mixed with siRNA targeting the CBS-coding region (Hs_CBS_5 and Hs_CBS_6), CTH-coding region (Hs_CTH_6, Hs_CTH_7, and Hs_CTH_8), MPST-coding region (Hs_MPST_7, Hs_MPST_6, Hs_MPST_5, and Hs_MPST_2), or Angptl4-coding region (Hs_Angptl4_5 and Hs_Angptl4_6) at a final concentration of 75 nM. Afterward, 7.5 µl of HiPerfect Transfection Reagent (Qiagen, Hilden, Germany) was added to the mixture and incubated for 10 min. The old medium in the plates was

replaced with 900 µl of full medium. Subsequently, the transfection mix was carefully added dropwise onto the cells. After 3 hr, an additional 1 mL of full medium was added to the plates. Negative control siRNA (All-Star Negative Control siRNA, Qiagen, Hilden, Germany) was used as a control. Transfection efficiency was assessed 72 hours post-transfection by RT-qPCR.

2.2.2. Proliferation Assay for Analyzing the Effect of CBS, CTH, MPST, and ANGPTL4 on Lymphangiogenesis *In Vitro*

In this study, the HDLECs were treated with different concentrations of aminooxy acetic acid (AOAA) (Sigma Aldrich, Taufkirchen, Germany) or ANGPTL4 (R&D Systems, Germany). Additionally, siRNA-transfected cells were used for 48 hours post-transfection for this experiment. naïve 3000 HDLECs and siRNA-transfected cells were seeded in 100µl complete medium in 96-well plates. The plates were left under the hood for 30 minutes to allow the cells to adhere and then incubated overnight in a humidified incubator at 37°C with 5% CO2. The remaining siRNA-transfected cells were returned to 6-well plates and placed in the incubator. The following day, the full medium was replaced with basal medium supplemented with 1% FCS (minimal medium) and incubated for 1 hour. After incubation, the basal medium was removed, and the non-transfected cells were treated with different concentrations of AOAA (4mM, 2mM, 1mM, 0.5mM & 0.25mM) or Angptl4(1, 10, 100, 1000 ng/ml). Unless otherwise stated, the transfected cells received only complete medium. Cell proliferation was measured by live cell imaging every 4 hours using the IncuCyteTM Zoom (Essen Biosciences, Hertfordshire, UK), monitoring an increase in cell density. The fold change in density was calculated within 24 hours using the IncuCyteTM software (Version 2016B and 2018A, Essen Biosciences, Hertfordshire, UK).

2.2.3. Apoptosis Assay

125,000 HDLEC cells were seeded onto a 6-well plate in 2 ml complete endothelial cell growth medium MV2 (PromoCell, Heidelberg, Germany) per well and incubated overnight to allow cell adhesion. The following day, the cells were incubated in basal medium supplemented with 1% FCS (minimal medium) for 1 hour. After treatment with

different concentrations of AOAA (4mM, 2mM, 1mM, 0.5mM & 0.25mM) for 24 hours, cells were harvested and stained using the BioLegend FITC Annexin V apoptosis detection kit with 7-aminoactinomycin D (7-AAD) according to the manufacturer's instructions. Cell samples were analyzed on a BD Biosciences FACSCanto II Flow Cytometer, and data were analyzed using FlowJo 8.7.3 software (Beckton Dickenson, Ashland, USA).

2.2.4. Migration Assay

In independent experiments, 10,000 HDLECs, non-transfected or transfected with CBS siRNAs, CTH siRNAs, or ANGPTL4 siRNA, were seeded in 100 µl of complete growth medium in 96-well plates. Each siRNA transfection was performed in a separate experimental setup to ensure a distinct analysis of the knockdown effects. The plates were left under the hood for 30 minutes to allow the cells to adhere, and then incubated overnight. The following day, the cells were incubated in basal medium supplemented with 1% FCS (minimal medium) for 1 hour. Scratches were made in each well using a 10µL pipette tip, and the medium was changed to either full medium or full medium containing the indicated concentrations of AOAA or ANGPTL4, for non-transfected cells. For siRNA-transfected cells, only a full medium was used. Wound closure was monitored by live cell imaging every 4 hours for 24 hours using the IncuCyteTM Zoom. The wound surface areas at each time point were measured using ImageJ (1.53K) software, and wound closure was calculated as the percentage of the healed scratch area compared to the original scratch area at 0 hours.

2.2.5. Tube Formation Assay

The tube formation assay was performed using µ-Slide angiogenesis assay (Ibidi, Martinsried, Germany) coated with Matrigel® (Corning, Kaiserslautern, Germany).

After coating the µ-Slides with Matrigel, 10,000 HDLECs, either transfected with siRNA or non-transfected, were seeded. The transfected cells were initially seeded in 50µl of basal medium with 1% FBS, and after 1 hour, the medium was replaced with complete endothelial cell growth medium MV2 (PromoCell, Heidelberg, Germany). The non-transfected cells were treated with varying concentrations of AOAA or ANGPTL4 in

50µl of the full medium for each well. Afterward, µ-Slides were then placed in the incubator. Images were taken after 4 hrs and 24 hours using a Zeiss Primo Vert inverted microscope fitted with an AxioCam ERc5s camera. The number of branches, loops, and branching points, as well as the length of the branches, were manually analyzed using ImageJ (1.53K) software.

2.2.6. RNA Isolation and cDNA Synthesis

125,000 naïve HDLECs were seeded in 6-well plates and left in an incubator at 37°C overnight to adhere. The cells were treated with different concentrations of AOAA or ANGPTL4 for 24 hours. After 24 hr, the cells were washed twice with cold PBS, and RNA was isolated using a mini kit from Qiagen. The concentration of RNA was determined using a NanoDrop 1000. For siRNA-transfected cells, RNA isolation was performed using the Qiagen minikit, and the concentration of RNA was determined using NanoDrop 1000. Complementary DNA (cDNA) synthesis was performed using the RevertAid First-Strand cDNA Synthesis Kit (ThermoScientific, Langenselbold, Germany) according to the manufacturer's instructions.

2.2.7. Analysis of mRNA Expression by Real-Time Quantitative PCR

For analysis of mRNA expression, 1000 ng of cDNA generated from each mRNA sample was used for real-time polymerase chain reaction (RT-PCR) in a BioRad CFX96 system using the quantitative (q)PCR SsoFast EvaGreen Supermix kit (BioRad, Munich, Germany) and specific primers; β2-macroglobulin, VEGF-C, VEGF-D, VEGF-R2, VEGF-R3, VEGF-A, CBS, and ANGPTL4. ß2-microglobulin was used as an endogenous control for normalization. Expression levels of the target genes were calculated relative to the levels found in unstimulated cells.

2.2.8. Immunofluorescence Staining of HDLECs for Examination of CBS Expression

To examine CBS expression after transfection with siRNA, 30,000 cells from 3-day post-transfected cultures were seeded in complete medium on coverslips in a 24-well

plate. The cells were allowed to attach overnight in a 37°C incubator. The following day, the cells were incubated with 500 µL of basal medium supplemented with 1% FCS for 1 hour. Subsequently, the medium was changed to full medium, and the cells were incubated for an additional 24 hours.

Cells were washed twice with 500 µL of phosphate-buffered saline (PBS) containing 1 mM $MgCl_2$ and 0.1 mM $CaCl_2$ (PBS^{++}). Next, the cells were fixed with 500 µL of 4% paraformaldehyde per well for 20 minutes. Permeabilization was then performed using 500 µL of PBS^{++} containing 0.1% Triton X-100 (PBS^{T++}) for 5 minutes at room temperature (RT). Following permeabilization, the cells were quenched with 1 mL of 50 mM NH_4Cl in PBS^{T++} for 5 minutes and then washed once with PBS^{T++}. Subsequently, the cells were blocked with 500 µL of PBS^{T++} containing 1% BSA for 1 hour at RT.

For staining, wet chambers were prepared using tissue towels and parafilm. Twenty microliters of the primary antibody solution, containing CBS (1:50) (Santa Cruz, Heidelberg, Germany) and p16 (1:1000) (Abcam, Amsterdam, Netherlands), were placed on top of the parafilm. Coverslips were then positioned over the antibody solution, with the cell sides facing down. The coverslips were then incubated for 60 minutes. After washing three times with 0.2% BSA/PBS^{T++}, 20 µL of the secondary antibody solution containing goat anti-mouse Alexa Fluor 488 (1:100) (Invitrogen, Darmstadt, Germany) and goat anti-rabbit Cy3 (1:100) (Dianova, Hamburg, Germany) was added to each coverslip, followed by another 45-minute incubation. Following the staining procedure, the coverslips were lifted, and DAPI was used to stain the total number of cells in each coverslip (1:5000 for 2 minutes at RT). The cells were then mounted in a mini drop of DAKO fluorescent mounting medium (DAKO) on slides. All staining processes were performed in the dark, and the slides were stored at 4°C.

In parallel, 30,000 HDLECs were seeded in complete medium on coverslips in a 24-well plate and treated with different concentrations of AOAA (4, 2, 1, 0.5, and 0.25 mM) for 24 hours, following the same immunofluorescence staining procedure as the CBS-transfected cells. Images were automatically captured with a fluorescence microscope (Olympus BX63), and quantification was performed using MATLAB R2021a (MathWorks Inc., Natick, USA).

2.2.9. Proliferation of transfected cells with CBS, CTH and MPST siRNA that were treated with AOAA

3000 HDLECs transfected separately with CBS, CTH, or MPST siRNA were seeded in 100 µl of complete medium in 96-well plates 72 hours post-transfection. The plate was then placed under the hood for 30 minutes to allow the cells to adhere. The cells were left to attach overnight. The next day, the cells were incubated in a basal medium supplemented with 1% FCS (minimal medium). After 1 hour, the medium was changed to either full medium or full medium containing 1mM and 4mM of AOAA (Sigma Aldrich, Taufkirchen, Germany). Cell proliferation was measured as an increase in cell density by live-cell imaging every 4 hours using the IncuCyte™ Zoom (Essen Biosciences, Hertfordshire, UK). For statistical analysis, the fold increase in density within 24 hours was calculated using the IncuCyte™ software (Versions 2016B and 2018A, Essen Biosciences, Hertfordshire, UK).

2.2.10. Evaluation of Fluorescence Intensity

For evaluation of CBS fluorescence staining, images taken with the fluorescence microscope (Olympus BX63) were loaded into MATLAB software (MathWorks, Inc., Natick, MA). Firstly, the background signal in the image was subtracted using a top-hat algorithm. Then, based on the saturation intensity value, the image was converted to a binary image using a threshold. Contiguous cells were separated using the watershed algorithm, and the mean fluorescence intensity was calculated. DAPI staining was used to determine the total number of cells in each image.

2.2.11. Suture-Induced Inflammatory Corneal Neovascularization Assay

The mouse model of suture-induced inflammatory corneal neovascularization was utilized to induce a rapid and strong inflammatory response in the cornea[60]. Each animal was weighed and deeply anesthetized using intraperitoneal injection of Ketamine (Ketanest-S) [100 mg/kg bodyweight] and Xylazine (Rompun) [10 mg/kg bodyweight], with a maximum injection volume of 0.1 ml/10g KG. Three sutures were

placed intrastromally in the right eye of each mouse using 11-0 nylon sutures (Serag Wiessner, Naila, Germany), with two stromal incursions extending over 120° of corneal circumference. The placement of sutures was standardized for optimal vascularization responses, with the outer suture point near the limbus and the inner suture point near the corneal center equidistant from the limbus. The sutures remained in the cornea for 14 days, and the corneas were treated three times a day with 3 µl eye drops using a 10 µl pipette.

To evaluate the effect of CBS on inflammation-induced lymphangiogenesis *in vivo*, a total of 24 C57BL/6 mice and 13 BALB/c mice were utilized. Of the C57BL/6 mice, 12 were treated with 3 µl of eye drops containing AOAA (4 mM) three times per day, while the remaining 12 received 3 µl of PBS three times per day as a control. Similarly, in the BALB/c group, seven mice were treated with AOAA, and the remaining six were treated with PBS as a control. Half of the C57BL/6 mice (6 treated with AOAA and 6 treated with PBS) and all the BALB/c mice were sacrificed on day 14, and their corneas were histologically analysed. The remaining C57BL/6 mice (6 treated with AOAA and 6 with PBS) were used for RNA isolation on day 14.

To study the effect of ANGPTL4 on inflammatory conditions,16 C57BL/6 mice were used. After suture placement, eight C57BL/6 mice were treated with 3 µL of recombinant murine Angiopoietin-like protein 4/Angptl4 (R&D Systems, Wiesbaden, Germany) (70 ng/3 µL) three times a day, while the remained mice (C57BL/6 x 8) were treated with 3 µL PBS three times a day as a control. In total, the mice were treated with 3000 ng of Angptl4 (R&D Systems, Wiesbaden, Germany) for 14 days.

Moreover, 8- to 12-week-old male and female CC008 (BOON_HF) and CC010 (NUK_AC) mice were used for the Suture-Induced Inflammatory Corneal Neovascularization Assay for CC Line Mice. The mice were purchased from Jackson Laboratories and bred at the University Hospital Animal Facility in Cologne, Germany. The sutures were left in the cornea for 14 days to induce neovascularization, after which the mice were sacrificed, and the corneas were histologically analysed on day 14.

2.2.12. Preparation of Corneal Whole Mounts and Immunohistochemistry

After sacrificing the mice, the whole excised cornea of each mouse was harvested and washed for 5 minutes with phosphate-buffered saline solution (PBS). The cornea was fixed in 4% PFA (Alfa Aesar, Kandel, Germany) for 1 hour at room temperature. The cornea was then cut under a stereo microscope, and the whole mounts were washed twice with 1 ml of PBS^{++T} for each sample. Subsequently, the whole mounts were placed in 50 µl blocking buffer containing 2% Bovine Serum Albumin (BSA) in PBS^{++T} for 2 hours on a shaker to block non-specific binding sites.

After the blocking step, the whole mounts were stained overnight with primary antibodies, including LYVE-1 antibody (1:200 dilution; AngioBio Co., Del Mar, CA) for staining lymphatic vessels and CD31 (1:200 dilution; OriGene Technologies GmbH, Herford, Germany) for staining blood vessels in 2% BSA in PBS^{T++} at 4°C. On the following day, the whole mounts were washed three times with PBS^{T++} on the shaker for 5 minutes each time. After washing, 50 µl of secondary antibodies in 2% BSA in PBS^{T++} were added to each washed whole mount for 1 hour in the dark. Goat anti-rabbit Alexa Fluor 488 (1:500 dilution; Invitrogen, Darmstadt, Germany) was used to detect LYVE-1, and goat anti-rat Alexa Fluor 555 (1:500 dilution; Invitrogen, Darmstadt, Germany) was used to detect CD31. After 1 hour, the whole mounts were washed three times for 5 minutes each time with PBS^{T++} at room temperature on a shaker. After the washing step, the whole mounts were stained overnight with 50 µl of F4/80-APC (1:100 dilution; Invitrogen, Darmstadt, Germany) in 2% BSA in PBS^{T++} at 4°C for detecting macrophages. On day 3, the whole mounts were washed three times with PBS^{T++} and once with PBS. Subsequently, the corneal whole mounts were transferred to SuperFrost slides (Menzel-Glaser, Braunschweig, Germany), covered with Dako fluorescent mounting medium (Dako, Hamburg, Germany), covered with glass micro coverslips, and stored at 4°C in the dark. Imaging was performed automatically using a fluorescence microscope (Olympus BX63; Olympus Deutschland GmbH).

2.2.13. Determination of Morphometric Parameters of naïve corneas

To study the effect of Angptl4 on lymphangiogenesis in naïve corneas *in vivo*, the whole right eye bulb of each mouse, purebred WT, and Angptl4−/− mice on a C57BL/6 background (Wageningen, Netherlands; a kind gift from Wageningen University), was used. The mice were housed under pathogen-free conditions and individually housed in temperature- and humidity-controlled environments. A total of 12 Angptl4-wild type (WT) mice and 10 Angptl4−/− mice were used in this study. The whole eye bulbs were washed with phosphate-buffered saline solution (PBS) and fixed in 4% PFA (Alfa Aesar, Kandel, Germany) for 2 hours at room temperature.

To identify additional novel modulators of lymphangiogenesis, naïve eyes from 9 different Collaborative Cross (CC) lines were obtained through collaboration with partners in Australia. Upon receipt, the entire eye bulbs were carefully enclosed and washed with phosphate-buffered saline (PBS), followed by fixation in 1 ml of 4% paraformaldehyde (PFA) (methanol-free) in PBS for 4 hours at room temperature. After the fixation process, the corneas were rinsed three times, each with 1 ml of PBS for 10 minutes. Subsequently, the corneas were immersed in 1 ml of 20% sucrose in PBS and incubated overnight at 4°C on a shaker. The eyes were then stored at -80°C for further analysis. Corneal Whole Mounts Immunohistochemistry was done as explained in part (2.2.12).

2.2.14. Determination of Inflammatory Limbal Lymphatic Vessel Area

For the analysis of inflammatory limbal vessel area, the surface area from whole mounts of treated and untreated mice was determined using an algorithm developed in the image analysis program Cell^F 3.4. The gray value images of the whole-mount images were modified by several filters. Lymphatic vessels were detected by a threshold setting, including bright vessels and excluding the dark background, as described previously[44]. The number of sprouts, branching points, and endpoints was counted manually using cellF^3.4 and related to the total corneal area (branching points, endpoints, and sprouts/mm^2).

2.2.15. RNA Isolation from Corneas and Reverse Transcription Polymerase Chain Reaction (RT-PCR)

RNA isolation was performed on corneas 14 days post-suture, treated with AOAA, or from naïve Angptl4-wt and Angptl4−/− mice. The central 2 mm of the corneas, collected from the left eyes of the same mice used in the experiment, were used for RNA isolation. The corneas were collected from the left eyes of the same mice used. For AOAA and PBS-treated corneas on day 14, the mice were sacrificed, and the central corneas were collected by excising the cornea above the limbus immediately after sacrificing the mice. Total RNA isolation from the cornea was performed using the RNAeasy micro kit (Qiagen, Hilden, Germany) following the manufacturer's instructions. DNA was digested from each sample using 10 µl of RNase-free DNase Set (**6.82 µg** of DNase I.) (Qiagen, Hilden, Germany) per sample. RNA concentrations were determined using NanoDrop 2000 (Thermo Scientific). The isolated RNAs were reverse-transcribed into single-stranded cDNA using the First Strand cDNA Synthesis Kit (Thermo-Scientific, Langenselbold, Germany). The RNA quality in each sample was determined using NanoDrop 2000 (Thermo Scientific). PowerTrack SYBR Green Master Mix (Thermo-Scientific, Langenselbold, Germany) and Applied Bioscience Quantstudio 6 (ThermoScientific, Langenselbold, Germany) were utilized, along with specific murine primers for Rsp29, Vegf-a, Vegf-c, Vegf-d, Vegf-r2, and Vegf-r3.

2.2.16. Preparation of CC Line Eyes for RNA Isolation

The RNA isolation, RNA sequencing, and subsequent analysis for the CC-line project were conducted in collaboration with the research group of Prof. Dr. med. André Reis, Institute of Human Genetics, University Hospital Erlangen, Friedrich-Alexander-Universität Erlangen-Nürnberg, Erlangen, Germany. The collaboration was crucial for the successful execution of these procedures, utilizing their established protocols and expertise.

Before RNA isolation, the enucleated whole right eye was dipped into 1 ml of RNAprotect Tissue Reagent (Qiagen, Hilden, Germany) right away at room temperature. The eyes were then left overnight at 4°C to allow thorough penetration of the tissue. The following day, the eyes were removed from the RNAprotect Tissue Reagent and transferred directly to -80°C for storage.

2.2.17. RNA Sequencing and Analysis of CC Line Eyes

For RNA sequencing, the center of the cornea was dissected using a 2mm punch, and total RNA was isolated using a routine method. RNA purity and concentration were determined using Nanodrop (Thermo Fisher Scientific), and RNA quality was assessed using the Agilent 2100 Bioanalyzer.

2.2.18. Whole Transcriptome Analysis by Sequencing of Total RNA and RNA Sequencing Data Analysis

Total RNA was extracted from naïve corneas of the CC-lines using the RNeasy Micro Kit (Qiagen, Hilden, Germany) following the manufacturer's protocol. After quality control on the Agilent Bioanalyzer, equal amounts of total RNA were pooled from three corneas of each CC-line mouse. Sequencing libraries were prepared using the Illumina Truseq stranded mRNA Kit from 500 ng pooled total RNA. The libraries were sequenced in a 100+100 bp paired-end format on an Illumina Hiseq 2500 platform. Raw reads underwent preprocessing steps where they were trimmed of poly-N-tails, bases with quality lower than 20, and clipped of potentially remaining sequencing adapters using cutadapt (version 1.10). Reads from (mt)-rRNA and (mt)-tRNA were filtered out.

To avoid the detection of false-positive differentially expressed genes resulting from lower alignability of non-C57BL/6 sequences, all SNPs and InDels from the Sanger mouse genomes project (Release 1505) for the seven other mouse strains were integrated into the GRCm38 reference genome using modtools (version 1.0.2). After alignment with Tophat2 (version 2.1.1) to these strain-specific genomes, the alignments were normalized to the reference using Lapels (version 1.1.1) and integrated into a single BAM file per strain using suspenders (version 0.2.2) according to mapping quality and complementary default criteria. Expression was then counted on the union of exons for each gene in the Ensembl mouse gene model (Release 94) with HTSeq (version 0.7.1). After filtering for consistently extremely lowly expressed genes with the function "filterByExpr" with default parameters, TMM values were calculated with the "cpm" both from the edgeR package.

2.2.19. Statistics and Reproducibility

All functional *in vitro* experiments were performed at least three times with at least four technical replicates for each experiment. For *in vivo* experiments, the sample size was determined for 5 individual animals. Statistical analysis of the functional studies was conducted using GraphPad Prism software version 8 (GraphPad Software, San Diego, CA). Statistical significance is presented as *$p < 0.05$, **$p < 0.01$, ***$p < 0.001$, ****$p < 0.0001$.

3. Results

3.1. Effects of CBS Inhibition on HDLECs

The potential roles of CBS in lymphangiogenesis were investigated both *in vitro* and *in vivo*. The initial step involved assessing the effects of CBS on various lymphangiogenic parameters, such as proliferation, migration, and tube formation of human dermal lymphatic endothelial cells (HDLECs).

3.1.1. Effects of CBS Inhibition by AOAA on Lymphatic Endothelial Cell Proliferation, Migration, and Tube Formation

Proliferation is the first step in this process. To analyse the effect of CBS on this process, the commonly used CBS inhibitor aminooxyacetic acid (AOAA) was applied. We observed that inhibition of CBS by AOAA resulted in a significant, dose-dependent reduction in the proliferation of HDLECs compared to control cells. The strongest inhibitory effect was observed at 2 mM and 4 mM AOAA after 24h of treatment, while 1 mM AOAA also led to a significant reduction. However, concentrations of 0.25mM and 0.5mM AOAA did not significantly affect proliferation (Figure 9A).

To investigate whether the observed decrease in proliferation was due to apoptosis, Annexin V staining was performed. Flow cytometry analysis showed no significant increase in Annexin V-positive HDLECs following AOAA treatment, indicating that CBS inhibition did not induce apoptosis. Interestingly, treatment with 4 mM AOAA even showed a slight anti-apoptotic trend (Figure 9B). Based on these results and preliminary optimization experiments, 1 mM and 4 mM AOAA were selected for subsequent experiments. These concentrations were chosen because 1 mM represents a submaximal inhibitory dose, while 4 mM provides a stronger, yet non-cytotoxic, inhibitory effect on lymphangiogenic processes, such as proliferation, migration, and tube formation.

The next step in the lymphangiogenic process involves the migration of lymphatic endothelial cells, which is essential for vessel formation and remodelling. To investigate this process, a scratch wound assay was performed to evaluate the migratory capacity of HDLECs under CBS inhibition. This assay allows the evaluation of cells to close a wound-like gap in a controlled environment and provides insights into how CBS

inhibition can influence lymphatic cell migration and thus the lymphangiogenic process. The results revealed that AOAA-treated HDLECs exhibited a significantly delayed directional migration, particularly with 1 mM AOAA and 4 mM AOAA, compared to control cells (Figure 9C). Since successful migration is critical for subsequent processes in lymphangiogenesis, the influence of AOAA on the tube formation ability of HDLECs was then investigated.

Treatment with 4 mM AOAA resulted in a significant increase in the number of loops, branching points, and branches after 4h compared to untreated control HDLECs, whereas 1mM AOAA did not result in a significant difference. Over time, the number of loops, branching points, and branches decreased, while the length of the branches increased, indicating a dynamic remodelling of tube-like structures (Figure 9D). Overall, these findings suggest that CBS plays a functional role in HDLEC proliferation, migration, and tube formation, and that its inhibition by AOAA affects these processes in a dose-dependent manner. Importantly, AOAA treatment did not induce apoptosis in HDLECs but did alter their migratory and tube-forming capabilities. Given the considerable inhibition of proliferation, migration, as well as the altered tube formation capacity observed with 4mM AOAA, this concentration was standardized for all subsequent experiments. The use of a constant AOAA concentration of 4 mM allows for a comprehensive assessment of the effects of CBS inhibition on lymphangiogenesis and may provide insight into potential therapeutic strategies targeting this signaling pathway (Figure 9).

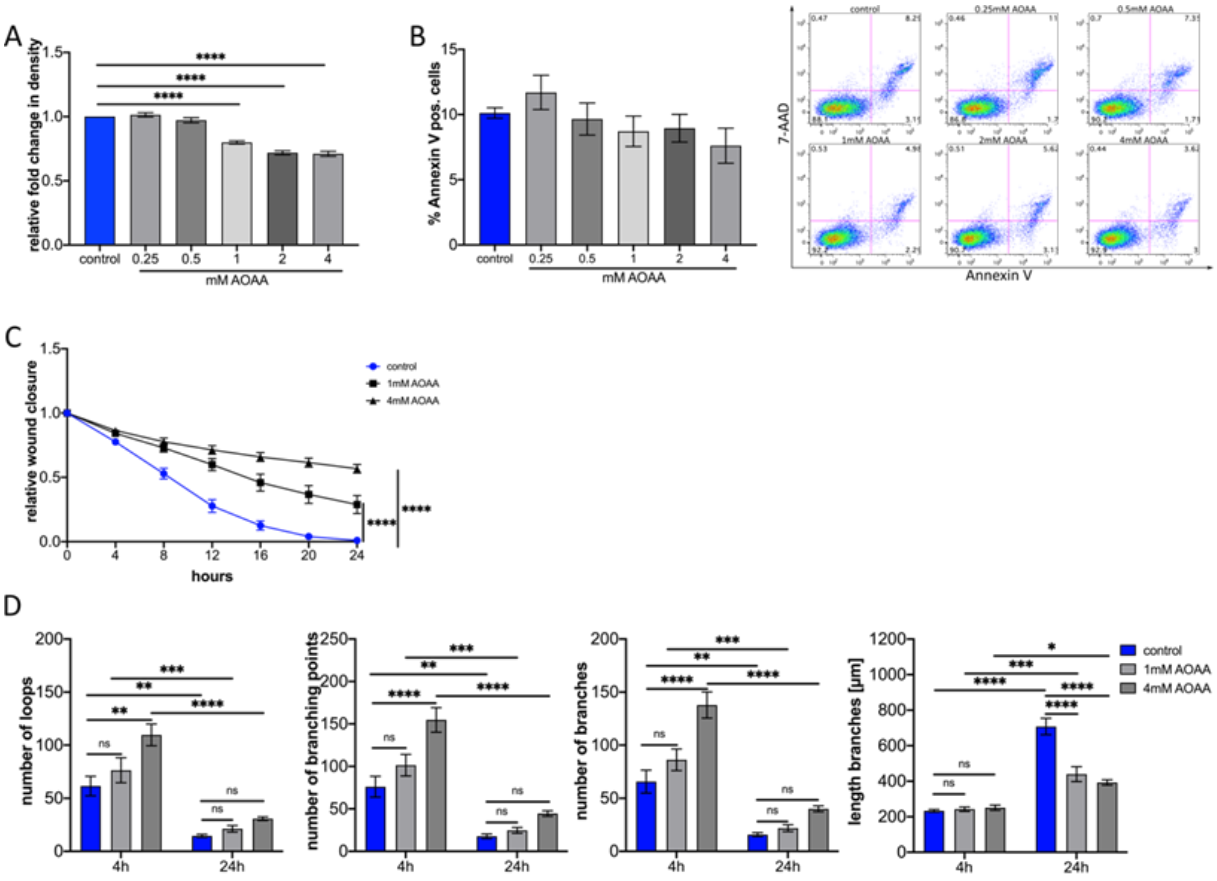

Figure 9. Effect of CBS inhibition by AOAA on HDLEC proliferation, migration, and tube formation efficiency. (A) Effect of various doses of AOAA on the proliferation efficiency of HDLECs after 24h (n=5). Proliferation was determined by using IncuCyte Zoom. (B) Quantification of flow cytometrically detected Annexin V-positive cells 24 hours after treatment with the indicated concentrations of AOAA and representative flow cytometry images (n=5). (C) AOAA treatment of HDLECs slowed wound closure compared to control cells in the wound healing assay (n=4). (D) Effect of 1mM and 4mM AOAA treatment on HDLECs on tube formation. The evaluation was performed after 4h and 24h (n=5). Statistical significance was analysed with one-way ANOVA and Dunnett's multiple comparison test, or two-way ANOVA and Tukey's multiple comparison test, or two-way ANOVA and Sidak's multiple comparisons test. **p<0.01; ***p < 0.001; ****p < 0.000.

3.1.2. CBS Inhibition by AOAA Reduces VEGFR-2 and -3 Expression in Lymphatic Endothelial Cells

To determine the influence of CBS inhibition using AOAA on the expression of VEGF-C and -D and their receptors, quantitative real-time PCR was performed. The qRT-PCR results indicated no significant change in the expression levels of VEGF-C and VEGF-D in HDLECs treated with 4mM AOAA compared to untreated control (Figure 10A). However, treatment with 4mM AOAA for 24 hours led to a significant

downregulation of VEGFR-2 and VEGFR-3 in HDLECs compared to untreated control cells (Figure 10B).

These findings indicate that CBS inhibition by AOAA reduced expression of VEGFR-2 and -3 in HDLECs, suggesting a potential role of CBS in regulating the VEGF signalling pathway involved in lymphangiogenesis.

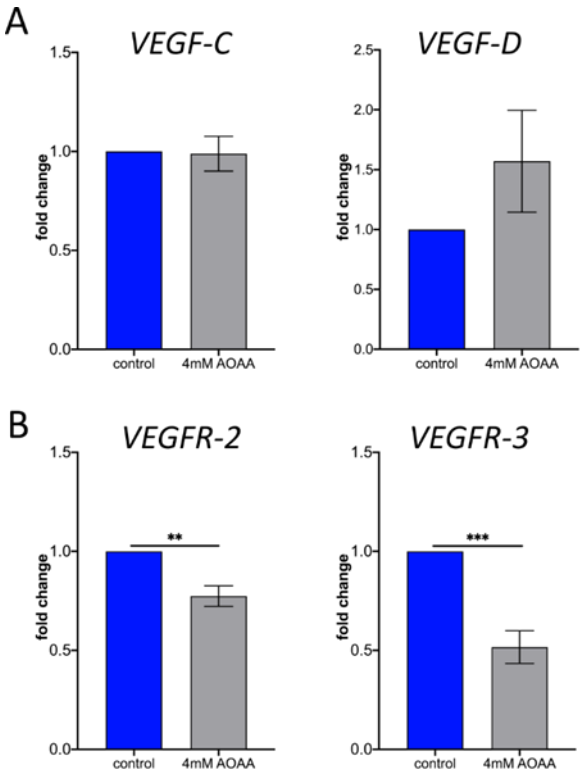

Figure 10. AOAA Treatment Reduces Expression of VEGFR2 and VEGFR3 in HDLECs without Major Effects on VEGF-C and VEGF-D. HDLECs were treated with indicated concentrations of AOAA for 24 hours. The mRNA levels for (A) VEGF-C and VEGF-D, and (B) VEGFR-2 and VEGFR-3 were assessed using real-time PCR. Statistical significance was analyzed with a two-tailed t-test (n=5). **p < 0.01; ***p < 0.001.

3.1.3. AOAA Treatment Do Not Induce Cellular Senescence in Human Dermal Lymphatic Endothelial Cells

To investigate the effects of AOAA treatment on cellular senescence in human dermal lymphatic endothelial cells (HDLECs), cells were exposed to varying concentrations of AOAA for 24 hours. Following treatment, immunofluorescence staining for the senescence marker $p16^{INK4A}$ was performed. The results revealed no significant changes in $p16^{INK4A}$ expression across the different AOAA concentrations (Figure 11a

& b), suggesting that AOAA treatment does not promote cellular senescence in these cells.

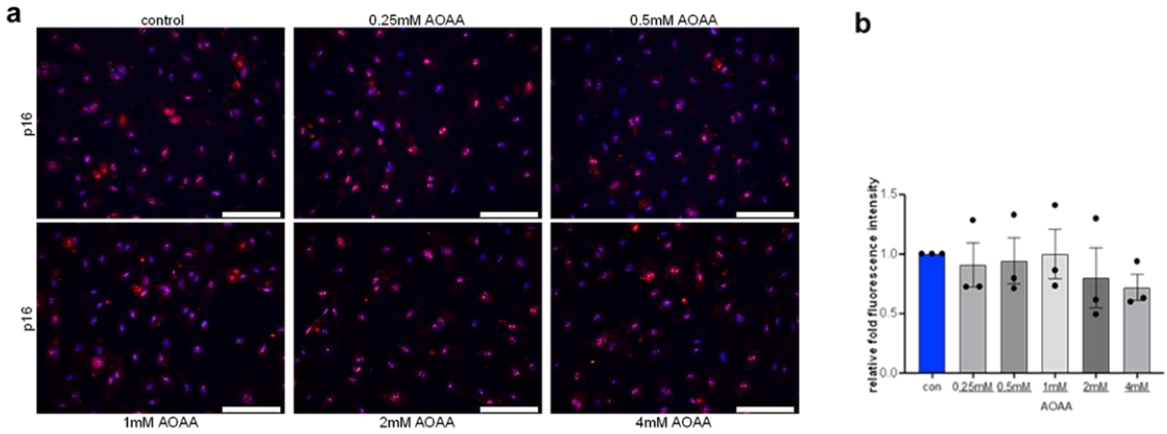

Figure 11. Effect of CBS inhibition by AOAA on p16^{INK4A} expression. (a) Representative immunofluorescence images of HDLECs treated with the indicated concentration of AOAA stained for p16^{INK4A}. Scale bars: 100 µm. (b) Quantification of immunofluorescence staining with the indicated concentration of AOAA stained for p16^{INK4A}. Data are presented as means ± SEM. Statistical significance was analysed with one-way ANOVA and Dunnett's multiple comparison test (n=3).

In summary, these findings indicate that treatment with the CBS pharmacological inhibitor AOAA affects the lymphangiogenic properties of lymphatic endothelial cells by reducing the expression of lymphangiogenic receptors VEGFR-2 and -3. This suggests a pro-lymphangiogenic role of CBS, at least *in vitro*, primarily through the regulation of VEGFR-2 and -3 expression on lymphatic endothelium.

3.1.4. Silencing of CBS decreases proliferation, migration, and tube formation in HDLECs

Gene silencing of CBS was performed to specifically investigate its role in lymphangiogenesis, as AOAA is a pharmacological inhibitor of both CBS and cystathionine-γ-lyase (CTH). This approach allowed us to confirm that the observed effects on HDLEC proliferation, migration, and tube formation were specifically attributable to CBS inhibition, thereby validating that the changes induced by AOAA are at least partially mediated through CBS downregulation in these cells. Therefore,

HDLECs were transfected with either siR_CBS-5, siR_CBS-6, or negative control (NC) siRNA. The efficiency of CBS knockdown in HDLECs was determined by qRT-PCR 72 hours post-transfection and confirmed by both RT-PCR and immunostaining (Figure 12A & 12B).

This approach allowed us to evaluate the influence of CBS silencing on the proliferation of HDLECs *in vitro*. The proliferation assay showed a significant decrease in proliferation in HDLECs transfected with either siR_CBS-5 or siR_CBS-6 after 24 hours compared with HDLECs transfected with NC siRNA (Figure 12C).

Apoptotic cells were assessed using Annexin V staining and flow cytometry to confirm that reduced CBS expression did not lead to increased apoptosis in HDLECs. FACS analysis further demonstrated that HDLECs transfected with siR_CBS-5 and siR_CBS-6 did not exhibit an increase in the number of Annexin V-positive cells compared with those transfected with NC siRNA. This observation suggests that the decrease in CBS levels achieved through targeted knockdown does not compromise cell viability, indicating that the regulatory effects of CBS on cellular processes are independent of apoptosis pathways (Figure 12D).

The influence of silencing CBS on the migration of HDLECs *in vitro* was subsequently assessed. The migration assay results demonstrated a significantly delayed wound closure in HDLECs transfected with either siR_CBS-5 or siR_CBS-6 compared with negative control (NC) siRNA-transfected HDLECs (Figure 12E), confirming that the delay in wound closure observed in HDLECs treated with AOAA is due to CBS inhibition.

Finally, the effect of CBS silencing on the tube formation of HDLECs *in vitro* was examined. The results showed that HDLECs transfected with either siR_CBS-5 or siR_CBS-6 exhibited a significantly increased number of loops, branching points, and branches compared to NC siRNA-transfected HDLECs after 4 hours. Additionally, CBS gene silencing with either siR_CBS-5 or siR_CBS-6 did not alter the length of the tubes compared to NC siRNA-transfected HDLECs at this time point. However, after 24 hours, the length of the tube in CBS-knockdown HDLECs (siR_CBS-5 or siR_CBS-6) was significantly shorter than in NC siRNA-transfected cells (Figure 12F).

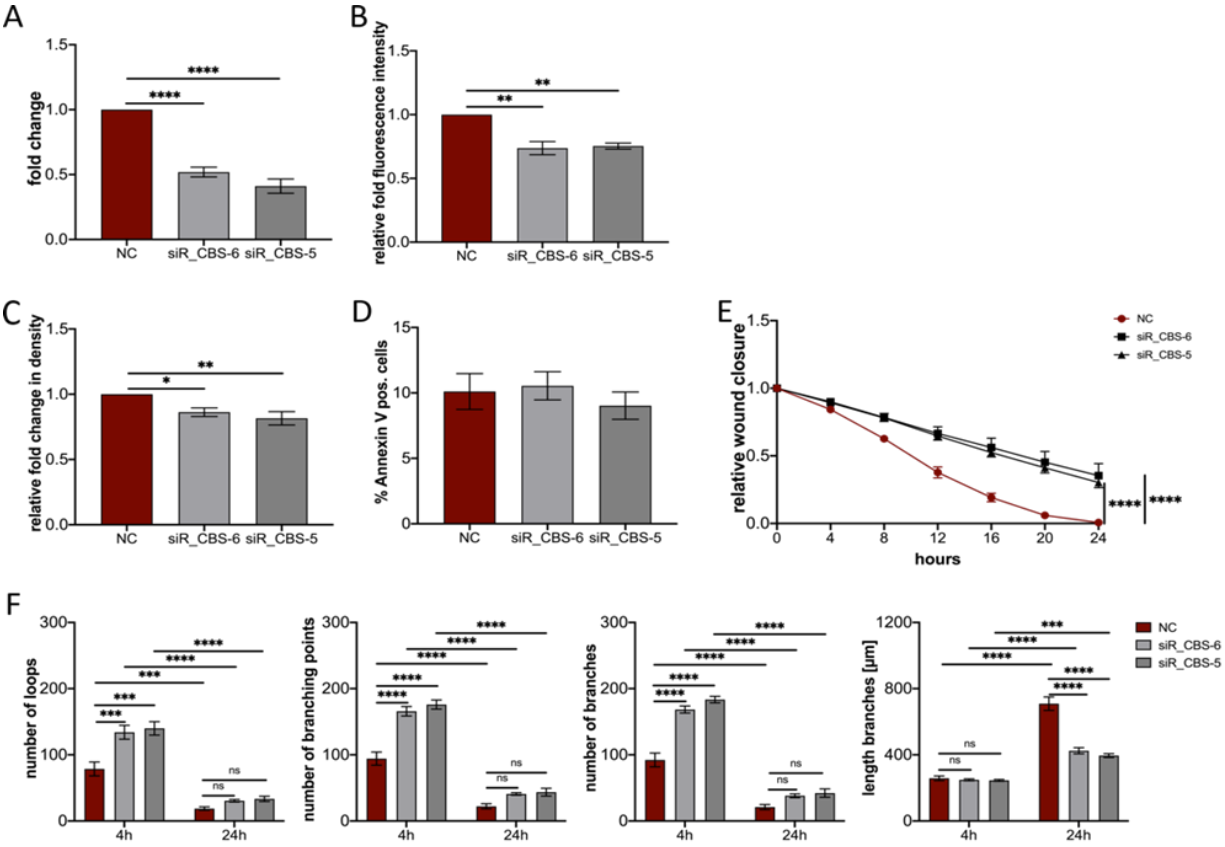

Figure 12. Silencing CBS Affects Proliferation, Migration, and Vessel Formation of HDLECs. (A) Efficiency of CBS knockdown determined by qRT-PCR 72 hours post-transfection. Reduced expression of CBS in HDLECs after 72 hours transfected with either siR_CBS-5, siR_CBS-6, or negative control (NC) siRNA (n=18). (B) Quantification of immunofluorescence staining of HDLECs transfected with either siR_CBS-5, siR_CBS-6, or negative control (NC) siRNA stained for CBS (n=3). (C) Effect of CBS silencing on HDLECs proliferation transfected with either siR_CBS-5 or siR_CBS-6 compared with NC siRNA-transfected cells. Proliferation was determined 72 hours after transfection using IncuCyte Zoom (n=5). (D) Quantification of flow cytometrically detected Annexin V-positive HDLECs 72 hours after transfection with either siR_CBS-5, siR_CBS-6, or negative control (NC) siRNA (n=5). (E) Wound healing assay with negative control (NC) siRNA, siR_CBS-5, or siR_CBS-6 siRNA-treated HDLECs after 72 hours of transfection (n=6). (F) Tube formation assay after 72 hours of transfection of HDLECs transfected with either negative control (NC) siRNA, siR_CBS-5, or siR_CBS-6 siRNA. Evaluation was performed after 4 hours and 24 hours (n=4). Statistical significance was analysed with one-way ANOVA and Dunnett's multiple comparison test or two-way ANOVA and Tukey's multiple comparison test. *p < 0.05; **p < 0.01; ***p < 0.001; ****p < 0.0001.

Over time, the number of loops, branching points, and branches significantly decreased. Conversely, at the 24-hour time point, the length of the branches increased compared with the 4-hour time point. These results demonstrate that siRNA-mediated CBS silencing in HDLECs recapitulated the effects of pharmacological inhibition by

AOAA on proliferation, migration, and tube formation. This confirms that the observed changes are directly attributable to reduced CBS activity in these cells.

3.1.5. Determination of the influence of silencing of CBS in HDLECs on the expression of VEGF-C, VEGF-D, VEGFR-2, and VEGFR-3 by Real-time PCR

The direct influence of CBS on the expression of the lymphangiogenic cytokines VEGF-C and VEGF-D and their receptors VEGF-R2 and VEGF-R3 was analysed using qRT-PCR. HDLECs were transfected with either siR_CBS-5, siR_CBS-6, or NC, and gene expression levels were assessed by qRT-PCR (Figure 13).

The qRT-PCR results showed that gene silencing of CBS with either siR-CBS-5 or siR-CBS-6 did not affect the expression of the lymphangiogenic cytokines VEGF-C and VEGF-D (Figure 13A). However, CBS knockdown in HDLECs led to a significant reduction in the expression of the lymphangiogenic receptors VEGFR-2 and VEGFR-3 (Figure 13B). The similarity between these results and those with 4mM AOAA treatment confirmed that the observed effects are attributable to CBS inhibition in HDLECs.

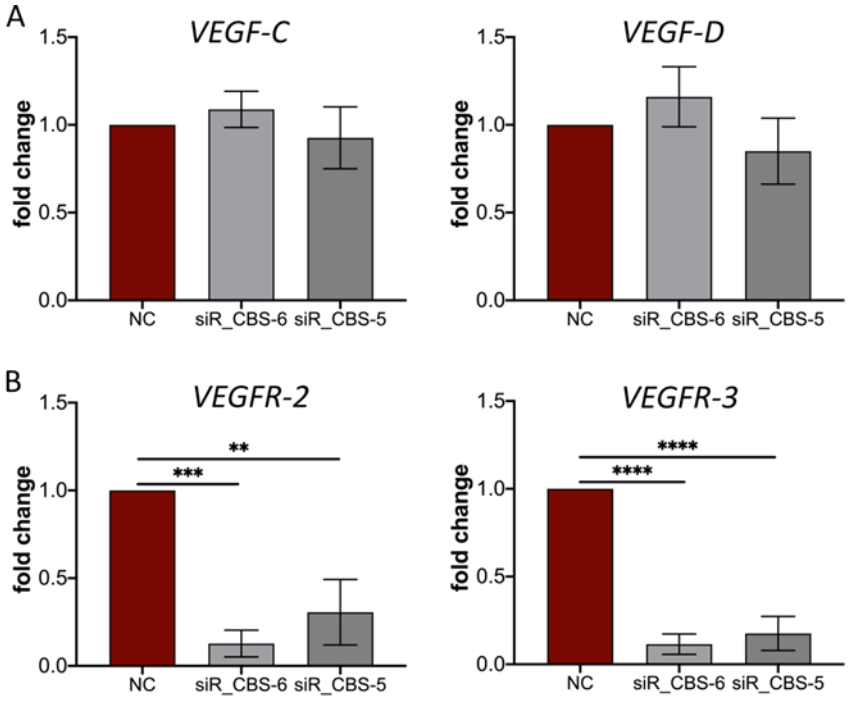

Figure 13. CBS Knockdown Reduces Expression of VEGF-R2 and VEGF-R3 on HDLECs without Affecting VEGF-C and VEGF-D Levels. Silencing of CBS in HDLEC with either siR-

CBS_5, siR-CBS_6, or negative control (NC). RNA was isolated 72 hours after transfection, and the level of mRNA for (A) VEGF-C and VEGF-D, (B) VEGFR-2, and VEGFR-3 was assessed using real-time PCR. Statistical significance was analysed with one-way ANOVA and Dunnett's multiple comparison test (n=5). **p < 0.01; ***p < 0.001; ****p < 0.0001.

3.1.6. CBS Gene Silencing Does Not Induce Cellular Senescence in Human Dermal Lymphatic Endothelial Cells

Next, HDLECs were transfected with siRNA targeting the CBS gene to explore the effects of CBS silencing on cell senescence. $p16^{INK4A}$ staining was performed on the transfected cells to assess potential impacts on senescence and apoptosis. The results showed a reduced intensity of $p16^{INK4A}$ staining in cells transfected with siR_CBS-5 or siR_CBS-6 compared to NC siRNA-transfected cells (Figure 14A & B). This reduction suggests that silencing the CBS gene does not induce senescence in HDLECs.

Collectively, these findings confirmed that neither AOAA treatment nor CBS gene silencing has a significant impact on inducing apoptosis or cellular senescence in HDLECs. Although there was a slight trend toward decreased $p16^{INK4A}$ expression with 4 mM AOAA treatment and a reduction in CBS expression following siRNA transfection, these changes did not culminate in senescence, highlighting the resilience of HDLECs to these interventions.

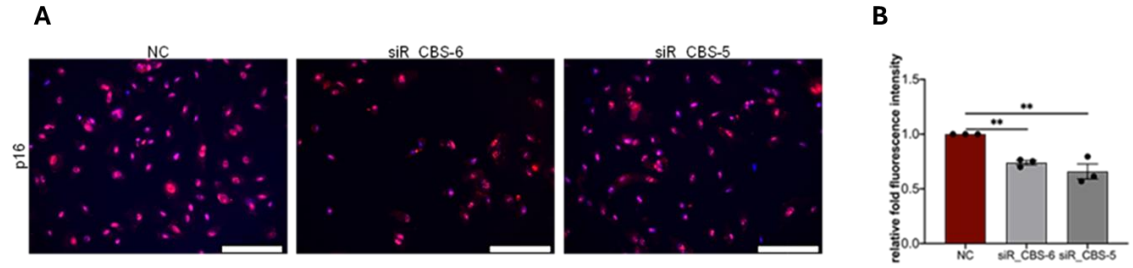

Figure 14. Effect of CBS gene silencing on $p16^{INK4A}$ expression. (A)Representative immunofluorescence images of HDLECs transfected with either siR_CBS-5, siR_CBS-6, or negative control (NC) siRNA stained for $p16^{INK4A}$. Scale bars: 100 µm. (B) Quantification of immunofluorescence staining of HDLECs transfected with either siR_CBS-5, siR_CBS-6, or negative control (NC) siRNA stained for $p16^{INK4A}$. Data are presented as means ± SEM. Statistical significance was analysed with one-way ANOVA and Dunnett's multiple comparison test (n=3). **p<0.01.

In summary, the results demonstrate that CBS influences proliferation, the formation of new tubes, migration, as well as the expression of the lymphangiogenic cytokine receptors VEGFR-2 and VEGFR-3 *in vitro*.

3.1.7. Impact of CTH and MPST Silencing on Lymphangiogenic Process in HDLECs

To determine the specific role of CTH in HDLEC lymphangiogenesis and clarify the effects of AOAA, specific siRNAs were used to silence CTH in HDLECs. This approach was essential to ascertain whether the inhibition of CTH could replicate the lymphangiogenic effects observed with AOAA treatment, which inhibits both CTH and CBS. By selectively silencing CTH, the experiments aimed to isolate its effects from those of CBS, thereby confirming that the impact of AOAA on HDLECs was primarily due to its inhibition of CBS. HDLECs were transfected with either siR_CTH-8, siR_CTH-7, or siR_CTH-6 and compared to the negative control (NC) siRNA 72 hours post-transfection. The downregulation of CTH expression in HDLECs, transfected with either siR_CTH-8, siR_CTH-7, or siR_CTH-6, was confirmed via qRT-PCR (Figure 15a). The results showed no significant changes in proliferation or wound closure compared with HDLECs transfected with negative control (NC) siRNA at 24 hours (Figure 15b &15c).

Additionally, 3-mercaptopyruvate sulfurtransferase (MPST) is another important enzyme involved in the production of hydrogen sulfide (H_2S), a gasotransmitter with various biological roles. Given H_2S's potential involvement in vascular biology, it is important to investigate the role of MPST in lymphangiogenic processes. To determine the influence of MPST on the proliferation and migration of HDLECs, HDLECs were transfected with either siR_MPST-7, siR_MPST-6, or siR_MPST-5 as well as siR_MPST-2, all specific siRNA targeting MPST. Transfection of HDLECs with different siRNAs for MPST resulted in a significant downregulation of MPST expression compared to HDLECs transfected with NC siRNA after 72 hours (Figure 15d). However, no significant difference in proliferation was observed in HDLECs transfected with any of the MPST-specific siRNAs (siR_MPST-2, -5, -6, or -7) compared to cells transfected with NC siRNA (Figure 15e).

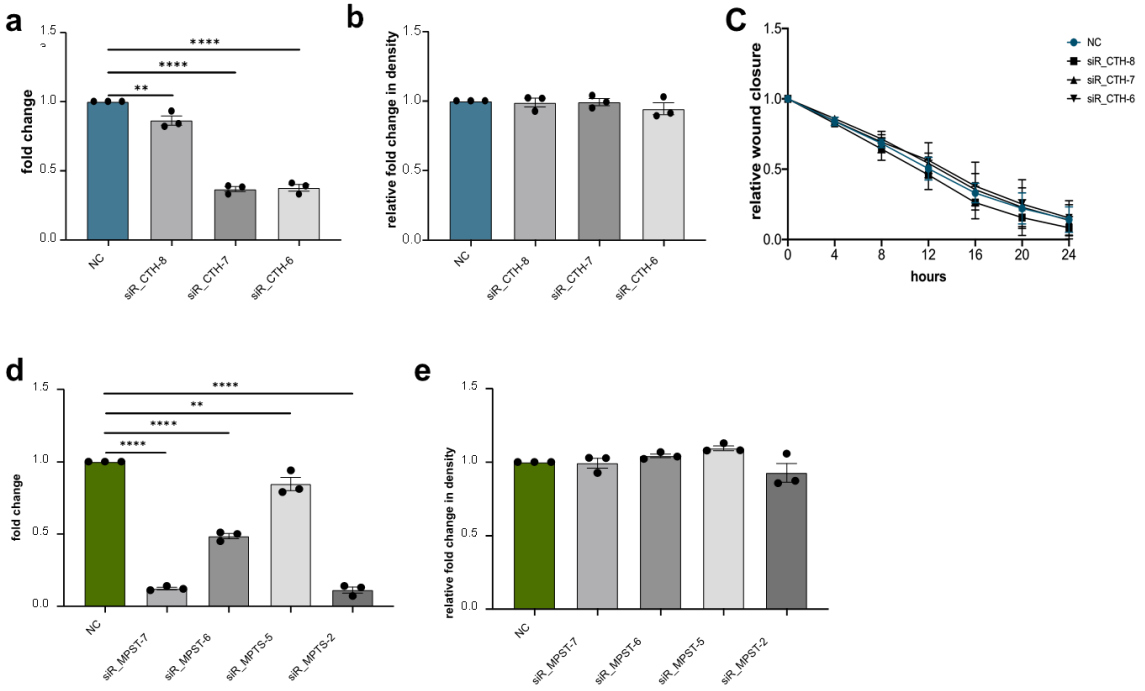

Figure 15. Silencing of CTH and MPST in HDLECS did not affect proliferation and migration. a) Efficiency of CTH knockdown determined by qRT-PCR 72h post-transfection. Reduced expression of CTH in HDLECs after 72h transfected with either siR_CTH-8, siR_CTH-7, siR_CTH-6, or negative control (NC) siRNA (n=3). (b) Effect of CTH silencing on HDLECs proliferation transfected with either siR_CTH-8, siR_CTH-7, or siR_CTH-6 compared with NC siRNA-transfected cells. Proliferation was 72h after transfection by using IncuCyte Zoom (n=3). (c) Wound healing assay with negative control (NC) siRNA, siR_CTH-8, siR_CTH-7, or siR_CTH-6 treated HDLECs after 72h transfection (n=3). (d) Efficiency of MPST knockdown determined by qRT-PCR 72h post-transfection. Reduced expression of MPST in HDLECs after 72h transfected with either siR_MPST7, siR_MPST-6, siR_MPST-5, siR_MPST-2 or negative control (NC) siRNA (n=3). (e) Effect of CTH silencing on HDLECs proliferation transfected with either siR_MPST-7, siR_MPST-6, siR_MPST-5, or siR_MPST-2 compared with NC siRNA-transfected cells. Proliferation was determined 72h after transfection by using IncuCyte Zoom (n=3). Data are presented as means ± SEM. Statistical significance was analysed with one-way ANOVA and Dunnett's multiple comparison test. **p<0.01; ****p < 0.0001.

3.1.8. Effects of AOAA Treatment Combined with Individual Gene Silencing of CBS, CTH, and MPST on HDLEC Proliferation

HDLECs were transfected with siRNA targeting CBS, CTH, or MPST to achieve gene knockdown. Following transfection, cells were treated with 1 mM and 4 mM AOAA for 24 hours. This experimental setup was specifically designed to determine whether the reduction in proliferation induced by AOAA was primarily due to the inhibition of CBS,

rather than MPST or CTH. Ensuring that observed changes in proliferation could be accurately attributed to the targeted silencing and subsequent AOAA treatment. HDLECs transfected with either siR_CBS-5 or siR_CBS-6 showed significant downregulation of proliferation after 24 hours compared to HDLECs transfected with NC siRNA (Figure 16a &16b). Furthermore, treatment of NC siRNA-transfected HDLECs with 1 mM and 4 mM AOAA led to significant downregulation of proliferation at 24 hours. Additionally, treatment of HDLECs transfected with either siR_CBS-5 or siR_CBS-6 with 1mM or 4mM AOAA did not further alter proliferation compared to NC control after 24 hrs (Figure 16b).

Similarly, gene silencing of CTH and MPST using either CTH (siR_CTH-8, siR_CTH_7, or siR_CTH-6) or MPST (siR_MPST-7, siR_MPST-6, or siR_MPST-5, or siR_MPST-2) resulted in effective downregulation of the respective genes compared to the corresponding NC negative control (Figure 16c & 16e). However, no difference in the proliferation was observed in HDLECs that were knocked down with either CTH (siR_CTH-8, siR_CTH-7, or siR_CTH-6) or MPST (siR_MPST-7, siR_MPST-6, or siR_MPST-5, or siR_MPST-2). Furthermore, treatment of HDLECs transfected with CTH (siR_CTH-8, siR_CTH-7, siR_CTH-6) or MPST (siR_MPST-7, siR_MPST-6, siR_MPST-5, siR_MPST-2) with 1 mM or 4 mM AOAA did not induce any statistically significant changes in proliferation compared to NC siRNA-transfected cells at 24 hr (Figure 16c-16f). Accordingly, these proliferation assay results indicate that AOAA affects HDLEC proliferation primarily through direct inhibition of CBS.

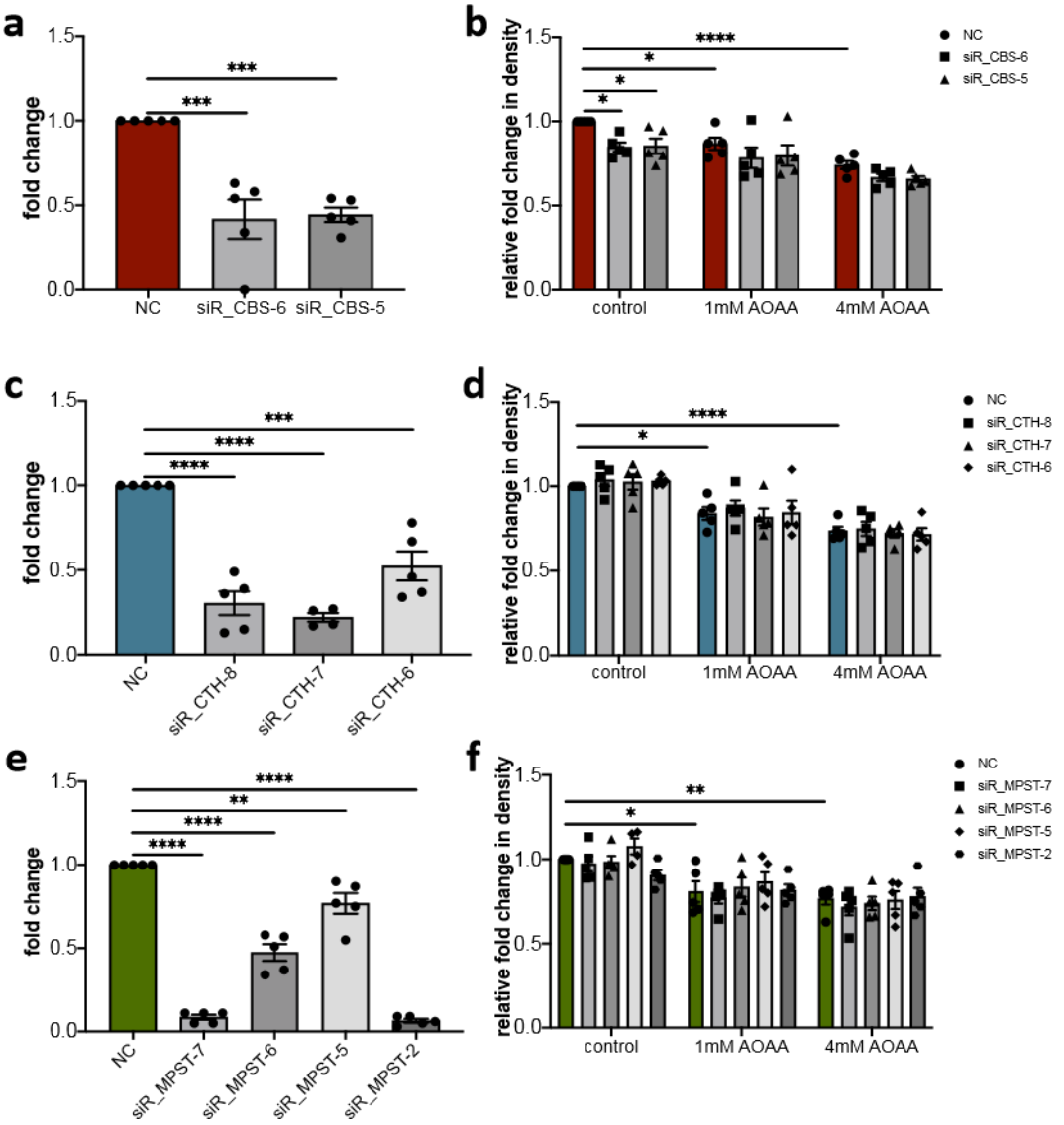

Figure 16. Additional treatment of HDLECs with AOAA after either silencing CBS, CTH, or MPST did not influence the proliferation of these cells. (a) Efficiency of CBS knockdown determined by qRT-PCR 72 hours post-transfection. Reduced expression of CBS in HDLECs after 72 hours transfected with either siR_CBS-5, siR_CBS-6, or negative control (NC) siRNA (n=5). (b) Effect of 1mM and 4mM AOAA on HDLECs proliferation transfected with either siR_CBS-5, siR_CBS-6, or negative control (NC) siRNA. Proliferation was determined 72 hours after transfection using IncuCyte Zoom (n=5). (c) Efficiency of CTH knockdown determined by qRT-PCR 72 hours post-transfection. Reduced expression of CTH in HDLECs after 72 hours transfected with either siR_CTH-8, siR_CTH-7, siR_CTH-6, or negative control (NC) siRNA (n=5).(d) Effect of 1mM and 4mM AOAA on HDLECs proliferation transfected with either siR_CTH-8, siR_CTH-7, or siR_CTH-6 compared with NC siRNA transfected cells. Proliferation was determined 72 hours after transfection using IncuCyte Zoom (n=5). (e) Efficiency of MPST knockdown determined by qRT-PCR 72 hours post-transfection. Reduced expression of MPST in HDLECs after 72 hours transfected with either siR_MPST-7, siR_MPST-6, siR_MPST-5, siR_MPST-2, or negative control (NC) siRNA (n=5).(f) Effect of 1mM and 4mM AOAA on HDLECs proliferation transfected with either siR_MPST-7, siR_MPST-6, siR_MPST-5, or siR_MPST-2 compared with NC siRNA transfected cells.

Proliferation was determined 72 hours after transfection using IncuCyte Zoom (n=5). Data are presented as means ± SEM. Statistical significance was analyzed with (a, c, e) one-way ANOVA and Tukey's multiple comparison test or (b, d, f) two-way ANOVA and Tukey's multiple comparison test. *p < 0.05 **p < 0.01; ***p < 0.001; ****p < 0.0001.

3.1.9. Determination of the influence of CBS on inflammatory lymphangiogenesis in C57BL/6N mice cornea

We previously observed significant differences in the limbal lymphatic vasculature of naive corneas between C57BL/6N and BALB/cN mice (Supplementary Figure 1)[45]. Given the *in vitro* findings demonstrating that gene silencing of CBS effects equivalent to pharmacological inhibition of CBS with AOAA in HDLECs, AOAA was used as an eye drop to investigate the role of CBS on inflammatory lymphangiogenesis *in vivo*. The suture-induced inflammatory corneal neovascularization model [61] was employed to analyse the outgrowth of lymphatic vessels into the normally avascular cornea. Mice corneas received eye drops containing 4mM AOAA or PBS immediately after sutures placement. Treatment was applied three times a day for 14 days (Figure 17A). To evaluate the influence of CBS on inflammatory lymphangiogenesis *in vivo*, whole corneas were prepared 14 days after treatment, and immunostaining for LYVE-1 was performed.

Subsequently, the total lymphatic vessel area in the cornea of 4mM AOAA and PBS-treated C57BL/6N mice was quantified (Figure 17B). The results demonstrate that corneas treated with 4mM AOAA exhibited a significantly lower lymphatic surface area compared to PBS-treated controls (Figure 17C). Additionally, analysis of corneas from AOAA-treated C57BL/6 mice shows a significantly reduced area covered with F4/80+ macrophages compared to PBS-treated corneas under inflammatory conditions (Figure 17D).

Together, these results indicate that inhibiting CBS in C57BL/6N mouse corneas suppresses inflammation-induced lymphangiogenesis *in vivo* after 14 days, suggesting that CBS contributes to lymphangiogenesis under inflammatory conditions *in vivo*.

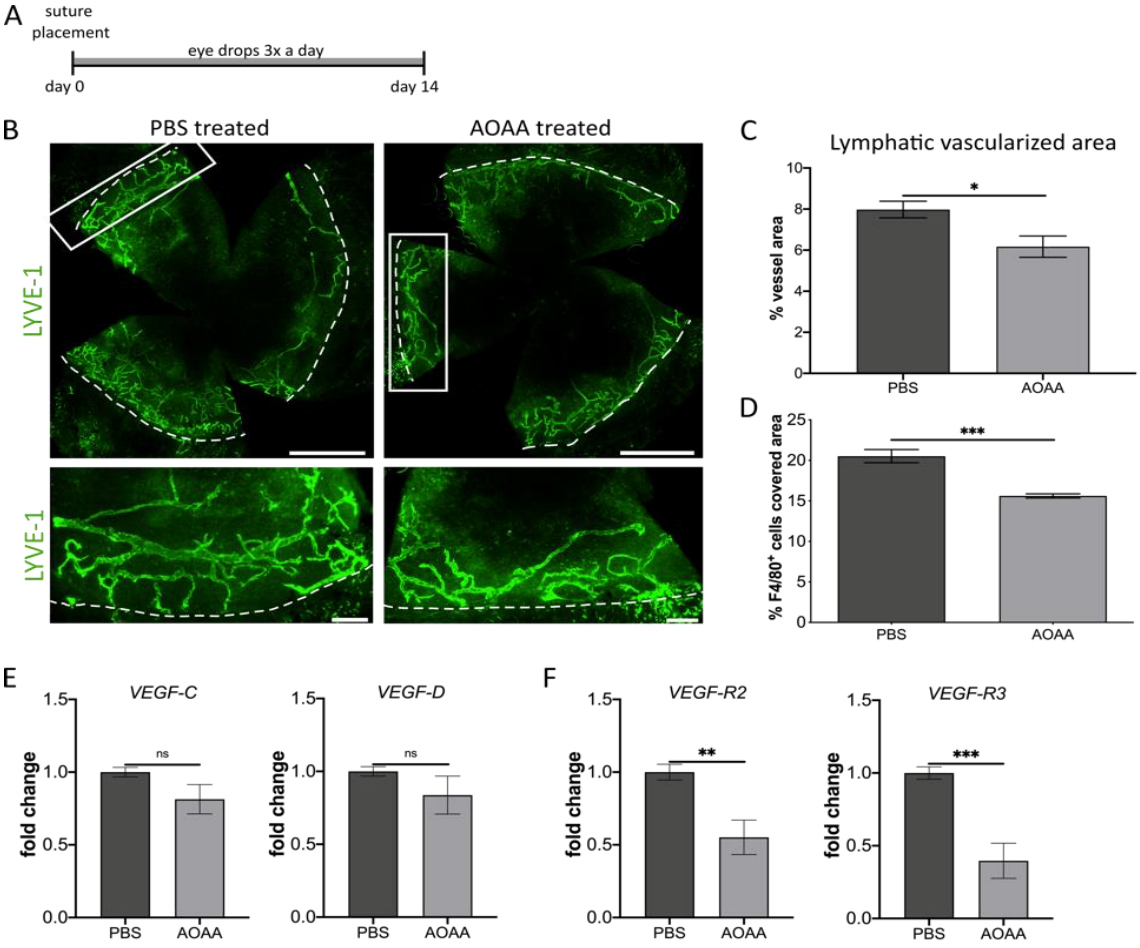

Figure 17. CBS Inhibition by AOAA Treatment Reduces Inflammation-Induced Lymphangiogenesis in C57BL/6N Mice. (A) Schematic representation of the suture-induced model of corneal neovascularization: Intrastromal sutures were placed into the cornea of the animals on day 0. Mice were then treated with AOAA (4mM) or PBS eyedrops three times a day for 2 weeks until the end of the experiment (day 14). (B) Representative corneal whole mounts showing inflammation-induced lymphangiogenesis of C57BL/6N mice stained for LYVE-1. The boxed areas in the top panels are shown at higher magnification in the bottom panels. Dashed lines indicate the border between the limbus and the cornea. Scale bars: 1 mm (top panel) and 200 µm (lower panel). (C) Quantification of the inflammatory lymphatic vascularized area of the whole mounts. Data are expressed as means ± SEM (n=6). (D) Quantification of the area covered with F4/80+ macrophages in the inflamed cornea. (E) Determination of mRNA levels of VEGF-C and VEGF-D. (F) Determination of mRNA levels of VEGF-R-2 and VEGF-R-3 in corneas of mice treated with AOAA (4mM) or PBS eyedrops for 14 days (n=8). A two-tailed t-test calculated statistical significance. *p<0.05; **p<0.01; ***p < 0.001.

3.1.10. Identification of the influence of inhibiting CBS on inflammatory lymphangiogenesis on lymphangiogenic factors via Real-time PCR

As observed in the *in vitro* studies, AOAA treatment of HDLECs led to the downregulation of VEGFR-2 and VEGFR-3 expression. To evaluate the effect of CBS inhibition *in vivo*, C57BL/6N mice were treated with 4 mM AOAA under inflammatory conditions for 14 days. Corneal inflammation was induced by sutures placement, followed by treatment with either 4 mM AOAA or PBS (control). Corneas were collected after 14 days, and RNA was isolated to examine the expression of Vegf-C, Vegf-D, and their receptors Vegfr-2 and Vegfr-3.

The expression of VEGF-C and VEGF-D showed no significant differences between AOAA-treated and PBS-treated corneas (Figure 14E). However, AOAA-treated corneas exhibited significantly decreased expression of VEGFR-2 and VEGFR-3 in the inflamed central cornea compared to PBS-treated corneas (Figure 14F). These findings indicate that AOAA treatment suppresses corneal inflammatory lymphangiogenesis, accompanied by a reduction in the expression of the lymphangiogenic receptors Vegfr-2 and Vegfr-3 (Figure 14F).

3.1.11. Determination of the Influence of CBS on Inflammatory Lymphangiogenesis in BALB/c Mice Cornea

The expression of Cbs in BALB/c mice is 35.7 times lower than in C57BL/6N mice. To investigate if AOAA could mitigate the effect of this lower Cbs expression in BALB/c mice, we utilized the established suture-induced inflammatory corneal neovascularization model [60]. Sutures were placed in the corneas of BALB/c mice, and the corneas were treated for fourteen days with either 4mM AOAA or PBS as a control. After fourteen days of treatment following the inflammatory insult, corneas were collected, and whole cornea staining was performed. The total surface area of the cornea of AOAA-treated BALB/c and PBS-treated BALB/c mice was analysed for vessels ingrown into the cornea (Figure 18A). Interestingly, although BALB/c mice exhibited a 35.7-fold lower Cbs expression in the cornea, AOAA-treated mice displayed a significantly reduced lymphatic vessel area following injury compared to PBS-treated

control BALB/c mice (Figure 18B). Furthermore, corneas treated with 4mM AOAA exhibited a markedly lower density of F4/80+ macrophages compared to the PBS-treated controls. This reduction suggests that AOAA treatment effectively diminishes macrophage infiltration, a key component of the corneal inflammatory response (Figure 18C).

These study outcomes indicate that CBS plays a fundamental role in inflammatory lymphangiogenesis, specifically in regulating VEGFR-2 and -3 expression in the cornea.

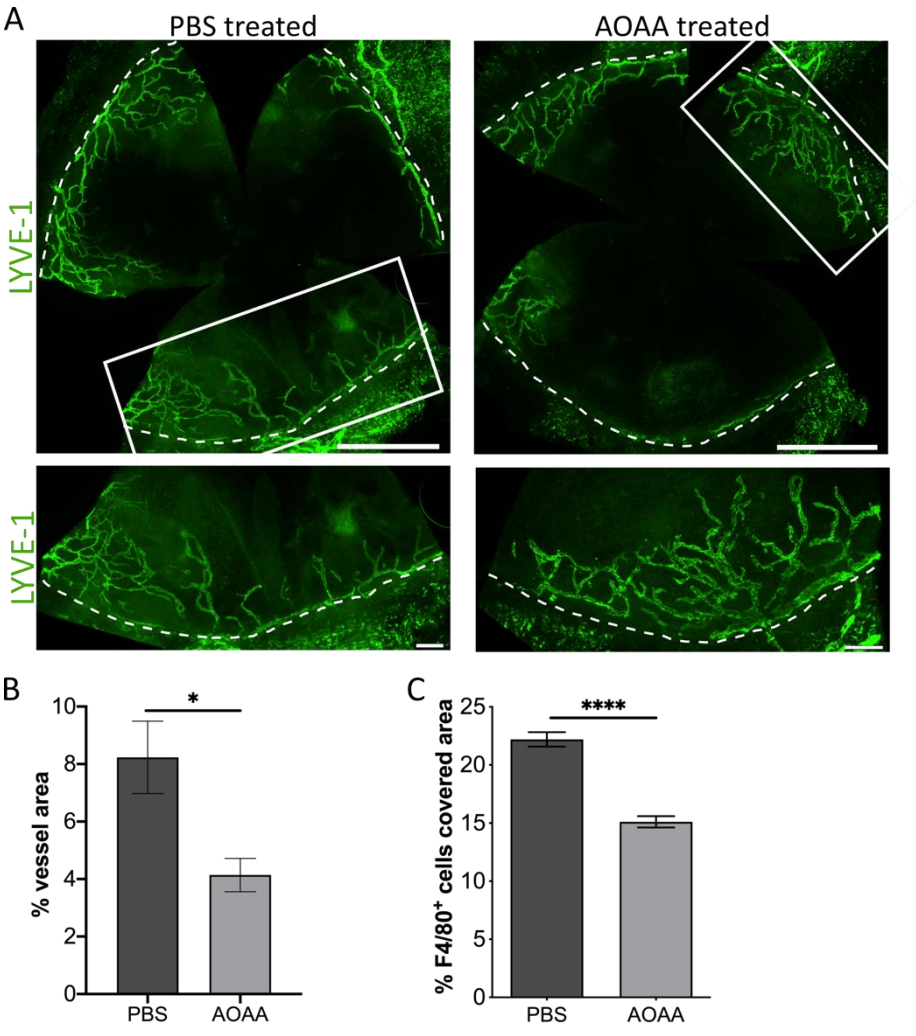

Figure 18. CBS Inhibition by AOAA Treatment Reduces Inflammation-Induced Lymphangiogenesis in BALB/cN Mice. (A) Representative corneal whole mounts showing inflammation-induced lymphangiogenesis of BALB/cN mice stained for LYVE-1. The boxed areas in the top panels are shown at higher magnification in the bottom panels. Dashed lines indicate the border between the limbus and the cornea. Scale bars: 1 mm (top panel) and 200 µm (lower panel). (B) Quantification of the inflammatory lymphatic vascularized area of the whole mounts. (C) Quantification of the area covered with F4/80+ macrophages in the inflamed

cornea. Data are expressed as means ± SEM (PBS n=7, AOAA n=6). Statistical significance was calculated by two-tailed t-test. *p<0.05.

3.2. Investigating the Influence of ANGPTL4 in Lymphangiogenesis ANGPTL4

The role of ANGPTL4 in lymphangiogenesis was functionally identified both *in vitro* and *in vivo*

The second potential candidate gene identified by QTL analysis and prioritization of QTL genes based on differential expression and public data is *ANGPTL4*. To investigate whether ANGPTL4 also has regulatory properties on lymphangiogenesis, initially, the complex process of lymphangiogenesis was studied to analyse the effect of ANGPTL4 *in vitro*. In these studies, the proliferation, migration, and tube formation of HDLECs were analysed by either treatment with recombinant human full-length ANGPTL4 or silencing ANGPTL4.

3.2.1. Determination of the Influence of ANGPTL4 on Proliferation, Migration and Formation of New Capillary Structures of HDLECs *in Vitro*

Proliferation is the initial step in studying lymphangiogenesis. To investigate the influence of ANGPTL4 on proliferation, HDLECs were treated with 1-1000 ng of recombinant human full-length ANGPTL4 for 24 hours. The results showed no difference between HDLECs treated with any concentrations of recombinant human full-length ANGPTL4 (1, 10, 100 &1000 ng/ml) compared to untreated HDLECs after 24 hours (Figure 19A).

To assess the effect of ANGPTL4 on lymphatic endothelial cell migration, a scratch wound assay was performed. HDLECs were treated with 1, 10, 100, and 1000 ng/ml of recombinant human full-length ANGPTL4 for 24 hours. The results indicated that treatment with 1000 ng/ml of recombinant human full-length ANGPTL4 significantly delayed wound closure compared to untreated HDLECs. In contrast, no significant differences were observed for HDLECs treated with 1,10 &100 ng/ml of recombinant human full-length ANGPTL4 compared to control HDLECs. These findings suggest

that a high dose of recombinant human full-length ANGPTL4 affects the migration of HDLECs (Figure 19B).

Subsequently, the next step in lymphangiogenesis was studied to determine if migrated cells could reorganize to form new capillary structures. HDLECs were treated with 1, 10, 100, and 1000 ng/ml of recombinant human full-length ANGPTL4, and their influence on the formation of new capillary structures was analysed. After 4 hours, HDLECs treated with recombinant human full-length ANGPTL4 (1, 10, 100, and 1000 ng/ml) exhibit significantly more loops, branching points, and branches compared to untreated control HDLECs. However, after 24 hours, no significant difference in the number of loops, branching points, and branches were observed between ANGPTL4-treated and control HDLECs (Figure 19C).

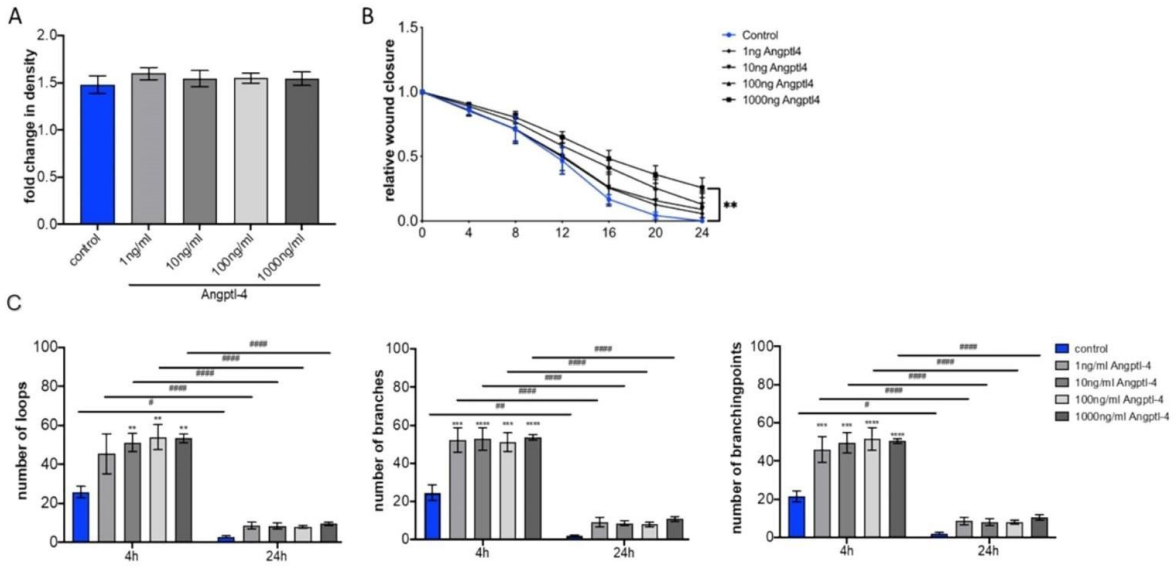

Figure 19. Identification of the Influence of ANGPTL4 on HDLECs' Formation of New Capillary Structures. (A)Effect of various concentrations of full-length ANGPTL4 on HDLEC proliferation after 24 hours (n=6). Proliferation was assessed using IncuCyte Zoom. (B) Migration assay results showing wound closure kinetics of HDLECs treated with different concentrations of ANGPTL4 compared to control cells (n=5). (C)Tube formation assay depicting the impact of ANGPTL4 treatment (1, 10, 100, & 1000 ng/ml) on HDLECs' ability to form capillary-like structures after 4 and 24 hours (n=4). Statistical significance was determined using one-way ANOVA and Dunnett's multiple comparison test or two-way ANOVA and Tukey's multiple comparison test or two-way ANOVA and Sidak's multiple comparisons test, where **p<0.01; $^{\#}$p<0.1; $^{\#\#}$p < 0.01; $^{\#\#\#\#}$p < 0.0001.

3.2.2. Real-time PCR was utilized to determine the influence of treating HDLECs with ANGPTL4 on VEGF-C, VEGF-D, VEGFR-2, and VEGFR-3 expression levels

To study the effects of full-length ANGPTL4 on the expression of cytokines VEGF-C and VEGF-D, as well as their receptors VEGFR-2 and VEGFR-3, HDLECs were treated with four different concentrations of full-length ANGPTL4 (1, 10, 100, and 1000 ng/ml). After 24 hours, RNA was isolated from both recombinant human full-length ANGPTL4-treated and untreated HDLECs. The qRT-PCR analysis revealed no significant differences in the expression of VEGF-C and VEGF-D, or their receptors VEGFR-2 and VEGFR-3, in HDLECs treated with any concentrations of recombinant human full-length ANGPTL4 compared to untreated controls after 24 hours (Figure 20). These results indicated that ANGPTL4 treatment does not significantly affect the expression of these vascular growth factors in HDLECs.

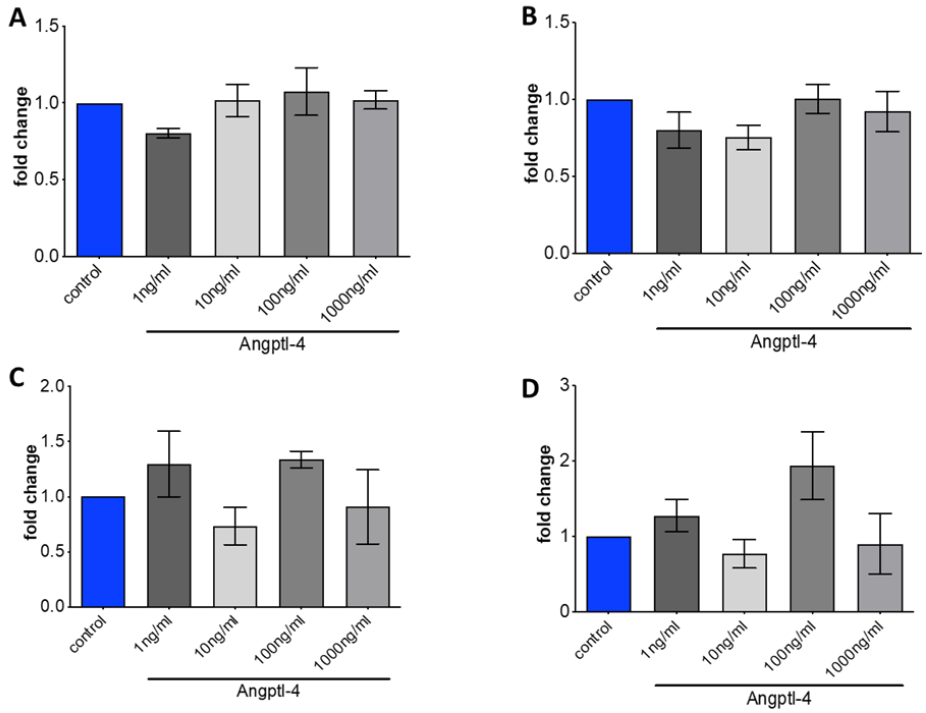

Figure 20. ANGPTL4-treated HDLECs show no significant effect on the expression of vascular growth factor. (A)The expression of VEGF-C in HDLECs treated with Angptl4 (gray bars) compared to the control group (blue bar) shows no significant difference. (B) The expression of VEGF-D in HDLECs treated with Angptl4 (gray bars) is like the control group (blue bar). (C) The expression level of VEGFR-2 shows no significant change in Angptl4-treated HDLECs (gray bars) compared to the control group (blue bar). The overlapping error bars indicate that any differences observed are not statistically significant. (D) The expression level of VEGFR-3 shows no significant change in Angptl4-treated HDLECs (gray bars)

compared to the control group (blue bar). RNA was assessed using real-time PCR. Statistical significance was analysed using one-way ANOVA and Dunnett's multiple comparison test (n=6).

3.2.3. Impact of ANGPTL4 Silencing on Proliferation, Migration, and Tube Formation in Human Dermal Lymphatic Endothelial Cells: *In Vitro* Analysis

The results demonstrated that treating HDLECs with different concentrations of ANGPTL4 allowed us to explore its effects on various stages of lymphangiogenesis. These findings prompted further investigation into the role of ANGPTL4 using a knockdown model using siRNA to better understand its specific contributions. Two specific siRNAs were employed to silence ANGPTL4 in HDLECs. The results showed a significant decrease in the expression of ANGPTL4 in HDLECs transfected with either siR_ANGPTL4-6 or siR_ANGPTL4-5 compared to the negative control (NC) siRNA 72 hours post-transfection (Figure 21A).

The influence of silencing ANGPTL4 on the proliferation and migration of HDLECs was then evaluated. HDLECs transfected with either siR_ANGPTL4-6 or siR_ANGPTL4-5 exhibited significantly increased proliferation after 24 hours compared to HDLECs transfected with NC siRNA (Figure 21B). Furthermore, the migration assay revealed that HDLECs transfected with either siR_ANGPTL4-6 or siR_ANGPTL4-5 demonstrated significantly faster wound closure compared to HDLECs transfected with NC siRNA after 24 hours (Figure 21C).

To further investigate the role of ANGPTL4 in lymphatic endothelial tube formation, a tube formation assay was conducted to compare the effects of ANGPTL4 gene silencing with those observed following ANGPTL4 treatment. Gene silencing of ANGPTL4 in HDLECs using siR_ANGPTL4-6 or siR_ANGPTL4-5 resulted in a significant decrease in the number of loops, branching points, and branches after 4 hours compared to NC siRNA-transfected HDLECs (Figure 21D). This reduction mirrors the effects observed in HDLECs treated with ANGPTL4, suggesting that both approaches have a similar impact on lymphangiogenic tube formation. However, after 24 hours, the number of loops, branching points, and branches in HDLECs transfected with siR_ANGPTL4-6 or siR_ANGPTL4-5 was comparable to that of NC siRNA-transfected cells, suggesting a transient effect of gene silencing. These findings

highlight the importance of ANGPTL4 in regulating tube formation in lymphatic endothelial cells, suggesting that gene silencing and direct ANGPTL4 treatment exert similar early-stage effects.

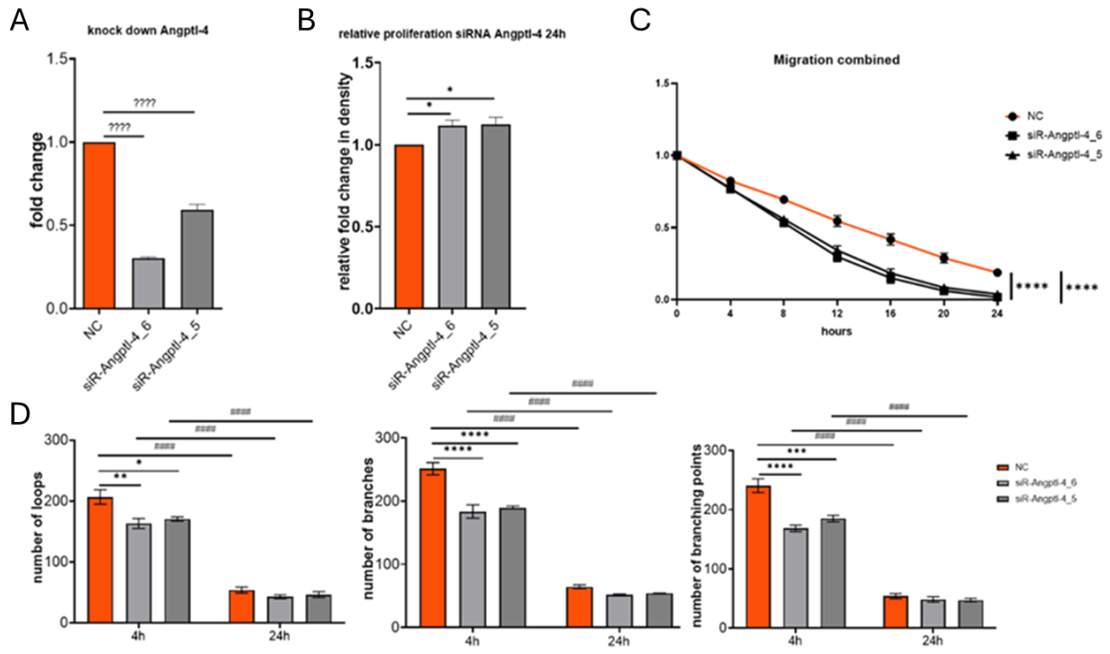

Figure 21. Silencing of Angptl4 Increases Proliferation, Migration, and Decreases Tube Formation *In Vitro* Using Two Different siRNAs, siR-Angptl4_6 & siR-Angptl4_5. (A) Efficiency of Angptl4 knockdown determined by qRT-PCR 72 hours post-transfection. Reduced expression of Angptl4 in HDLECs after 72 hours of transfection with either siR_ANGPTL4-6, siR_ANGPTL4-5, or negative control (NC) siRNA (n=6). (B) Effect of silencing Angptl4 using siR Angptl4_6 & siR Angptl4_5 on HDLEC proliferation after 24 hours (n=4). Proliferation was assessed using IncuCyte Zoom. (C) Migration assay results showing the impact of Angptl4 silencing on HDLEC migration kinetics compared to control cells (n=6). (D) Tube formation assay depicting the effects of Angptl4 silencing using siR Angptl4_6, siR Angptl4_5 on HDLECs' ability to form capillary-like structures(n=4). Statistical significance was determined using one-way ANOVA and Dunnett's multiple comparison test, or two-way ANOVA and Tukey's multiple comparison test, or two-way ANOVA and Sidak's multiple comparisons test, where **p<0.01; ***p < 0.001; ****p < 0.0001; ####p < 0.0001.

3.2.4. Investigating the influence of ANGPTL4 silencing on the expression of VEGF-C, VEGF-D, VEGFR-2, and VEGFR-3 in HDLECs

The effect of ANGPTL4 silencing in HDLECs using either siR_ANGPTL4-6 or siR_ANGPTL4-5 on the expression of cytokines VEGF-C and VEGF-D, as well as their receptors VEGFR-2 and VEGFR-3, was analysed by qRT-PCR. HDLECs were harvested 72 hours post-transfection, and RNA was isolated for qRT-PCR analysis,

comparing results with HDLECs transfected with NC siRNA. The qRT-PCR results revealed a significant downregulation in the expression of VEGF-C and VEGF-D in HDLECs transfected with either siR-ANGPTL4-6 or siR-ANGPTL4-5 compared to the negative control after 72 hours (Figure 22A). In contrast, there were no significant differences in the expression of VEGFR-2 and VEGFR-3 between HDLECs transfected with either siR_ANGPTL4-6 or siR_ANGPTL4-5 compared to HDLECs transfected with NC siRNA after 72 hours (Figure 22B).

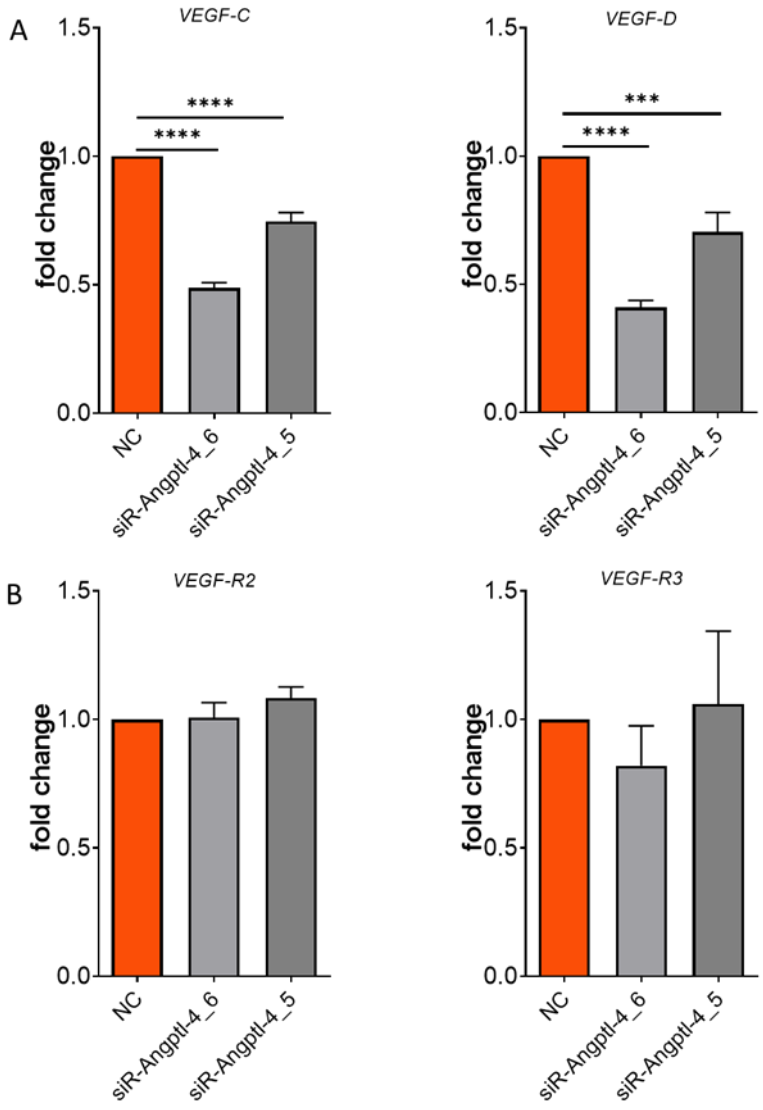

Figure 22. ANGPTL4 Knockdown Reduces Expression of VEGF-C and VEGF-D in HDLECs. Down-regulation of Angptl4 in HDLECs with either siR-ANGPTL4_6, siR-ANGPTL4_5, or negative control (NC). RNA was isolated 72 hours after transfection, and the level of mRNA for (A) VEGF-C and VEGF-D, and (B) VEGFR-2 and VEGFR-3. RNA was assessed using real-time PCR. Statistical significance was analysed using one-way ANOVA and Dunnett's multiple comparison test (n=6). ***p < 0.001; ****p < 0.0001.

In summary, these findings indicate that ANGPTL4 influences lymphangiogenesis *in vitro* by modulating HDLEC proliferation, tube formation, migration, and the expression of lymphangiogenic cytokine receptors VEGF-C and VEGF-D.

3.2.5. Angiopoietin-like4 knock out (Angptl4−/−) mice have more lymphatic surface area compared to naïve WT mice

To determine the influence of ANGPTL4 on lymphangiogenesis *in vivo*, the limbal lymphatic vasculature of naïve cornea from Angptl4−/− mice and WT littermates was analysed. Therefore, whole mounts were prepared and stained for the lymphatic marker LYVE-1. The Angptl4−/− mice showed a significantly larger lymphatic vascularized area compared with their wild-type littermates (Figure 23A). However, further morphometric analysis revealed no differences in the numbers of endpoints, branching points, or sprouts between Angptl4 -/- and WT mice (Figure 24B, C, and D). These findings indicate that Angptl4 is involved in developmental lymphangiogenesis in the cornea *in vivo.*

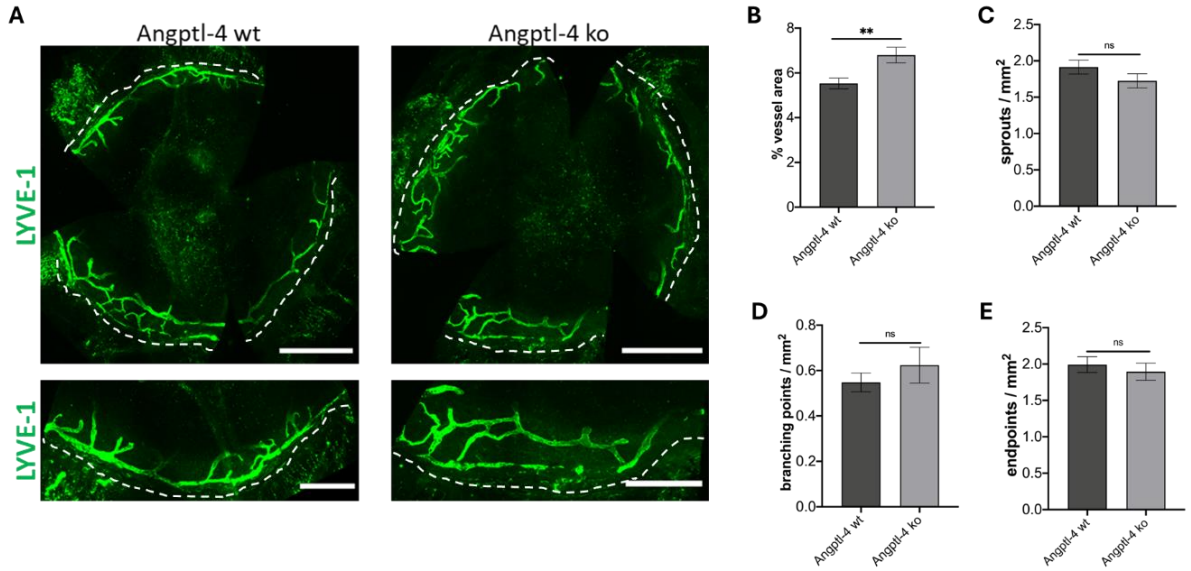

Figure 23. Angptl4 knockout reduces lymphangiogenesis in vivo. (A) Representative corneal whole mounts showing naïve Angptl4−/− mice were compared to naïve WT mice by analysing corneal whole-mount staining with LYVE-1. Dashed lines indicate the border between the limbus and the cornea. (B) Quantification of lymphatic vessel area of the whole mounts. (C) Quantification of the number of sprouts per square mm² in the whole mounts. (D) Quantification of the lymphatic vascularized area of the whole mounts. (E) Quantification of the number of Endpoints per square mm^2 in the whole mounts. Data are expressed as means ±

SEM (WT mice n=12, Angptl4−/− mice n=10). Statistical significance was calculated by a two-tailed t-test, **p<0.01.

Additionally, the corneas were stained for the macrophage marker F4/80+ (Figure 24A) and endothelial cell marker CD31 (Figure 24C). Analysis of naïve Angptl4−/− mice showed a greater area covered with F4/80+ macrophages (Figure 24B) and significantly larger blood surface area compared to naïve WT corneas (Figure 24D). These findings suggest that Angptl4 is involved in the developmental regulation of both lymphatic and blood vasculature in the cornea.

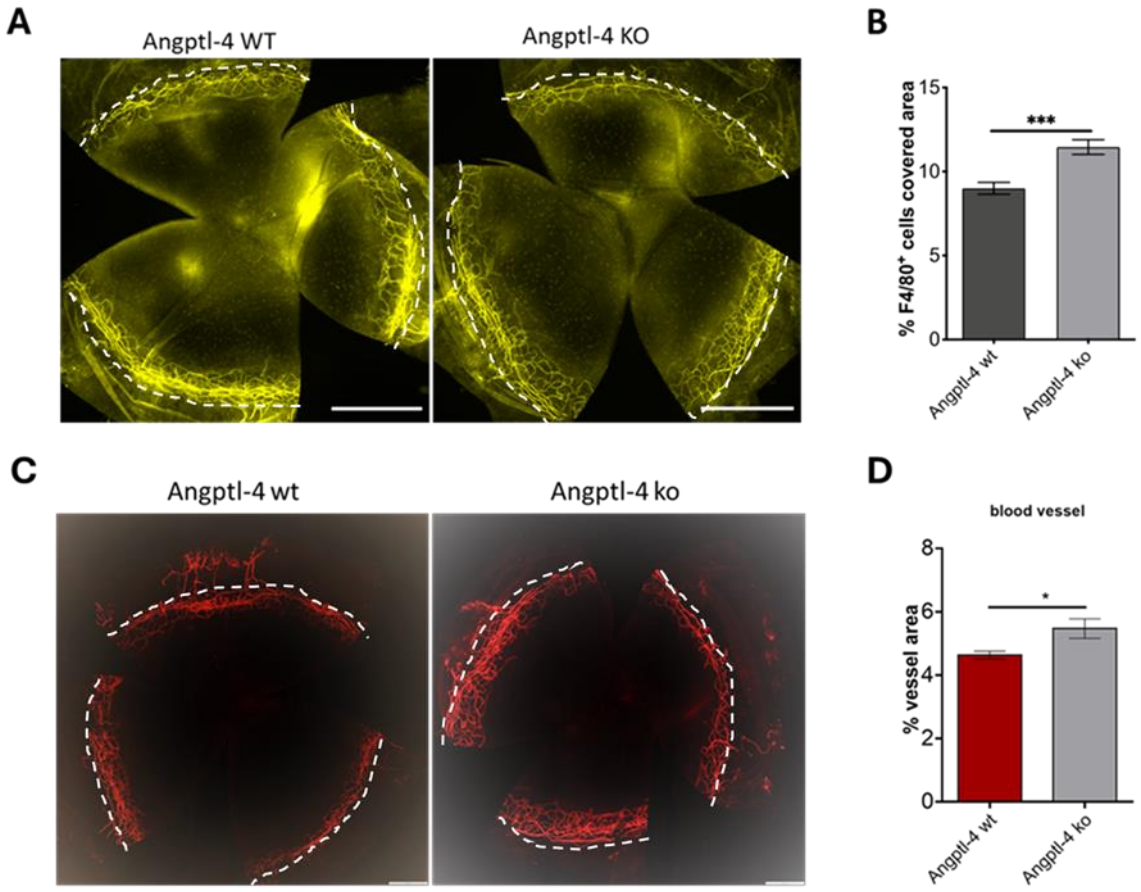

Figure 24. Whole amount staining of Corneas of naïve Angptl4−/− Mice vs. Wild-Type Mice. Dashed lines indicate the border between the limbus and the cornea. Scale bars: 1 mm. (A) Representative corneal whole mounts stained for F4/80+ Cells. (B) This graph shows the number of F4/80+ cells (macrophages) in the corneas of wild-type (WT) mice (depicted by the dark grey bar) compared to Angptl4 knockout (KO) mice. (C)Representative corneal whole mounts stained for CD31. (D) This graph displays the blood vessel area in the corneas of WT mice (indicated by the red bar) versus Angptl4 KO mice (shown by the grey bar). Data are

expressed as means ± SEM (WT Mice n=12, Angptl4-KO Mice n=10). Statistical significance was calculated by two-tailed t-test <0.05 ***p<0.001.

3.2.6. The impact of Angptl4 knockout on the expression of Vegf-A, Vegf-C, Vegf-D, Vegfr-2, and Vegfr-3 was determined using real-time PCR.

To investigate the influence of Angptl4 on the expression of lymphangiogenic cytokines, RNA was isolated from the central cornea, and the expression of Vegf-A, Vegf-C, Vegf-D, and their receptors Vegfr-2 and Vegfr-3 was analysed using qRT-PCR. The results showed that the expression of Vegf-A and Vegf-C was significantly lower in the corneas of naïve Angptl4−/− mice compared to WT mice (Figure 25A & B). In contrast, the expression levels of Vegf-D, Vegfr-2, and Vegfr-3 were not significantly different between naïve Angptl4−/− and WT corneas (Figure 25C, D & E).

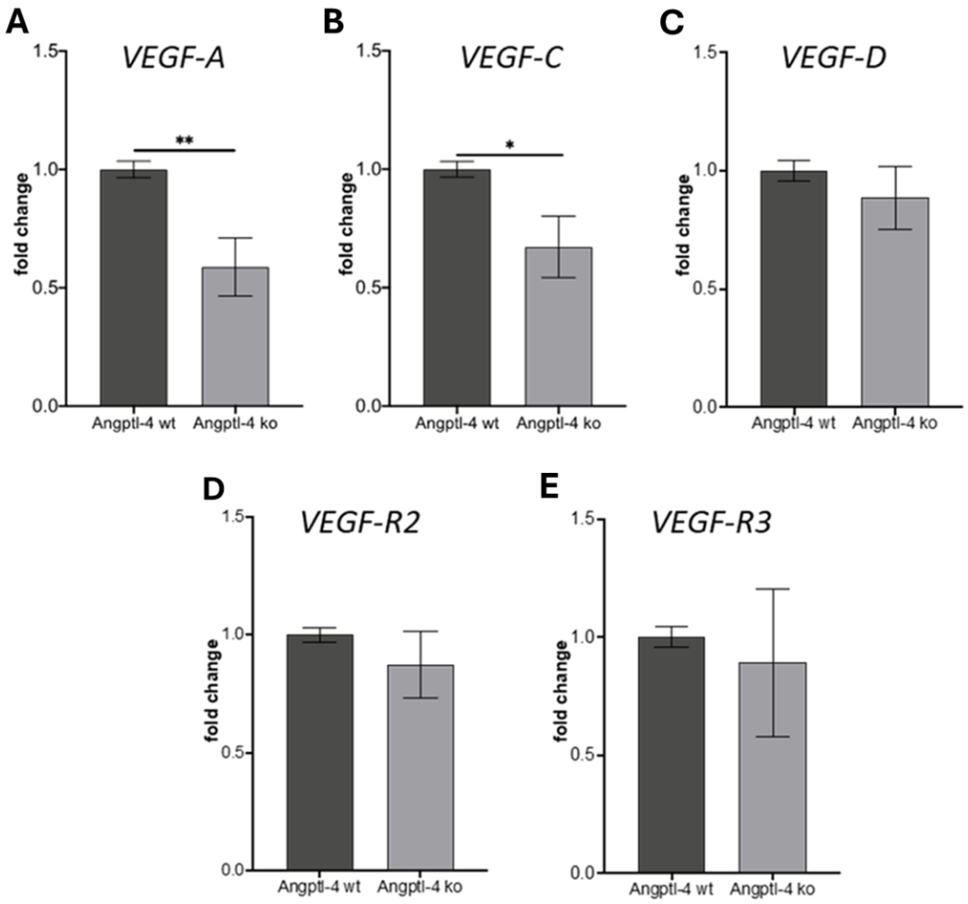

Figure 25. Angptl4 knockout mice show significantly reduced expression of lymphangiogenic receptors Vegf-A and Vegf-C. Determination of mRNA levels of (A) VEGF-A, (B) VEGF-C, (C) VEGF-D, (D) VEGFR-2, and (E) VEGFR-3 in corneas of naïve Angptl4−/− mice compared to naïve WT controls (WT mice n=12, Angptl4−/− mice n=10). Statistical significance was calculated by a two-tailed t-test *p<0.05; **p<0.01.

3.2.7. Treatment of C57BL/6 mice with recombinant Angptl4 leads to reduced inflammation-induced lymphangiogenesis

To assess the impact of Angptl4 on inflammation-induced lymphangiogenesis in C57BL/6N mice corneas, recombinant murine full-length Angptl4 was administered as eye drops. Lymphatic vessel ingrowth into the normally avascular cornea was induced using the suture-induced inflammatory corneal neovascularization model [60], and then the animals were treated with either recombinant murine full-length Angptl4 or PBS as eye drops for 14 days (Figure 26A). Subsequently, all corneas were analysed to evaluate the influence of Angptl4 on inflammatory lymphangiogenesis *in vivo*. Corneas from both Angptl4- and PBS-treated mice were stained for LYVE-1, CD31, and F4/80+ macrophages for comparison.

The total surface area of the corneal ingrown vessel was quantified in Angptl4- and PBS-treated C57BL/6N mice. The results demonstrated that treatment with Angptl4 significantly reduced the lymphatic vascularized area compared to PBS-treated corneas (Figure 26B & C). Additionally, corneas treated with recombinant murine full-length Angptl4 showed a significantly lower blood area under inflammatory conditions compared to PBS-treated controls (Figure 26D). Similarly, Angptl4-treated corneas showed a significantly lower area covered with F4/80+ macrophages compared to PBS-treated corneas (Figure 26E).

Therefore, the results indicate that treatment with Angptl4 effectively reduced inflammation-induced lymphangiogenesis in C57BL/6 mouse corneas *in vivo* over 14 days.

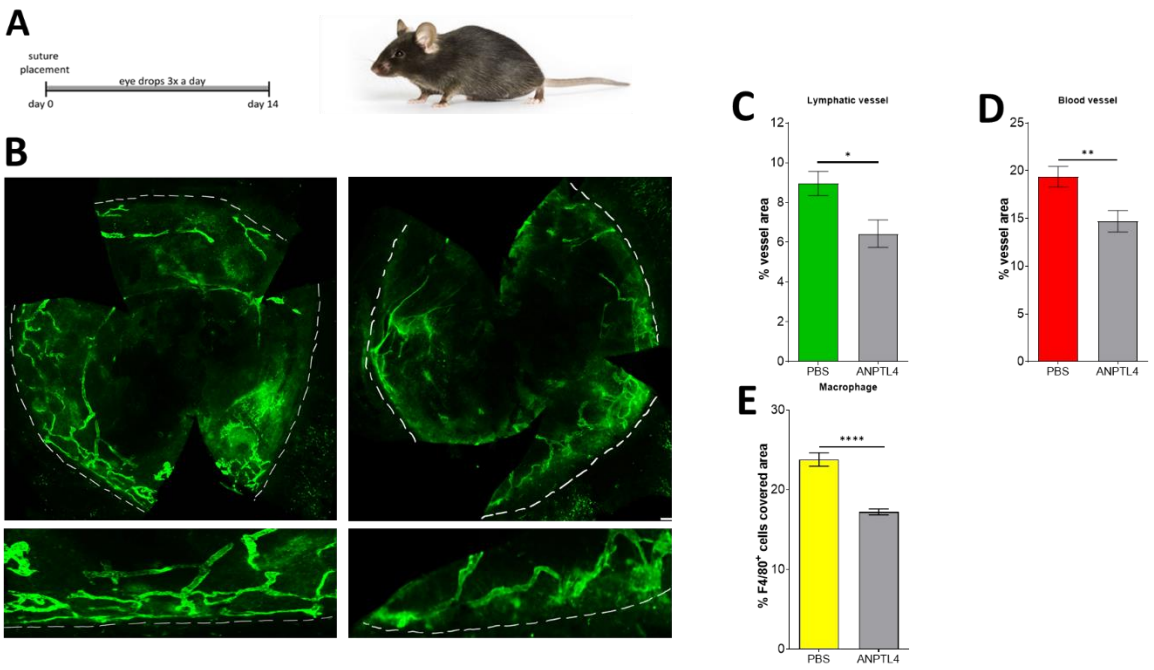

Figure 26. Angplt4 Treatment Reduces Inflammation-Induced Lymphangiogenesis in C57BL/6N Mice. (A) Schematic representation of the suture-induced model of corneal neovascularization: Intrastromal sutures were placed into the cornea of the animals on day 0. Mice were then treated with Angptl4 or PBS eyedrops three times a day for 2 weeks until the end of the experiment (day 14). (B) Representative corneal whole mounts showing inflammation-induced lymphangiogenesis of C57BL/6N mice stained for LYVE-1. (C) Quantification of the inflammatory lymphatic vascularized area of the whole mounts. (D) Quantification of the inflammatory vessel area in mm² of the mouse cornea. (E) Quantification of the area covered with F4/80+ macrophages in the inflamed cornea. Data are expressed as means ± SEM (PBS n=8, Angptl4 n=8). Statistical significance was calculated by a two-tailed t-test *p<0.05, **p<0.01, ****p<0.0001.

3.3. Determination of Limbal Lymphatic Vasculature Variation Among Collaborative Cross Mice

3.3.1. The limbal lymphatic vasculature in naïve corneas varied among different Collaborative Cross mice

In this study, the limbal lymphatic vasculature in naïve corneas was examined across 9 different Collaborative Cross (CC) line strains using immunofluorescence staining with lymphatic vessel endothelial hyaluronan receptor 1 (LYVE-1) (Figure 27). The limbal lymphatic surface area, representing the corneal area covered by circular limbal lymphatic vessels and their extension into the cornea, was quantified through analysis of immunofluorescence images.

Immunofluorescence staining revealed significant differences in developmental lymphangiogenesis among CC lines. Specifically, CC-lines PAT_CD, BOON_HF, LOT_EC, and ROGAN_CF exhibited minimal lymphatic vessels in the limbus region, whereas CC-lines LUF_AD, FIV_AC, CIS_AD, LAT_AD, and NUK_AC displayed prominent circular lymphatic vessels extending into the cornea (Figure 27).

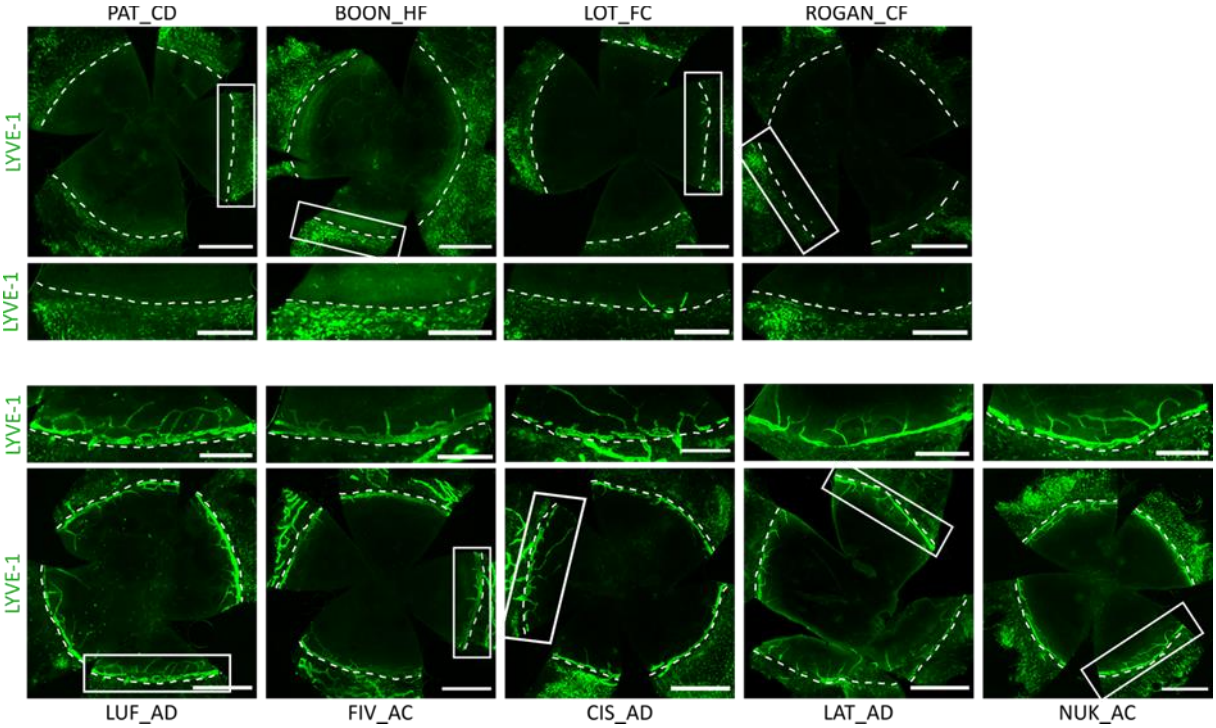

Figure 27. Immunofluorescence Staining of Resting Limbal Lymphatic Vasculature in Untreated Corneas of Several Collaborative Cross (CC) Mouse Strains: Significant Differences in Developmental Lymphangiogenesis among CC Mice. Representative corneal whole mounts of naïve corneas from PAT_CD, BOON_HF, LOT_FC, ROGAN_CF, LUF_AD, FIV_AC, CIS_AD, LAT_AD, and NUK_AC were stained for LYVE-1. The top panels display the entire corneas, while the boxed areas are magnified in the bottom panels. Dashed lines delineate the border between the limbus and the cornea.

The mean resting limbal vascular area for each strain is summarized in Table 8. No significant difference was found among the CC-lines PAT_CD, BOON_HF, LOT_EC, and ROGAN_CF. However, these four lines exhibited highly significant differences ($p < 0.001$) when compared to the other five CC strains: LUF_AD, FIV_AC, CIS_AD, LAT_AD, and NUK_AC. LUF_AD exhibited the largest limbal vascular area and showed significant differences compared to FIV_AC ($p < 0.05$) and highly significant differences from CIS_AD, LAT_AD, and NUK_AC ($p < 0.0001$; Figure 24A).

In comparison, the “high-lymphangiogenic” C57BL/6 mouse exhibited a limbal lymphangiogenic vascular area of 3.45% ± 0.39 (Figure 28A, dashed line). This indicates that the C57BL/6 mouse has an intermediate lymphatic vessel area compared to the CC lines LUF_AD, FIV_AC, CIS_AD, LAT_AD, and NUK_AC, which show significantly larger lymphatic vessel areas, and CC lines PAT_CD, BOON_HF, LOT_EC, and ROGAN_CF, which display little to no lymphatic vessel development (Figure 28A).

To determine the total corneal area, the main limbal lymphatic vessel was used as the outer boundary. The mean total corneal area for each strain is also displayed in Table 8. Among the strains, FIV_AC showed a significantly larger total corneal area compared to PAT_CD ($p < 0.001$), whereas CIS_AD ($p < 0.05$) and LAT_AD ($p < 0.01$) exhibited significantly smaller total corneal areas (Figure 28B).

To analyse the complexity of the lymphatic vessel network in the CC lines, the number of sprouts, the number of branching points, and the number of endpoints were quantified and related to the corneal area. For the number of sprouts per corneal area, PAT_CD, BOON_HF, LOT_EC, and ROGAN_CF did not differ significantly from one another but showed significant differences ($p < 0.0001$) compared to LUF_AD, FIV_AC, CIS_AD, LAT_AD, and NUK_AC (Figure 28C). Additionally, LUF_AD showed significant differences compared to FIV_AC ($p < 0.05$), LAT_AD ($p < 0.05$), and NUK_AC ($p < 0.05$) (Figure 28C).

The number of branching points per corneal area for each strain is shown in Figure 28D and Table 8. The four strains (PAT_CD, BOON_HF, LOT_EC, and ROGAN_CF) did not differ significantly from one another. However, significant differences were observed between these lines and LUF_AD ($p < 0.0001$), CIS_AD ($p < 0.0001$), LAT_AD ($p < 0.0001$), and NUK_AC ($p < 0.0001$). Moreover, LOT_EC showed significant differences compared to LAT_AD ($p < 0.001$) and highly significant differences compared to LUF_AD ($p < 0.0001$), CIS_AD ($p < 0.0001$), and NUK_AC ($p < 0.0001$). Notable differences were detected among the five CC lines with high lymphatic vessel areas (Figure 28A).

LUF_AD differed significantly from FIV_AC ($p < 0.05$), LAT_AD ($p < 0.05$), and NUK_AC ($p < 0.05$). The average values for endpoints per corneal area are shown in Figure 28E and Table 8. The strains PAT_CD, BOON_HF, LOT_EC, and ROGAN_CF

showed no significant differences from one another but differed significantly from the other lines (LUF_AD, FIV_AC, CIS_AD, LAT_AD, NUK_AC). Among the high-lymphangiogenic lines, LUF_AD differed significantly from FIV_AC ($p < 0.0001$) and CIS_AD ($p < 0.05$), while FIV_AC differed significantly from LAT_AD ($p < 0.01$) and NUK_AC ($p < 0.01$). In conclusion, the morphometric parameters of the nine different CC lines revealed significant differences across all measured parameters, demonstrating clear strain-dependent differences in corneal lymphatic development.

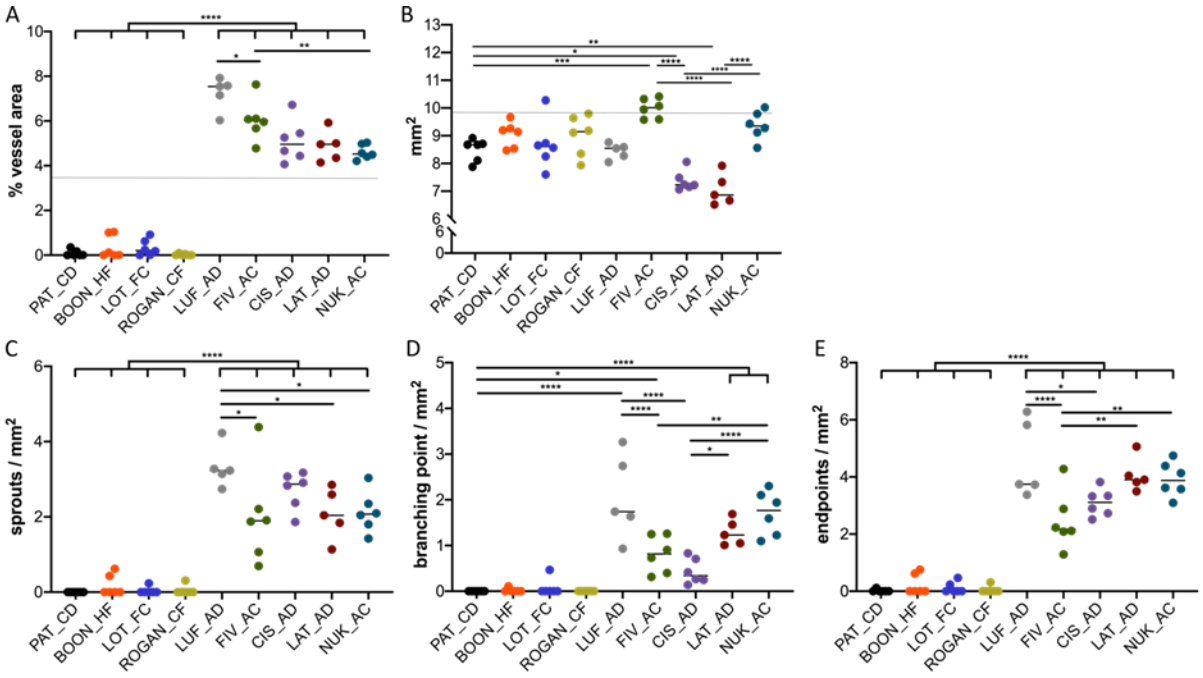

Figure 28. The phenotype of Resting Limbal Lymphatic Vasculature of the Collaborative Cross Mice (Developmental Lymphangiogenesis). (A)Quantification of the lymphatic vascularized area. (B)The whole cornea area. Further characterization of the lymphatic vessel architecture by the number of sprouts (C), the number of branching points (D), and the number of endpoints (E). Data are expressed as means ± SEM. PAT_CD (n=6), BOON_HF (n=6), LOT_EC (n=6), ROGAN_CF (n=6), LUF_AD (n=5), FIV_AC (n=6), CIS_AD (n=6), LAT_AD (n=5), NUK_AC (n=6). Statistical significance was calculated by one-way ANOVA and Tukey multiple comparison test. *p<0.05; **p<0.01; ***p < 0.001; ****p < 0.0001.

Table 8. Quantification of morphometric parameters in different CC mice strains

Strain	Limbal Vessel Area (% ± SD)	Total Corneal Area (mm^2 ± SD)	Corneal Vessel Area (mm^2 ± SD)	Branch Points ($1/mm^2$ ± SD)	Endpoints ($1/mm^2$ ± SD)
PAT_CD	0.09 ± 0.14	8.49 ± 0.41	0 ± 0	0 ± 0	0.02 ± 0.5
BOON_HF	0.36 ± 0.51	9.05 ± 0.46	0.18 ± 0.28	0.02 ± 0.04	0.23 ± 0.36
LOT_EC	0.33 ± 0.37	8.68 ± 0.89	0.04 ± 0.10	0.08 ± 0.19	0.12 ± 0.20
ROGAN_CF	0.03 ± 0.04	9.00 ± 0.73	0.05 ± 0.13	0 ± 0	0.05 ± 0.13
LUF_AD	7.24 ± 0.73	8.44 ± 0.28	3.32 ± 0.55	2.06 ± 0.93	4.59 ± 1.35
FIV_AC	6.04 ± 0.92	9.99 ± 0.35	2.02 ± 1.29	0.81 ± 0.41	2.48 ± 1.02
CIS_AD	5.10 ± 0.94	7.37 ± 0.36	2.70 ± 0.50	0.44 ± 0.28	3.11 ± 0.48
LAT_AD	4.87 ± 0.70	7.06 ± 0.57	2.09 ± 0.67	1.29 ± 0.29	4.07 ± 0.59
NUK_AC	4.61 ± 0.33	9.37 ± 0.51	2.13 ± 0.54	1.71 ± 0.49	3.93 ± 0.61

3.3.2. Determining the growth factors involved in lymphangiogenesis in various Collaborative Cross (CC) line mice.

Given that lymphangiogenesis is primarily regulated by members of the VEGF family, we investigated whether different Collaborative Cross (CC) mouse lines exhibit differential expression of VEGF members in the naïve central cornea. The expression profile in the central cornea was analysed using RNA sequencing.

Among vascular growth factors, VEGF-A showed the highest expression in the central cornea across all CC lines, along with the vascular growth factor receptor VEGFR-2 (Figure 29). Among the four CC lines with a low lymphatic vascularized area, BOON_HF exhibited a significantly higher VEGF-A expression compared to the other three lines (Figure 29A). Additionally, ROGAN_CF showed elevated expression of VEGFR-1 (Figure 29D), while the PAT_CD showed higher expression of VEGFR-2 (Figure 29E). Otherwise, the CC lines displayed comparable expression levels of vascular growth factors and their receptors.

In contrast, among the CC lines with a high lymphatic vascularized area, FIV_AC and LUF_AD exhibited lower expression of VEGF-A and VEGF-D compared to other highly vascularized CC lines (Figure 29A & 29C). FIV_AC also showed reduced expression of VEGFR-1 and VEGFR-3, whereas LUF_AD exhibited low expression of VEGFR-1 only. NUK_AC showed low expression of VEGF-D and VEGFR-3, but moderate expression of VEGF-A and VEGFR-1 compared to other highly vascularized lines. In contrast, LUF_AD showed the highest expression of VEGF-C and VEGFR-3, while

CIS_AD exhibited the highest expression of VEGF-D and VEGFR-1. Among all CC lines, BOON_HF showed the highest expression of VEGF-A, and PAT_CD the highest expression of VEGFR-2 (Figure 29).

The rank order of the expression of different vascular growth factors is as follows. For VEGF-A: BOON_HF > LAT_AD > LOT_EC > CIS_AD > NUK_AC > ROGAN_CF > LUF_AD > PAT_CD > FIV_AC; for VEGF-C: LUF_AD > CIS_AD > PAT_CD > ROGAN_CF > FIV_AC > LOT_EC > BOON_HF > LAT_AD > NUK_AC; and for VEGF-D: CIS_AD > LAT_AD > PAT_CD > ROGAN_CF > BOON_HF > LOT_EC > LUF_AD > NUK_AC > FIV_AC (Figure 29A-C). These vascular growth factors signal through their receptors VEGFR-1, -2, and -3. The rank order of expression for these receptors in each CC line is as follows. For VEGFR-1: CIS_AD > LAT_AD > ROGAN_CF > BOON_HF > NUK_AC > PAT_CD > LOT_EC > LUF_AD > FIV_AC; for VEGFR-2: PAT_CD > BOON_HF > ROGAN_CF > FIV_AC > LUF_AD > NUK_AC > CIS_AD > LOT_EC > LAT_AD; and for VEGFR-3: LUF_AD > LAT_AD > CIS_AD > PAT_CD > ROGAN_CF = NUK_AC > LOT_EC > BOON_HF > FIV_AC (Figure 29D-F).

In conclusion, the CC lines analysed in this study exhibited significant variation in the expression of lymphangiogenic growth factors and their receptors. These differences in both lymphatic vascularized area and vascular growth factor expression profile highlighted the substantial genetic variability in the regulation of lymphangiogenesis among CC strains derived from the original eight CC founder strains.

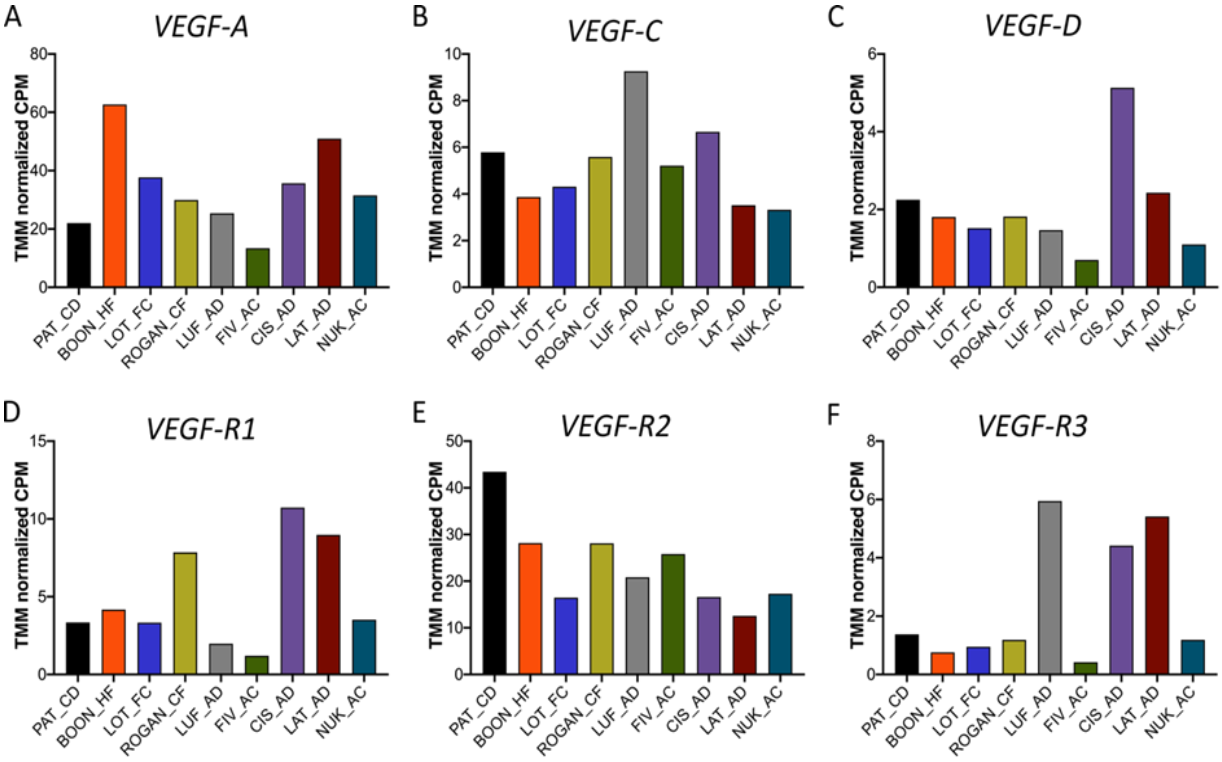

Figure 29. Illustrates the strain-dependent differences in the expression of vascular growth factor family members in Collaborative Cross (CC) mice. RNA was isolated from the central 2 mm of naïve corneas from various CC lines, and sequencing libraries were prepared. Equal amounts of total RNA were pooled from three corneas of each CC line. Raw reads were processed to trim poly-N-tails, and expression levels were counted for VEGF-A, VEGF-C, VEGF-D, VEGF-R-1, VEGF-R-2, and VEGF-R-3. Transcript per million (TMM) values were calculated using the "cpm" method from the edgeR package. (n=3)

3.3.3. Comparative Analysis of Suture-Induced Lymphangiogenesis in Collaborative Cross Lines BOON-HF and NUK-AC

The determination of growth factors involved in lymphangiogenesis across different CC lines reveals substantial variation in lymphatic vascularized areas in the naïve cornea, accompanied by a diverse expression profile of lymphangiogenic growth factors. This observation raises the question of whether animals exhibiting either extremely low or extremely high lymphatic vascularized areas are still capable of responding to an inflammatory stimulus.

For this purpose, two extreme CC lines were selected: BOON_HF, which exhibits nearly no lymphvascularized area in the naïve cornea (0.36% ± 0.51% vessel area, Figure 28A), and NUK_AC, which displays high lymphvascularized area in the naïve cornea (4.61% ±0.33% vessel area, Figure 28A). These lines were chosen as representative models for low and high lymphangiogenic potential, respectively.

Inflammation-induced lymphangiogenesis was assessed using the previously described suture-induced corneal vascularization model. Fourteen days after suture placement, the total surface area of ingrown vessels in the cornea was analysed using immunofluorescence staining with LYVE1 (Figure 30A). The results demonstrate a significant induction of inflammation-induced lymphangiogenesis in both CC lines.

Under inflammatory conditions bordering on naïve corneas, BOON_HF (7.25% ± 3.28% vessel area) exhibits a significantly lower lymph vascularized area compared to NUK_AC (11.94% ± 3.33% vessel area) (Figure 30B). However, relative to their respective naive states, BOON_HF showed a dramatic 20-fold increase in lymphatic vascularized area following inflammation. On the other hand, NUK_AC demonstrates only a 2.5-fold increase in lymphatic vascularized area following inflammation compared to the resting limbal vasculature. These findings indicate that, despite the nearly complete absence of resting limbal vasculature in BOON_HF, this mouse line exhibits a significantly greater relative increase in inflammation-induced lymphangiogenesis compared to the highly vascularized NUK_AC line.

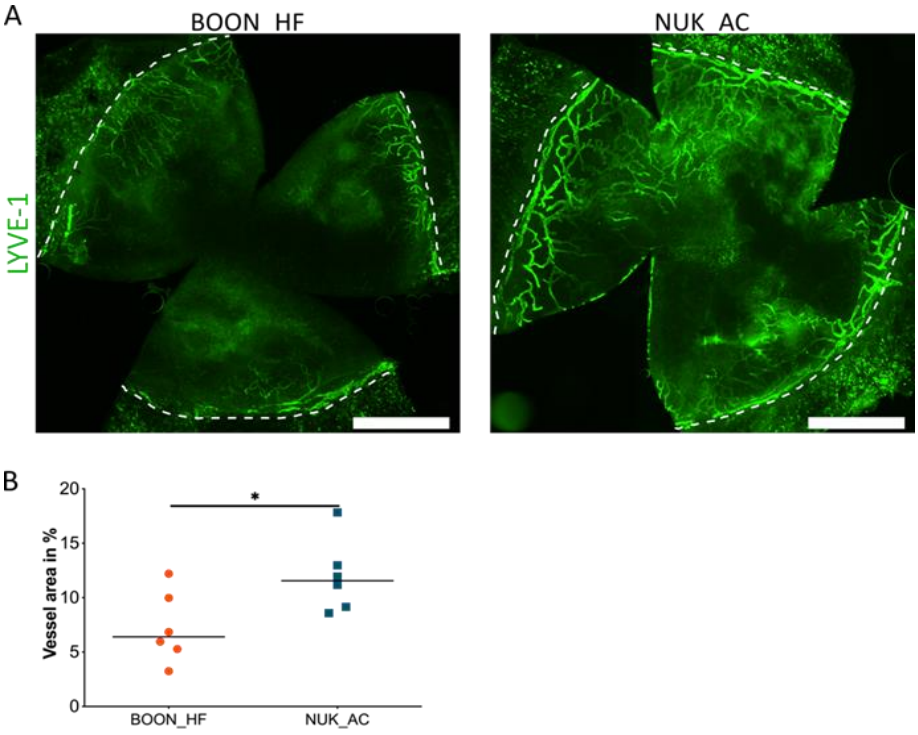

Figure 30. Significant Strain-Dependent Differences in Inflammation-Induced Lymphangiogenesis.(A)Representative corneal whole mounts of inflammation-induced lymphangiogenesis of BOON_HF and NUK_AC stained for LYVE-1. Dashed lines show the border between the limbus and the cornea scale bars: 1 mm. (B) Quantification of the

inflammatory lymphatic vascularized area of the whole mounts. Data are expressed as means ± SEM (n=6). Statistical significance was calculated by a two-tailed t-test, *p<0.05.

4. Discussion

The term "corneal (lymph)angiogenic privilege" refers to the cornea's unique ability to remain free of both blood and lymphatic vessels under normal physiological conditions. This privilege is crucial for maintaining avascularity, which is essential for optimal visual function. The absence of blood and lymphatic vessels in the healthy cornea is a fundamental characteristic that contributes to its transparency and visual clarity[21, 42]. The balance between anti(lymph)angiogenic factors, which inhibit new vessel formation, and pro(lymph)angiogenic factors, which promote vascular growth, is tightly regulated[37]. This regulation prevents vascular infiltration that could compromise vision by maintaining corneal transparency and preventing pathological conditions such as corneal neovascularization[62, 63].

The lymphatic vascular system is essential for various physiological processes, including dietary fat absorption, immune surveillance, and maintaining tissue fluid balance. In the context of corneal graft survival, lymphatic vessels play a significant role by transporting antigens and antigen-presenting cells to regional lymph nodes, which can lead to sensitization and graft rejection[37, 60]. Similarly, in cancer, lymphatic vessels are key mediators of metastasis, providing pathways for tumor cells to disseminate from primary sites to distant organs through tumor-associated lymphangiogenesis[64]. Studies have shown that the presence of lymphatic vessels, whether in the corneal recipient bed or in tumors, is associated with adverse outcomes, such as reduced graft survival or cancer progression[37, 60, 62, 63]. Conversely, therapeutic strategies aimed at inhibiting or regressing lymphatic vessels have demonstrated promise in improving graft survival and limiting cancer metastasis[58, 64]. Recent studies highlight the critical role of lymphangiogenic factors, such as VEGF-C and VEGF-D, and their receptors VEGFR-2 and VEGFR-3, in promoting the formation of new lymphatic vessels[65-67].

In the cornea, lymphangiogenesis contributes to various pathological conditions, including dry eye disease, corneal graft rejection, ocular allergies, and microbial keratitis. Under such pathological conditions, the cornea loses its (lymph)angiogenic privilege, leading to the ingrowth of blood and lymphatic vessels. While the mechanisms underlying pathological corneal hemangiogenesis are well-characterized[68], our understanding of lymphangiogenesis, particularly its guidance mechanisms, remains limited. Recent reviews have emphasized the importance of

elucidating lymphatic endothelial guidance and its role in ocular disease pathogenesis [12]. This lack of clarity is mirrored in cancer research, where the role of lymphangiogenesis in facilitating metastasis remains underexplored[68-70].

In this regard, Rohan et al. demonstrated that genetic factors significantly influence lymphangiogenesis during tumor progression, underscoring the importance of model selection in lymphatic research[71]. Similarly, Nakao et al. investigated the roles of VEGF-C and its receptor VEGFR-3 in lymphangiogenesis using genetically modified mouse models, emphasizing their relevance in identifying therapeutic targets[72]. Consistent with these findings, our previous studies confirmed that genetic background profoundly impacts lymphatic vessel development in the corneal model, underscoring the need for careful consideration of mouse strain selection in lymphatic research[46].

By utilizing mice with varying genetic predispositions, researchers can better explore the interplay between genetic background and lymphangiogenic responses, thereby gaining a deeper understanding of the molecular regulators involved.

Specifically, the naïve corneas of C57BL/6N mice exhibited a significantly larger lymphatic vascularized area compared with those of BALB/cN mice (Supplementary Figure 1A and B)[45]. To further assess the complexity of the lymphatic network, we quantified the number of sprouts, branching points, and endpoints in the naïve corneas of both strains. C57BL/6N mice displayed significantly higher numbers of sprouts, branching points, and endpoints relative to the total corneal area (Supplementary Figure 1C), indicating a denser and more intricate lymphatic vessel network[45].

Quantitative trait locus (QTL) analysis can be applied when genetic variability exists across a population and the trait of interest is measurable, such as lymphatic vessel area in the cornea. By correlating phenotypic differences with genetic markers in a genetically diverse intercross population, QTL mapping enables the identification of genomic regions associated with lymphangiogenesis. Subsequent analysis of genes within these regions has previously identified tyrosinase as a novel endogenous regulator of both developmental and inflammatory lymphangiogenesis in the mouse cornea[44].

In this study, CBS has been identified as a novel regulator of lymphangiogenesis. CBS plays a central role in the transsulfuration pathway of sulfur amino acids metabolism, catalyzing the initial and rate-limiting step in this pathway. Additionally, CBS is involved

in desulfuration reactions that lead to the production of hydrogen sulfide (H_2S), a gaseous signaling molecule with diverse physiological functions[73]. In humans, CBS is primarily expressed in the brain, liver, kidney, pancreas, and, to a lesser extent, in endocrine and lymphoid tissues[74, 75].

Previous studies have demonstrated that CBS promotes tumor growth and cell proliferation in various cancers, including colon, ovarian, prostate, and breast cancer [76]. Interestingly, inhibiting CBS, either through RNA interference or pharmacological inhibitors like aminooxyacetate (AOAA), reduces tumor growth, suggesting that CBS functions as a tumor promoter[77]. This inhibition also affects tumor angiogenesis, indicating that CBS serves as a dual regulator of both tumor growth and blood vessel formation[78]. CBS expression has been detected in multiple ocular tissues, including the conjunctiva, iris, ciliary body, and cornea, underscoring its presence in various eye compartments[79, 80]. Acting through paracrine mechanisms, CBS can modulate the tumor microenvironment and promote angiogenesis, with potential implications for eye health and disease[73, 76]. Importantly, CBS deficiency has been associated with a range of ocular disorders, including ectopic lentis, myopia, retinal degeneration, optic atrophy, glaucoma, corneal abnormalities, and cataracts, which are often observed in patients with homocystinuria caused by CBS mutations. Specifically, CBS deficiency has been linked to corneal pathologies such as corneal thinning and keratoconus[81, 82]. These manifestations likely result from elevated homocysteine levels, which disrupt normal corneal structure and function, thereby contributing to disease progression.

In humans, CBS exists as a tetramer composed of 63 kDa subunits. Alongside CBS, two other enzymes, MPST and CTH, are involved in the enzymatic production of H_2S [73, 83]. H_2S has been shown to elicit various cellular responses[83, 84], including endothelial cell angiogenic activities, vascular formation[85, 86], angiogenesis[85, 86], and epithelial-mesenchymal transition[87]. Moreover, H_2S has been demonstrated to enhance mitochondrial activity and reduce reactive oxygen species (ROS) levels[88].

Under normal conditions, CBS is primarily localized in the cytosol, although it can also be found in the mitochondria in certain tissues[89, 90]. The expression of CBS is highly regulated at multiple levels, including transcriptional, epigenetic, post-transcriptional, or hormonal regulation[91]. Additionally, CBS expression can be induced by growth

and differentiation hormones such as transforming growth factor-α (TGF-α), epidermal growth factor (EGF), and cAMP[92].

Deficiency of CBS in mice leads to a range of phenotypic abnormalities, including premature death, loss of visceral fat, hyperhomocysteinemia (elevated levels of homocysteine in the blood), liver steatosis (accumulation of fat in the liver), growth retardation, and impaired bone mineralization[73]. Additionally, CBS knockout mice develop progressive endothelial dysfunction, characterized by extensive vascular remodeling, thickened blood vessel walls, and higher blood pressure[73, 93].

AOAA is the most potent pharmacological inhibitor of CBS[91]. However, AOAA also inhibits additional pyridoxal-5-phosphate (PLP)-dependent enzymes, including DOPA decarboxylase, CTH, alanine transaminase, glutamate decarboxylase, alanine racemase, histidine decarboxylase, D-amino acid transaminase, and aspartate transaminase[73]. The anticancer effects of AOAA have been demonstrated in various experimental models, including patient-derived colon cancer xenografts and breast cancer xenografts[94, 95].

Saha et al. reported that AOAA inhibits endothelial cell migration and proliferation of HUVECs[94, 96]. Herein, we used AOAA to investigate its *in vitro* effects on CBS in its role in regulating lymphangiogenesis, a process involving the migration and proliferation of HDLECs.

Our results showed that AOAA treatment significantly reduced HDLEC proliferation in a dose-dependent manner without inducing apoptosis. Specifically, treatment with 1 mM AOAA results in a marked reduction in HDLEC proliferation and delayed wound healing, whereas lower concentrations had minimal impact on proliferation. Interestingly, tube formation by HDLECs was unaffected at 1 mM AOAA, but was inhibited at higher concentrations (4 mM). These findings suggest that the inhibitory effects of AOAA on HDLEC proliferation are concentration dependent.

Consistent with our findings, Szabo et al. observed reduced proliferation in colon cancer cells following treatment with 1 mM AOAA, while non-tumorigenic colon epithelial cells were unaffected[94]. In contrast, Hellmich et al. reported that a concentration as low as 300 μM AOAA suppressed proliferation in HCT116 cells[97]. These discrepancies indicate that AOAA's inhibitory effects may be cell-type specific and concentration-dependent.

Furthermore, our study investigated the impact of AOAA on the organization of LECs into capillary structures and cell migration, which are crucial aspects of lymphangiogenesis. We found that wound closure was delayed by AOAA treatment, indicating impaired migration. However, AOAA also enhances cellular branching, suggesting a potential role in promoting capillary network organization. These findings highlight the complex and context-dependent effects of CBS inhibition on different stages of lymphangiogenesis.

Since AOAA targets pyridoxal-5′-phosphate-dependent enzymes, including CTH[98, 99], which is expressed in endothelial cells and regulates various endothelial functions[83, 100]. To further elucidate the specific role of CBS, gene silencing studies were conducted. Lymphatic endothelial cells were transfected with small interfering RNA (siRNA) specific to CBS, and multiple lymphangiogenic parameters were evaluated 72 hours post-transfection, including the assessment of apoptotic cells using Annexin V staining.

By employing gene-silencing approaches, we were able to specifically attribute the observed effects to CBS inhibition, thereby elucidating its role in modulating lymphatic endothelial cells' behaviour. In addition, we investigate the potential involvement of CBS, CTH, and 3-MPST in lymphangiogenesis to determine whether AOAA specifically targets CBS or if it also affects the other enzymes in the transsulfuration pathway.

Interestingly, HDLECs treated with CBS-specific siRNA exhibited a marked reduction in proliferation, delayed wound healing, and impaired tube formation compared to control cells. Importantly, there was no increase in the number of apoptotic cells, indicating that the observed effects were not due to induction of apoptosis but rather specific to CBS inhibition.

These findings provide strong evidence for the involvement of CBS in regulating lymphangiogenesis and highlight its potential as a therapeutic target for modulating lymphatic vessel formation and function. Notably, silencing CBS in HDLECs produced lymphangiogenic effects similar to those observed with treatment with AOAA, including reduced proliferation, delayed wound healing, and impaired tube formation.

On the other hand, gene silencing of CTH, the second enzyme in the transsulfuration pathway, did not significantly affect lymphangiogenesis. To further elucidate the specificity of AOAA, transfected cells were treated with two distinct concentrations of

AOAA in the context of gene silencing experiments targeting CBS, CTH, and MPST. The results clearly demonstrated that AOAA selectively inhibits CBS activity, without affecting CTH or MPST, confirming CBS as its primary target in lymphangiogenesis regulation.

Recent studies indicate that CBS silencing in HUVECs reduces proliferative and migratory capacity[96] and induces early senescence[101]. Pharmacological inhibition of CBS with AOAA has similarly been shown to cause cell cycle arrest and decreased proliferation in various cell types, including myeloma cells[102]. IncCBS-deficient (Cbs-/-) mice, livers exhibit increased expression of senescence-related mRNAs p21, Pai-1, Mcp1, and Il-6[13].

Building on these observations, the current study examined whether similar effects occur in HDLECs. Both CBS-specific siRNA knockdown and AOAA treatment decreased proliferation and migration, while enhancing tube formation in HDLECs. Importantly, neither 24-hour AOAA treatment nor 96-hour transfection with CBS-specific siRNAs induced cellular senescence. These findings suggest that CBS inhibition reduces lymphangiogenic activity without triggering senescence in lymphatic endothelial cells, although other studies have reported senescence in HUVECs following CBS inhibition[101].

In the context of this study, treatment with AOAA in gene silencing of CBS led to decreased transcriptional levels of VEGFR-2 and VEGFR-3 in HDLECs, highlighting a potential mechanism by which CBS regulates lymphangiogenesis through VEGF receptor modulation.

The VEGF family plays a central role in angiogenesis, the process by which new blood vessels form from existing ones. This complex process encompasses several critical stages, such as endothelial cell proliferation, migration, and tube formation. VEGF-A, in particular, is crucial for maintaining endothelial cell functionality and promoting angiogenesis[32, 60]. The signaling cascade, mediated through VEGFR-2 and Neuropilin-1 (NRP-1), facikitates vascular repair and endothelial responses[103].

The VEGF family is also involved in lymphangiogenesis, with VEGF-C and VEGF-D stimulating lymphatic endothelial cell migration and proliferation through their receptors, VEGFR-2 and VEGFR-3[35, 65, 67].

In line with this, our experiments showed that both CBS-specific siRNA-mediated gene silencing and pharmacological inhibition of CBS with AOAA reduced proliferation, migration, and tube formation in HDLECs, accompanied by a marked decrease in VEGF receptor expression.

Emerging evidence also links CBS deficiency to ocular manifestations, including lens abnormalities, myopia, and retinal degeneration[80]. Research by Tawfik et al. demonstrates that in Cbs-/- animals exhibit elevated homocysteine levels associated with significant changes in retinal vasculature, including increased VEGF mRNA and protein expression, suggesting a compensatory mechanism to counteract vascular function[104]. Additionally, Persa et al. mapped the distribution of CBS across ocular compartments, offering a detailed understanding of its local effects and potential therapeutic targets[80].

The study revealed a notable expression of CBS in the anterior segment of the eye, including the cornea, ciliary body, iris, and conjunctiva, in a 17-year-old donor[80]. Interestingly, the distribution pattern of CBS in the anterior segment of the eye does not appear to change with age. Among the regions of the eye expressing CBS, the corneal epithelial layer exhibited significantly higher CBS activity compared to other areas[80].

This observation suggests that the corneal epithelial cells are particularly active in CBS-mediated processes. One possible explanation for this could be the entry of oxygen from the surrounding environment into the corneal epithelium, leading to the generation of reactive oxygen species (ROS) within the cells. ROS are known to be potent activators of CBS, which could contribute to the higher levels of CBS activity observed in the corneal epithelial layer[105].

To investigate the role of CBS in inflammation-induced lymphangiogenesis, we utilized the suture-induced corneal neovascularization assay[48, 60]. Sutures were placed in the corneal stroma of C57BL/6N and BALB/cN mice, mimicking inflammatory conditions triggering immune cell infiltration, including macrophages and dendritic cells [1, 106, 107]. This model elicited marked proliferation of lymphatic vessels, demonstrating an active lymphangiogenic response and highlighting CBS's regulatory role in both inflammatory responses and lymphatic vessel development *in vivo*[73, 102]. Macrophages play a pivotal role in this process by secreting paracrine factors,

including VEGF-C and VEGF-D[90], binding to VEGFR-2 and VEGFR-3 on endothelial cells, and thereby driving hemangiogenesis and lymphangiogenesis. These achievements could highlight critical pathways through which inflammatory responses promote vascular remodeling and growth[106]. The influence of CBS on tumor and blood vessel growth has been extensively studied using various *in vivo* and *in vitro* models[94, 96]. As reported, in xenograft models, gene silencing of CBS has been associated with a decrease in the density and number of CD31-positive blood vessels, indicating a reduction in overall blood vessel formation and density of the tumor microenvironment. It also demonstrates a distinct impact on vascular architecture by producing larger and structurally mature blood vessels[94].

Collectively, these findings indicate that CBS is a crucial regulator of lymphangiogenesis by stimulating HDLEC proliferation and migration, likely through the upregulation of VEGFR-2 and VEGFR-3. This role is evident both in vitro and in vivo, particularly during inflammation-induced lymphangiogenesis. Thus, CBS emerges as a novel endogenous modulator and a potential therapeutic target for disorders associated with abnormal lymphatic function, including corneal graft rejection or lymphedema.

Building on the identification of CBS as an endogenous regulator of lymphangiogenesis through quantitative trait locus (QTL) analysis, our study further identified ANGPTL4 as an additional regulator identified within the same QTL framework. This finding underscores the contribution of multiple genetic loci in lymphatic vessel development and highlights ANGPTL4 as a novel candidate for elucidating the molecular mechanisms underlying lymphangiogenesis. ANGPTL4 plays a complex role in the vascular system. Its impact on physiological and pathological processes is context-dependent, reflecting its diverse regulatory function [108, 109]. As a member of the angiopoietin-like (ANGPTL) superfamily of secreted proteins, ANGPTL4 is known to modulate angiogenesis by influencing EC behavior. These include inhibiting endothelial adhesion, migration, and sprouting, thereby suppressing angiogenesis and metastasis under certain conditions[108]. However, in specific pathological settings, such as arthritis and certain tumors, ANGPTL4 can shift its role to promote vascular permeability and enhance angiogenesis[110].

ANGPTL4 is widely expressed in various tissues, with the highest expression levels in the liver and adipose tissue (AT). It is also detected, though at lower levels, in tumor

cells, macrophages, placental tissue, and vascular endothelium. In contrast, its expression is relatively low in the heart and muscle. The protein exists in distinct isoforms, each with specialized functions. The full-length ANGPTL4 and its N-terminal fragment (nANGPTL4) bind to and inhibit lipoprotein lipase (LPL), thereby regulating lipid metabolism. In contrast, the C-terminal fragment (cANGPTL4) is primarily implicated in non-metabolic pathways[109, 111-113]. Additionally, ANGPTL4 expression is strongly upregulated under hypoxic conditions, particularly in necrotic tumor zones, and is markedly elevated in tumor cells of conventional renal cell carcinoma, indicating its potential role in tumor adaptation and progression[109, 110, 113].

The connection between ANGPTL4 and ocular diseases is particularly noteworthy, as ANGPTL4 has been implicated in conditions characterized by altered vascular permeability and inflammation within the eye. Aberrant expression of ANGPTL4 in ocular tissues may contribute to pathologies such as diabetic retinopathy and age-related macular degeneration, where dysregulated angiogenesis and vascular leakage play central roles[114, 115]. Understanding the mechanistic involvement of ANGPTL4 in these disorders could lead to novel therapeutic approaches aimed at modulating its activity to restore vascular integrity and function.

These findings highlight the multifaceted biological function of ANGPTL4 and its involvement in various physiological and pathological processes, including lymphangiogenesis. The anti-lymphangiogenic properties of ANGPTL4 identified in this study suggest its potential as a target for modulating lymphatic vessel growth and function in different disease contexts. Tumor-derived cleaved ANGPTL4 (cANGPTL4) has been shown to disrupt endothelial continuity through direct interactions with integrin α5β1, VE-cadherin, and claudin-5, ultimately compromising junction integrity. Similarly, ANGPTL4 modulates vascular junctions via integrin signaling, highlighting its role in maintaining endothelial barrier function and potentially modulating pathological lymphangiogenesis[109, 113] . The structural similarity of ANGPTL4 to members of the angiopoietin family has attracted considerable interest, as it is involved in various physiological and pathological processes[109].

ANGPTL4 has been linked to anoikis resistance, altered redox regulation, angiogenesis, and vascular permeability[109, 116]. These findings highlight the multifaceted function of ANGPTL4 in cellular and molecular pathways that influence

tissue homeostasis, vascular integrity, and disease progression. Previous investigations of ANGPTL4 expression involved examining its secretion in the conditioned media of HEK293 cells transfected with ANGPTL4 cDNA[110]. Both mouse and human ANGPTL4 proteins, with molecular weights exceeding 50 kDa, were detected in the culture media, whereas only modest levels were observed in the cell lysate[117]. SDS-PAGE and Western blot analysis techniques confirm these findings. Under non-reducing conditions (without 2-mercaptoethanol), ANGPTL4 exhibits oligomerization, consistent with the behaviours of proteins containing a coiled-coil domain, similar to those found in other angiopoietin family members[117].

The role of Angptl4 signaling in vascular function was further explored by evaluating its effects on VEGF-induced endothelial proliferation and chemotaxis. VEGF application to both HUVECs and human dermal microvascular endothelial cells (HDMVECs), resulting in a marked increase in BrdU incorporation, indicating enhanced proliferative activity. Remarkably, when Angptl4 was applied in a dose-dependent manner, it effectively inhibited VEGF-induced BrdU incorporation, demonstrating its capacity to suppress VEGF-induced proliferation[117]. These findings suggest that ANGPTL4 functions as a negative modulator of VEGF signaling, thereby serving as an important regulatory factor in angiogenesis.

In recent years, Angptl4 has emerged as a key regulator of angiogenesis, although its role in lymphangiogenesis remains relatively understudied. Investigating the role of Angptl4 in lymphangiogenesis is significant for several reasons[108]. Elucidating its involvement provides valuable insight into the mechanisms driving lymphatic vessel growth and function under both physiological and pathological conditions[109]. Given the critical role of lymphatic vessels in immune surveillance, fluid homeostasis, and disease progression, understanding how ANGPTL4 influences lymphangiogenesis may uncover novel therapeutic targets for a wide range of diseases[113]. It also inhibits angiogenesis and vascular leakiness, suggesting a potential role in modulating pathological lymphangiogenesis[117]. In the cornea, dysregulated lymphangiogenesis is a key factor in graft rejection, as lymphatic vessels facilitate the migration of antigen-presenting cells and alloimmune responses[118, 119]. Therefore, targeting ANGPTL4-mediated lymphatic remodeling could provide a novel strategy to improve corneal graft survival and modulate immune rejection.

Furthermore, the identification of ANGPTL4 as a potential biomarker for lymphatic-related diseases holds clinical significance. Studies have implicated ANGPTL4 expression in lymphatic vessel density and lymph node metastasis in certain cancers, suggesting its potential utility as both a prognostic marker and therapeutic target[120]. Investigating the role of ANGPTL4 in lymphangiogenesis may, therefore, lead to the development of biomarker-based strategies for disease diagnosis, prognosis, and treatment selection[121].

Targeting lymphangiogenesis has emerged as a promising therapeutic approach for diseases such as cancer and lymphedema. Understanding how ANGPTL4 regulates lymphatic vessel growth and function could help identify novel biomarkers and therapeutic targets, offering opportunities to modulate lymphangiogenesis and improve outcomes in lymphatic-related disorders[83].

Thus, elucidating ANGPTL4-mediated mechanisms is essential for advancing our understanding of lymphatic diseases and for developing effective interventions for conditions associated with abnormal lymphatic vessel growth. The potential influence of ANGPTL4 on VEGF-induced chemotaxis was examined in Brain-derived Endothelial Cells, clone 3 (bEND3), and HUVECs. It was found that ANGPTL4 reduced VEGF-induced chemotaxis in both cell types in a dose-dependent manner. Importantly, the basal level of migration in HUVECs and bEND3 cells was not affected by treatment with ANGPTL4 alone, indicating that Angptl4 specifically interfered with VEGF-induced chemotactic responses without altering baseline migration levels. The impact of ANGPTL4 on tube formation was also investigated in HUVECs grown on Matrigel. Tube formation involves the development of pathogenic alterations, where endothelial cells arrange themselves around a lumen, forming tubular structures[122].

Previous studies using a mouse corneal model and the Miles vascular permeability assay have demonstrated that ANGPTL4 effectively inhibits endothelial cell proliferation, chemotactic activity, tube formation, angiogenesis, and vascular leakiness *in vivo*. These comprehensive findings strongly suggest that ANGPTL4 exerts potent antiangiogenic effects, positioning it as a key regulator of vascular integrity and endothelial function[109, 122].

In the current study, it was observed that gene silencing with ANGPTL4-specific siRNA led to increased proliferation and migration, while reducing tube formation in HDLECs.

Conversely, treatment of HDLECs with 1000ng/ml of ANGPTL4 decreased migration and enhanced tube formation in the assay. These findings suggest that ANGPTL4 may play a context-dependent role in regulating endothelial cell behavior, potentially exhibiting both pro- and anti-angiogenic effects depending on the cellular context and ANGPTL4 concentration.

Both *in vitro* and *in vivo* experiments revealed that recombinant human cANGPTL4 and tumor-derived cANGPTL4 increased vascular permeability. These findings were corroborated by experiments demonstrating that cANGPTL4 enhanced vascular leakiness and facilitated lung metastasis in mice. This was further validated by comparing Angptl4-deficient and wild-type mice injected with either control or Angptl4-knockdown tumors[109, 113].

Mechanistically, cANGPTL4 exerts its effects on vascular permeability through integrin α5β1-mediated PAK/Rac signaling, which leads to decreased endothelial cell-cell adhesion and increased vascular leakiness. Thus, cANGPTL4 plays a critical role in modulating endothelial barrier function and may contribute to the metastatic potential of tumors through this mechanism[109, 113].

The role of ANGPTL4 in regulating angiogenesis and vascular permeability remains complex, with studies reporting both increases and decreases in vascular leakiness under different pathophysiological conditions. These discrepancies may arise from differences in experimental design, such as the use of distinct ANGPTL4 isoforms (full-length vs. cleaved forms), primarily in *in vitro* systems, as well as the utilization of a complete knockout animal to investigate its effects on the endothelium[109, 123].

While most research has focused on the paracrine effects of ANGPTL4 on ECs, its potential cell-autonomous effects have been largely overlooked, despite its high expression in ECs. This dual role suggests that ANGPTL4 may regulate vascular permeability through both paracrine signaling, affecting neighboring cells, and cell-autonomous mechanisms, directly modulating the behavior of the expressing cell. These findings add further complexity to our understanding of ANGPTL4's role in angiogenesis and vascular homeostasis, highlighting the need for additional studies to explore these distinct pathways[109].

Deficiency in ANGPTL4 has been associated with the amplification of lipid-sensitive genes and the promotion of macrophage lipid absorption[124].

Hemangiogenesis and lymphangiogenesis are primarily mediated by members of the VEGF family and their corresponding receptors. VEGF-A activates VEGFR-1 and VEGFR-2, while VEGF-C and VEGF-D activate VEGFR-2 and VEGFR-3. Notably, VEGFR-3 is unique to lymphangiogenesis, although VEGFR-2 can also contribute to this process. Both VEGFR-1 and VEGFR-2 play an essential role in hemangiogenesis. During development, the binding of VEGF-C to VEGFR-3 is crucial for lymphatic vessel formation. The angiogenic properties of VEGF-A, particularly its role in tumor formation, have been extensively studied[125].

The previous findings indicate that the introduction of a pellet containing VEGF alone resulted in the formation of new capillary vessels extending from the corneal limbus towards the pellet. However, when a pellet containing both VEGF and Angptl4 was implanted, corneal neovascularization towards the pellet was significantly inhibited. This inhibition was evident in multiple parameters of ocular neovascularization, including maximal vessel length, clock hours, and vessel area, all of which were notably reduced compared to VEGF-induced neovascularization[117].

Through our experimental analyses, we discovered that naïve Angptl4−/− mice exhibited a marked increase in both blood and lymphatic vessel surface areas in the cornea compared to wild-type (WT) mice. Under inflammatory conditions, 14 days after treatment with recombinant ANGPTL4 protein, revealed a significant reduction in vascularized areas of the cornea compared to PBS-treated controls, supporting the observations from the Angptl4 knockout model. Furthermore, we observed that the corneas of naïve Angptl4−/− mice had a significantly larger area covered by $F4/80^{+}$ macrophages than those of WT mice. Treating C57BL/6N mice with recombinant ANGPTL4 resulted in a marked decrease in inflammation-induced lymphangiogenesis, underscoring the modulatory role of ANGPTL4. Our data demonstrate that ANGPTL4 reduces both blood and lymphatic vessel formation and limits macrophage infiltration during corneal inflammation. Together, these findings establish ANGPTL4 as a key endogenous regulator of inflammatory lymphangiogenesis and immune cell recruitment in the cornea, thereby contributing to the maintenance of corneal immune privilege.

In this study, we further observed that the levels of VEGF-A and VEGF-C expression in the corneas of naïve Angptl4−/− mice were significantly higher than those in WT mice. However, there were no differences in the expression levels of VEGF-D, VEGFR-

2, and VEGFR-3 between the corneas of naïve Angptl4 -/- and WT mice. In conclusion, these findings underscore the significant role of ANGPTL4 as a regulator of lymphangiogenesis. Moreover, the molecular insights provided by these studies suggest that lymphangiogenesis regulators may exert their effects through distinct molecular pathways compared to the conventional VEGF-dependent mechanism. These results also emphasize the likelihood that additional factors, beyond growth factors, contribute to the regulation of both lymphangiogenesis and angiogenesis, warranting further exploration and investigation. In conclusion, the findings of these studies underscore the significant role of ANGPTL4 as a regulator of lymphangiogenesis.

In general, CBS and ANGPTL4 are emerging as significant regulators in the realm of vascular biology, particularly in the context of lymphangiogenesis and angiogenesis. CBS is traditionally recognized for its role in sulfur amino acid metabolism and the production of hydrogen sulfide[75]. Our studies demonstrated that CBS expression correlates with lymphatic vessel growth, and inhibition of CBS in mice led to impaired lymphangiogenesis under inflammatory conditions. This effect appears to be mediated, at least in part, by the local AOAA treatment, which reduced the expression of key growth factors and receptors, including VEGFR-2 and VEGFR-3, during the suture-induced inflammatory response. The specificity of this effect is underscored by the finding that control animals did not show a reduction in lymphatic surface area following the injury.

Although ANGPTL4 is traditionally associated with lipid metabolism, recent studies have highlighted its significant influence on angiogenesis and vascular permeability. Depending on the biological context, ANGPTL4 can exhibit both pro-angiogenic and anti-angiogenic properties. Specifically, *in vitro* studies have shown that ANGPTL4 inhibits VEGF-induced endothelial cell proliferation, migration, and tube formation. These anti-angiogenic effects are further supported by *in vivo* studies, which demonstrate that ANGPTL4 suppresses VEGF-induced corneal neovascularization and inhibits tumor angiogenesis, reinforcing its potential as a therapeutic target in conditions characterized by excessive vascular growth[117].

Our study advances the understanding of the complex regulatory networks that control vascular development and homeostasis. By identifying CBS and ANGPTL4 as novel regulators of lymphangiogenesis and angiogenesis, we highlight new potential targets

for therapeutic interventions in vascular-related disorders such as cancer metastasis, lymphedema, and ocular neovascularization. Future research exploring the modulation of CBS and ANGPTL4 signaling pathways may pave the way for innovative treatments aimed at improving vascular health and graft survival.

Building upon these findings, research on the CC-line mice enhances our understanding of the genetic factors that influence lymphangiogenesis in the cornea. By studying the genetic variations among different strains of mice, researchers can identify key genes involved in the regulation of lymphatic vessel growth. This knowledge may facilitate the discovery of novel endogenous modulators of lymphangiogenesis, providing potential targets for therapeutic intervention in conditions characterized by abnormal corneal vascularization. Initially, studies using two phenotypically distinct mouse strains provided a basic model for investigating genetic influences on disease traits. However, this approach has limitations, primarily due to the restricted genetic variability between just two strains. The transition to the model of CC lines overcomes these limitations by utilizing a genetically diverse panel of mice, which better reflects the genetic complexity found in human populations. This shift not only enhances the reliability of the findings but also increases the potential for discovering more comprehensive genetic interactions that govern lymphatic development and disease.

Moreover, the limbal region serves as a critical anatomical and physiological boundary between the highly vascularized conjunctiva and the avascular cornea [60]. In conclusion, this study highlights significant variations in the developmental limbal lymphatic vascularity of naïve corneas across the CC-lines examined, along with diversity in the expression of vascular growth factors. In the context of ocular health, the delicate balance between pro- and anti-(lymph) angiogenic factors plays a crucial role in maintaining corneal transparency and visual acuity[61]. Disruption of this equilibrium, due to factors such as infections or ocular injuries, including burns, can lead to pathological neovascularization, characterized by the ingrowth of blood and lymphatic vessels into the typically avascular cornea. The infiltration of lymphatic vessels into the cornea poses significant challenges, particularly in corneal transplantation, a primary treatment for conditions that cause corneal opacification [60]. The presence of lymphatic vessels increases the risk of immune reactions during transplantation, potentially leading to graft rejection and compromised visual outcomes

[126]. Moreover, aberrant vascularization impairs corneal transparency, reducing vision quality and negatively affecting the patient’s quality of life.

The mouse is the most used mammalian model in biomedical research. Knockout mice and the mouse reference genome primarily originate from the widely used inbred mouse strain, C57BL/6J. Other strains, such as the BALB/c sub-strains, have also been extensively employed in immunology and infectious disease research[127]. Our previous studies[45] and Nakao et al.[72] have demonstrated strain-specific differences in the development of the naïve cornea's limbal lymphatic vasculature, as well as in VEGF-C-driven and inflammation-induced lymphangiogenesis. Specifically, C57BL/6 mice typically exhibit a 'high-lymphangiogenic' phenotype with pronounced limbal lymphatic vessel structure, whereas BALB/c mice display a 'low-lymphangiogenic' phenotype with weaker limbal lymphatic vessel structure[45].

Comparative gene expression analysis of naïve corneas from low-lymphangiogenic BALB/c mice and high-lymphangiogenic C57BL/6 mice revealed several differentially expressed genes[46]. Alongside the well-established inhibitor thrombospondin-1 (TSP-1)[47], two additional candidate genes were identified: plasminogen activator, tissue (plat/tPA), and tumor necrosis factor-related apoptosis-inducing ligand (trail/Tnfsf10)[46]. These findings confirm the role of these genes as novel endogenous regulators of lymphangiogenesis.

The wide genetic diversity of the human population is not fully represented in traditional mouse models. However, collaborative cross (CC) mice, developed from eight distinct founder strains (five traditional laboratory strains: C57BL/6, 129S1/SvlmJ, A/J, NOD/ShiLtJ, and NZO/HiLtJ, and three wild-derived inbred strains: CAST/EiJ, PWK/PhJ, and WSB/EiJ), better reflect the complexity of the human genome[128]. The CC mice incorporate over 90% of common genetic variation, enabling the analysis of common human diseases arising from interactions between allele combinations and the environment[129].

Analysis of the limbal lymphatic vasculature in the naïve corneas of the nine different CC mouse lines reveals clear differences. Limbal lymphatic vessels were largely absent in the CC mouse lines PAT_CD, BOON_HF, LOT_EC, and ROGAN_CF, although they were present in the low-lymphangiogenic BALB/c animals[45]. Thus, these CC lines PAT_CD, BOON_HF, LOT_EC, and ROGAN_CF exhibit a phenotype

that can be characterized as "extremely low-lymphangiogenic." In contrast, the limbal lymphatic vasculature of the CC lines LUF_AD, FIV_AC, CIS_AD, LAT_AD, and NUK_AC was markedly higher than that of the "high-lymphangiogenic" C57BL/6 mice, representing an “extremely high-lymphangiogenic” phenotype.

The suture-induced corneal neovascularization assay was employed to examine the behavior of the "extreme low-lymphangiogenic" (BOON_HF) and "extreme high-lymphangiogenic" (NUK_AC) CC mouse lines during inflammatory conditions[60].

In comparison to BOON_HF, NUK_AC exhibited a resting lymphatic vascularized area in the naïve cornea that was 12.8-fold greater. However, 14 days after an inflammatory insult, the lymphatic vascularized area in NUK_AC was only 1.7-fold greater than in BOON_HF.

The lymphatic vascularized area differed markedly between resting and inflamed conditions, increasing 2.6-fold in NUK_AC and 7.8-fold in BOON_HF. Despite being highly lymphangiogenic under resting conditions, NUK_AC displayed a comparatively subdued response to inflammatory stimuli. In contrast, BOON_HF, which lacks lymphatic vessels in the resting state, exhibits a pronounced inflammatory lymphangiogenic response. This observation aligns with previous findings in C57BL/6 mice and suggests that the response to inflammation is influenced by the baseline level of vascularization. Mice with a higher “lymphatic vascular reserve” in the cornea, such as NUK_AC, require a proportionally smaller response to cope with inflammatory challenges, whereas those with fewer pre-existing vessels, like BOON_HF, exhibit a more pronounced compensatory reaction. Thus, in our studies, mice with a higher lymphatic vasculature in the cornea show a proportionally smaller increase in lymphangiogenesis when challenged with inflammation. These results clearly demonstrate that the genetic background of mice significantly influences the lymphangiogenic response to inflammatory stimuli.

The CC lineage has long provided an invaluable animal model for studying the genetics of complex diseases such as heart disease [130], diabetic retinopathy, cancer[131-133], infectious disorders[128, 130, 134], inflammatory bowel diseases[135], diabetes[136-138], and immunological variants[138]. Recently, Abu-Toamih Atamni et al. identified two genes critical for regulating glucose tolerance, highlighting the influence of genetic factors[136].

Various morphometric techniques can reliably quantify the lymphangiogenesis in mouse corneas. Phenotypic and genotypic data, including molecular markers, can be combined using quantitative trait locus (QTL) analysis to identify candidate genes contributing to the observed variance of the investigated trait[139]. Two mouse strains with distinct phenotypes can be deliberately crossed to generate a population with both genetic and phenotypic diversity, facilitating subsequent QTL analysis[140].

We were able to identify tyrosinase using such an intercross and confirmed it as a unique regulator of lymphangiogenesis in both inflammatory and developmental contexts[44].

The Collaborative Cross (CC) resource highlights the complex nature of genetic regulation, as demonstrated by the divergent phenotypes observed in two albino strains (CIS and NUK), despite both strains lacking tyrosinase activity. This discrepancy underscores the interplay of multiple genetic factors contributing to phenotypic variation in lymphangiogenesis. Genetically diverse mouse strains provide valuable opportunities for identifying novel regulators of lymphangiogenesis. Moreover, the cornea serves as an excellent model for applying QTL analysis, enabling the uncovering of genetic mechanisms governing lymphatic regulatory pathways.

Interestingly, the expression of VEGFs and their receptors in the CC mice does not always align with the observed lymphangiogenic phenotypes. While differences in lymphangiogenesis were expected to correlate with changes in VEGF expression, our results show a lack of congruence between the phenotype and the expression of VEGFs and their receptors. This suggests that regulation of lymphangiogenesis is influenced by factors beyond VEGF signaling, potentially involving other molecular pathways or genetic modifiers. These findings underscore the complexity of lymphangiogenesis regulation and highlight the utility of the CC resource in identifying novel endogenous modulators that could be targeted for therapeutic intervention in lymphangiogenesis-related diseases.

Briefly, this study highlights significant variations in the developmental limbal lymphatic vasculature of naïve corneas across the CC-lines examined, alongside diversity in the vascular growth factor expression. The extremely high- and low-lymphangiogenic CC-line mice BOON_HF and NUK_AC exhibited distinct inflammation-induced lymphangiogenic responses relative to each other, as well as compared to their naïve

corneas. These findings underscore the complexity of the genetic regulation of lymphangiogenesis and its responses to inflammatory stimuli.

Researchers investigating lymphatic disorders and utilizing CC lines to explore the genetics of complex diseases can benefit from these insights. The observed variations in lymphangiogenic responses across different genetic backgrounds emphasize the importance of considering genetic diversity when studying disease mechanisms and developing targeted therapeutic interventions.

Conclusion and Outlook

This thesis has made significant contributions to our understanding of the lymphatic system, particularly through the identification and characterization of novel endogenous modulators of lymphangiogenesis such as CBS and ANGPTL4. The insights gained from studying these key molecules deepen our fundamental understanding of lymphatic biology and highlight potential therapeutic targets, offering new perspectives on controlling pathological processes associated with lymphedema and cancer metastasis. Identifying key genetic factors that regulate lymphangiogenesis could lead to novel therapeutic approaches for managing these conditions. Furthermore, our research on lymphangiogenesis has important implications for ocular diseases, particularly those involving corneal inflammation, graft rejection, or other ocular pathologies where lymphangiogenesis plays a critical role. By identifying novel regulatory factors, our study contributes to the development of new therapeutic strategies for treating these conditions and improving patient outcomes.

While the findings are promising, this study is not without limitations. The reliance on standard mouse models in the initial phases restricted the exploration of genetic diversity and its impact on lymphangiogenesis. Although CBS and ANGPTL4 were identified as critical regulators, the specific genetic models employed may not fully capture the intricate genetic and environmental interactions influencing lymphatic system behaviors in human populations. Further research should validate these findings across more genetically diverse models, such as Collaborative Cross (CC) mice, to enhance the translational relevance of the results.

The groundwork laid by this research opens numerous avenues for further investigation. Future studies should focus on exploring the molecular pathways influenced by CBS and ANGPTL4, employing diverse genetic models and initiating clinical trials to validate and extend these findings. Leveraging the genetic diversity of CC mice could yield deeper insights into how these proteins regulate lymphangiogenesis under various genetic and environmental contexts. There is also a substantial potential for developing targeted therapies that modulate the activity of these proteins, which could transform the treatment of diseases associated with abnormal lymphatic growth or function.

In conclusion, this thesis has not only highlighted crucial molecular mechanisms underlying lymphangiogenesis but has also identified CBS and ANGPTL4 as key therapeutic targets for a range of diseases. Continued exploration of these proteins and their pathways, particularly in genetically diverse models, could lead to significant advancements in the treatment of lymphatic-related disorders. Ultimately, such progress will improve patient outcomes and contribute meaningfully to the broader field of vascular biology. Also, the CC lines represent a powerful and promising model for identifying further potential new modulators of lymphangiogenesis.

References

1. Patel, S.P. and R. Dana, *Corneal lymphangiogenesis: implications in immunity.* Semin Ophthalmol, 2009. **24**(3): p. 135-8.
2. Randolph, G.J., et al., *The Lymphatic System: Integral Roles in Immunity.* Annu Rev Immunol, 2017. **35**: p. 31-52.
3. Ohtani, O. and Y. Ohtani, *Structure and function of rat lymph nodes.* Arch Histol Cytol, 2008. **71**(2): p. 69-76.
4. Swartz, M.A., *The physiology of the lymphatic system.* Adv Drug Deliv Rev, 2001. **50**(1-2): p. 3-20.
5. Alitalo, K., *The lymphatic vasculature in disease.* Nat Med, 2011. **17**(11): p. 1371-80.
6. Mueller, S.N. and R.N. Germain, *Stromal cell contributions to the homeostasis and functionality of the immune system.* Nat Rev Immunol, 2009. **9**(9): p. 618-29.
7. Mowat, A.M. and W.W. Agace, *Regional specialization within the intestinal immune system.* Nat Rev Immunol, 2014. **14**(10): p. 667-85.
8. Murphy, K. and C. Weaver, *Janeway's immunobiology*. 9th edition. ed. 2016, New York, NY: Garland Science/Taylor & Francis Group, LLC. xx, 904 pages.
9. Schmid-Schonbein, G.W., *Microlymphatics and lymph flow.* Physiol Rev, 1990. **70**(4): p. 987-1028.
10. Hughes, C.E., et al., *Antigen-Presenting Cells and Antigen Presentation in Tertiary Lymphoid Organs.* Front Immunol, 2016. **7**: p. 481.
11. Cueni, L.N. and M. Detmar, *The lymphatic system in health and disease.* Lymphat Res Biol, 2008. **6**(3-4): p. 109-22.
12. Patnam, M., et al., *Lymphangiogenesis Guidance Mechanisms and Therapeutic Implications in Pathological States of the Cornea.* Cells, 2023. **12**(2).
13. Utyro, O., J. Perla-Kajan, and H. Jakubowski, *The Cbs Locus Affects the Expression of Senescence Markers and mtDNA Copy Number, but not Telomere Dynamics in Mice.* Int J Mol Sci, 2020. **21**(7).
14. Rehman, I., B. Hazhirkarzar, and B.C. Patel, *Anatomy, Head and Neck, Eye*, in *StatPearls*. 2024: Treasure Island (FL).
15. Li, S.Z. and A.K. Jain, *Encyclopedia of biometrics*. 2009, New York: Springer.
16. Pal, I. and J.D. Ramsey, *The role of the lymphatic system in vaccine trafficking and immune response.* Adv Drug Deliv Rev, 2011. **63**(10-11): p. 909-22.
17. Hsu, M.C. and M. Itkin, *Lymphatic Anatomy.* Tech Vasc Interv Radiol, 2016. **19**(4): p. 247-254.
18. Jalkanen, S. and M. Salmi, *Lymphatic endothelial cells of the lymph node.* Nat Rev Immunol, 2020. **20**(9): p. 566-578.
19. Oliver, G., et al., *The Lymphatic Vasculature in the 21(st) Century: Novel Functional Roles in Homeostasis and Disease.* Cell, 2020. **182**(2): p. 270-296.
20. Lee, H.K., S.M. Lee, and D.I. Lee, *Corneal Lymphangiogenesis: Current Pathophysiological Understandings and Its Functional Role in Ocular Surface Disease.* Int J Mol Sci, 2021. **22**(21).
21. Cursiefen, C., et al., *Lymphatic vessels in vascularized human corneas: immunohistochemical investigation using LYVE-1 and podoplanin.* Invest Ophthalmol Vis Sci, 2002. **43**(7): p. 2127-35.
22. Cassin, B. and M.L. Rubin, *Dictionary of Eye Terminology*. 2006: Triad Pub.

23. Goldstein, E.B. and T. Learning, *Sensation and Perception*. 2007: Thomson Wadsworth.
24. Clahsen, T., et al., *The novel role of lymphatic vessels in the pathogenesis of ocular diseases.* Prog Retin Eye Res, 2023. **96**: p. 101157.
25. Rama, P., et al., *Limbal stem-cell therapy and long-term corneal regeneration.* N Engl J Med, 2010. **363**(2): p. 147-55.
26. Sasamoto, Y., et al., *Repairing the corneal epithelium using limbal stem cells or alternative cell-based therapies.* Expert Opin Biol Ther, 2018. **18**(5): p. 505-513.
27. Cursiefen, C., et al., *Corneal lymphangiogenesis: evidence, mechanisms, and implications for corneal transplant immunology.* Cornea, 2003. **22**(3): p. 273-81.
28. Dana, M.R., et al., *Corneal neovascularization after penetrating keratoplasty.* Cornea, 1995. **14**(6): p. 604-9.
29. Ambati, B.K., et al., *Corneal avascularity is due to soluble VEGF receptor-1*. Nature, 2006. **443**(7114): p. 993-7.
30. Presta, M., et al., *Fibroblast growth factor/fibroblast growth factor receptor system in angiogenesis.* Cytokine Growth Factor Rev, 2005. **16**(2): p. 159-78.
31. Cao, R., et al., *PDGF-BB induces intratumoral lymphangiogenesis and promotes lymphatic metastasis.* Cancer Cell, 2004. **6**(4): p. 333-45.
32. Avraamides, C.J., B. Garmy-Susini, and J.A. Varner, *Integrins in angiogenesis and lymphangiogenesis.* Nat Rev Cancer, 2008. **8**(8): p. 604-17.
33. Kajiya, K., et al., *Hepatocyte growth factor promotes lymphatic vessel formation and function.* EMBO J, 2005. **24**(16): p. 2885-95.
34. Tammela, T. and K. Alitalo, *Lymphangiogenesis: Molecular mechanisms and future promise.* Cell, 2010. **140**(4): p. 460-76.
35. Achen, M.G., et al., *Vascular endothelial growth factor D (VEGF-D) is a ligand for the tyrosine kinases VEGF receptor 2 (Flk1) and VEGF receptor 3 (Flt4).* Proc Natl Acad Sci U S A, 1998. **95**(2): p. 548-53.
36. Singh, N., et al., *Soluble vascular endothelial growth factor receptor 3 is essential for corneal alymphaticity.* Blood, 2013. **121**(20): p. 4242-9.
37. Cursiefen, C., *Immune privilege and angiogenic privilege of the cornea*. Chem Immunol Allergy, 2007. **92**: p. 50-57.
38. Delgado, M. and D. Ganea, *Vasoactive intestinal peptide: a neuropeptide with pleiotropic immune functions.* Amino Acids, 2013. **45**(1): p. 25-39.
39. Dall'Olmo, L., et al., *Alpha-melanocyte stimulating hormone (alpha-MSH): biology, clinical relevance and implication in melanoma*. J Transl Med, 2023. **21**(1): p. 562.
40. White, M.F., *IRS proteins and the common path to diabetes.* Am J Physiol Endocrinol Metab, 2002. **283**(3): p. E413-22.
41. Kubota, T., et al., *Impaired insulin signaling in endothelial cells reduces insulin-induced glucose uptake by skeletal muscle.* Cell Metab, 2011. **13**(3): p. 294-307.
42. Cursiefen, C., et al., *Nonvascular VEGF receptor 3 expression by corneal epithelium maintains avascularity and vision.* Proc Natl Acad Sci U S A, 2006. **103**(30): p. 11405-10.
43. Clahsen, T., et al., *Role of Endogenous Regulators of Hem- And Lymphangiogenesis in Corneal Transplantation*. J Clin Med, 2020. **9**(2).
44. Buttner, C., et al., *Tyrosinase Is a Novel Endogenous Regulator of Developmental and Inflammatory Lymphangiogenesis.* Am J Pathol, 2019. **189**(2): p. 440-448.
45. Regenfuss, B., et al., *Genetic heterogeneity of lymphangiogenesis in different mouse strains.* Am J Pathol, 2010. **177**(1): p. 501-10.

46. Regenfuss, B., et al., *The Naive Murine Cornea as a Model System to Identify Novel Endogenous Regulators of Lymphangiogenesis: TRAIL and rtPA*. Lymphat Res Biol, 2015. **13**(2): p. 76-84.
47. Cursiefen, C., et al., *Thrombospondin 1 inhibits inflammatory lymphangiogenesis by CD36 ligation on monocytes*. J Exp Med, 2011. **208**(5): p. 1083-92.
48. Bock, F., et al., *Improved semiautomatic method for morphometry of angiogenesis and lymphangiogenesis in corneal flatmounts*. Exp Eye Res, 2008. **87**(5): p. 462-70.
49. Schallreuter, K.U., et al., *Regulation of melanogenesis--controversies and new concepts*. Exp Dermatol, 2008. **17**(5): p. 395-404.
50. Svenson, K.L., et al., *Multiple trait measurements in 43 inbred mouse strains capture the phenotypic diversity characteristic of human populations*. J Appl Physiol (1985), 2007. **102**(6): p. 2369-78.
51. Capecchi, M.R., *Gene targeting in mice: functional analysis of the mammalian genome for the twenty-first century*. Nat Rev Genet, 2005. **6**(6): p. 507-12.
52. Singer, J.B., et al., *Genetic dissection of complex traits with chromosome substitution strains of mice*. Science, 2004. **304**(5669): p. 445-8.
53. Andersson, U. and K.J. Tracey, *Reflex principles of immunological homeostasis*. Annu Rev Immunol, 2012. **30**: p. 313-35.
54. Keane, T.M., et al., *Mouse genomic variation and its effect on phenotypes and gene regulation*. Nature, 2011. **477**(7364): p. 289-94.
55. Roberts, A., et al., *The polymorphism architecture of mouse genetic resources elucidated using genome-wide resequencing data: implications for QTL discovery and systems genetics*. Mamm Genome, 2007. **18**(6-7): p. 473-81.
56. Collaborative Cross, C., *The genome architecture of the Collaborative Cross mouse genetic reference population*. Genetics, 2012. **190**(2): p. 389-401.
57. Pomp, D. and K.L. Mohlke, *Obesity genes: so close and yet so far*. J Biol, 2008. **7**(9): p. 36.
58. Pan, J., et al., *Strategies for generating mouse model resources of human disease*. Protein Cell, 2023. **14**(12): p. 866-870.
59. Churchill, G.A., et al., *The Collaborative Cross, a community resource for the genetic analysis of complex traits*. Nat Genet, 2004. **36**(11): p. 1133-7.
60. Cursiefen, C., et al., *VEGF-A stimulates lymphangiogenesis and hemangiogenesis in inflammatory neovascularization via macrophage recruitment*. J Clin Invest, 2004. **113**(7): p. 1040-50.
61. Bock, F., et al., *Bevacizumab as a potent inhibitor of inflammatory corneal angiogenesis and lymphangiogenesis*. Invest Ophthalmol Vis Sci, 2007. **48**(6): p. 2545-52.
62. Hos, D., et al., *Immune reactions after modern lamellar (DALK, DSAEK, DMEK) versus conventional penetrating corneal transplantation*. Prog Retin Eye Res, 2019. **73**: p. 100768.
63. Dietrich, T., et al., *Cutting edge: lymphatic vessels, not blood vessels, primarily mediate immune rejections after transplantation*. J Immunol, 2010. **184**(2): p. 535-9.
64. Schoppmann, S.F., *Lymphangiogenesis, inflammation and metastasis*. Anticancer Res, 2005. **25**(6C): p. 4503-11.
65. Chen, J.C., et al., *The role of the VEGF-C/VEGFRs axis in tumor progression and therapy*. Int J Mol Sci, 2012. **14**(1): p. 88-107.

66. Scavelli, C., et al., *Crosstalk between angiogenesis and lymphangiogenesis in tumor progression*. Leukemia, 2004. **18**(6): p. 1054-8.
67. Su, J.L., et al., *The role of the VEGF-C/VEGFR-3 axis in cancer progression*. Br J Cancer, 2007. **96**(4): p. 541-5.
68. Zhang, R., et al., *Mechanisms of angiogenesis in tumour*. Front Oncol, 2024. **14**: p. 1359069.
69. Saman, H., et al., *Inducing Angiogenesis, a Key Step in Cancer Vascularization, and Treatment Approaches*. Cancers (Basel), 2020. **12**(5).
70. Hooglugt, A., et al., *Endothelial YAP/TAZ Signaling in Angiogenesis and Tumor Vasculature*. Front Oncol, 2020. **10**: p. 612802.
71. Rohan, R.M., et al., *Genetic heterogeneity of angiogenesis in mice*. FASEB J, 2000. **14**(7): p. 871-6.
72. Nakao, S., et al., *Lymphangiogenesis and angiogenesis: concurrence and/or dependence? Studies in inbred mouse strains*. FASEB J, 2010. **24**(2): p. 504-13.
73. Zuhra, K., et al., *Cystathionine-beta-Synthase: Molecular Regulation and Pharmacological Inhibition*. Biomolecules, 2020. **10**(5).
74. Bao, L., et al., *Identification and tissue distribution of human cystathionine beta-synthase mRNA isoforms*. Arch Biochem Biophys, 1998. **350**(1): p. 95-103.
75. Kabil, O., et al., *The quantitative significance of the transsulfuration enzymes for H2S production in murine tissues*. Antioxid Redox Signal, 2011. **15**(2): p. 363-72.
76. Zhu, H., et al., *Cystathionine beta-Synthase in Physiology and Cancer*. Biomed Res Int, 2018. **2018**: p. 3205125.
77. Bhattacharyya, S., et al., *Cystathionine beta-synthase (CBS) contributes to advanced ovarian cancer progression and drug resistance*. PLoS One, 2013. **8**(11): p. e79167.
78. Szabo, C. and A. Papapetropoulos, *Hydrogen sulphide and angiogenesis: mechanisms and applications*. Br J Pharmacol, 2011. **164**(3): p. 853-65.
79. Uhlen, M., et al., *Proteomics. Tissue-based map of the human proteome*. Science, 2015. **347**(6220): p. 1260419.
80. Persa, C., et al., *The distribution of cystathionine beta-synthase (CBS) in the eye: implication of the presence of a trans-sulfuration pathway for oxidative stress defense*. Exp Eye Res, 2006. **83**(4): p. 817-23.
81. Kraus, J.P., et al., *Cystathionine beta-synthase mutations in homocystinuria*. Hum Mutat, 1999. **13**(5): p. 362-75.
82. Mudd, S.H., et al., *Glycine N-methyltransferase deficiency: a novel inborn error causing persistent isolated hypermethioninaemia*. J Inherit Metab Dis, 2001. **24**(4): p. 448-64.
83. Kanagy, N.L., C. Szabo, and A. Papapetropoulos, *Vascular biology of hydrogen sulfide*. Am J Physiol Cell Physiol, 2017. **312**(5): p. C537-C549.
84. Jiang, W., et al., *H(2)S promotes developmental brain angiogenesis via the NOS/NO pathway in zebrafish*. Stroke Vasc Neurol, 2021. **6**(2): p. 244-251.
85. Majumder, A., et al., *Hydrogen sulfide improves postischemic neoangiogenesis in the hind limb of cystathionine-beta-synthase mutant mice via PPAR-gamma/VEGF axis*. Physiol Rep, 2018. **6**(17): p. e13858.
86. Qi, Q.R., et al., *Enhanced Stromal Cell CBS-H2S Production Promotes Estrogen-Stimulated Human Endometrial Angiogenesis*. Endocrinology, 2020. **161**(11).

87. Wang, M., et al., *Hydrogen sulfide modulates epithelial-mesenchymal transition and angiogenesis in non-small cell lung cancer via HIF-1alpha activation*. Biochem Pharmacol, 2020. **172**: p. 113775.
88. Rao, G., et al., *Cystathionine beta synthase regulates mitochondrial dynamics and function in endothelial cells*. FASEB J, 2020. **34**(7): p. 9372-9392.
89. Szabo, C., et al., *Regulation of mitochondrial bioenergetic function by hydrogen sulfide. Part I. Biochemical and physiological mechanisms*. Br J Pharmacol, 2014. **171**(8): p. 2099-122.
90. Teng, H., et al., *Oxygen-sensitive mitochondrial accumulation of cystathionine beta-synthase mediated by Lon protease*. Proc Natl Acad Sci U S A, 2013. **110**(31): p. 12679-84.
91. Hellmich, M.R., et al., *The therapeutic potential of cystathionine beta-synthetase/hydrogen sulfide inhibition in cancer*. Antioxid Redox Signal, 2015. **22**(5): p. 424-48.
92. Enokido, Y., et al., *Cystathionine beta-synthase, a key enzyme for homocysteine metabolism, is preferentially expressed in the radial glia/astrocyte lineage of developing mouse CNS*. FASEB J, 2005. **19**(13): p. 1854-6.
93. Eberhardt, R.T., et al., *Endothelial dysfunction in a murine model of mild hyperhomocyst(e)inemia*. J Clin Invest, 2000. **106**(4): p. 483-91.
94. Szabo, C., et al., *Tumor-derived hydrogen sulfide, produced by cystathionine-beta-synthase, stimulates bioenergetics, cell proliferation, and angiogenesis in colon cancer*. Proc Natl Acad Sci U S A, 2013. **110**(30): p. 12474-9.
95. Thornburg, J.M., et al., *Targeting aspartate aminotransferase in breast cancer*. Breast Cancer Res, 2008. **10**(5): p. R84.
96. Saha, S., et al., *Cystathionine beta-synthase regulates endothelial function via protein S-sulfhydration*. FASEB J, 2016. **30**(1): p. 441-56.
97. Hellmich, M.R., et al., *Efficacy of Novel Aminooxyacetic Acid Prodrugs in Colon Cancer Models: Towards Clinical Translation of the Cystathionine beta-Synthase Inhibition Concept*. Biomolecules, 2021. **11**(8).
98. Asimakopoulou, A., et al., *Selectivity of commonly used pharmacological inhibitors for cystathionine beta synthase (CBS) and cystathionine gamma lyase (CSE)*. Br J Pharmacol, 2013. **169**(4): p. 922-32.
99. Stottrup, N.B., et al., *Inhibition of the malate-aspartate shuttle by pre-ischaemic aminooxyacetate loading of the heart induces cardioprotection*. Cardiovasc Res, 2010. **88**(2): p. 257-66.
100. Szabo, C., *Hydrogen sulfide, an enhancer of vascular nitric oxide signaling: mechanisms and implications*. Am J Physiol Cell Physiol, 2017. **312**(1): p. C3-C15.
101. Albertini, E., et al., *Cystathionine beta synthase modulates senescence of human endothelial cells*. Aging (Albany NY), 2012. **4**(10): p. 664-73.
102. Zhang, M., et al., *Cystathionine beta Synthase/Hydrogen Sulfide Signaling in Multiple Myeloma Regulates Cell Proliferation and Apoptosis*. J Environ Pathol Toxicol Oncol, 2020. **39**(3): p. 281-290.
103. Soker, S., et al., *VEGF165 mediates formation of complexes containing VEGFR-2 and neuropilin-1 that enhance VEGF165-receptor binding*. J Cell Biochem, 2002. **85**(2): p. 357-68.
104. Tawfik, A., et al., *Alterations of retinal vasculature in cystathionine-Beta-synthase mutant mice, a model of hyperhomocysteinemia*. Invest Ophthalmol Vis Sci, 2013. **54**(2): p. 939-49.

105. Liu, N., X. Lin, and C. Huang, *Activation of the reverse transsulfuration pathway through NRF2/CBS confers erastin-induced ferroptosis resistance.* Br J Cancer, 2020. **122**(2): p. 279-292.
106. Hadrian, K., et al., *Macrophage-Mediated Tissue Vascularization: Similarities and Differences Between Cornea and Skin*. Front Immunol, 2021. **12**: p. 667830.
107. Maruyama, K., et al., *The maintenance of lymphatic vessels in the cornea is dependent on the presence of macrophages.* Invest Ophthalmol Vis Sci, 2012. **53**(6): p. 3145-53.
108. Galaup, A., et al., *Angiopoietin-like 4 prevents metastasis through inhibition of vascular permeability and tumor cell motility and invasiveness.* Proc Natl Acad Sci U S A, 2006. **103**(49): p. 18721-6.
109. Fernandez-Hernando, C. and Y. Suarez, *ANGPTL4: a multifunctional protein involved in metabolism and vascular homeostasis.* Curr Opin Hematol, 2020. **27**(3): p. 206-213.
110. Le Jan, S., et al., *Angiopoietin-like 4 is a proangiogenic factor produced during ischemia and in conventional renal cell carcinoma*. Am J Pathol, 2003. **162**(5): p. 1521-8.
111. Tan, M.J., et al., *Emerging roles of angiopoietin-like 4 in human cancer.* Mol Cancer Res, 2012. **10**(6): p. 677-88.
112. Zhu, P., et al., *Angiopoietin-like 4: a decade of research*. Biosci Rep, 2012. **32**(3): p. 211-9.
113. Huang, R.L., et al., *ANGPTL4 modulates vascular junction integrity by integrin signaling and disruption of intercellular VE-cadherin and claudin-5 clusters.* Blood, 2011. **118**(14): p. 3990-4002.
114. Hato, T., M. Tabata, and Y. Oike, *The role of angiopoietin-like proteins in angiogenesis and metabolism*. Trends Cardiovasc Med, 2008. **18**(1): p. 6-14.
115. Yang, X., Y. Cheng, and G. Su, *A review of the multifunctionality of angiopoietin-like 4 in eye disease.* Biosci Rep, 2018. **38**(5).
116. Adeshakin, F.O., et al., *Mechanisms for Modulating Anoikis Resistance in Cancer and the Relevance of Metabolic Reprogramming*. Front Oncol, 2021. **11**: p. 626577.
117. Ito, Y., et al., *Inhibition of angiogenesis and vascular leakiness by angiopoietin-related protein 4.* Cancer Res, 2003. **63**(20): p. 6651-7.
118. Qazi, Y. and P. Hamrah, *Corneal Allograft Rejection: Immunopathogenesis to Therapeutics.* J Clin Cell Immunol, 2013. **2013**(Suppl 9).
119. Di Zazzo, A., et al., *Management of high-risk corneal transplantation*. Surv Ophthalmol, 2017. **62**(6): p. 816-827.
120. Padua, D., et al., *TGFbeta primes breast tumors for lung metastasis seeding through angiopoietin-like 4.* Cell, 2008. **133**(1): p. 66-77.
121. Hwang, I., et al., *Tumor-associated macrophage, angiogenesis and lymphangiogenesis markers predict prognosis of non-small cell lung cancer patients.* J Transl Med, 2020. **18**(1): p. 443.
122. Valenzuela, D.M., et al., *Angiopoietins 3 and 4: diverging gene counterparts in mice and humans.* Proc Natl Acad Sci U S A, 1999. **96**(5): p. 1904-9.
123. Sodhi, A., et al., *Angiopoietin-like 4 binds neuropilins and cooperates with VEGF to induce diabetic macular edema*. J Clin Invest, 2019. **129**(11): p. 4593-4608.
124. Oteng, A.B., et al., *Characterization of ANGPTL4 function in macrophages and adipocytes using Angptl4-knockout and Angptl4-hypomorphic mice.* J Lipid Res, 2019. **60**(10): p. 1741-1754.

125. Dakowicz, D., M. Zajkowska, and B. Mroczko, *Relationship between VEGF Family Members, Their Receptors and Cell Death in the Neoplastic Transformation of Colorectal Cancer*. Int J Mol Sci, 2022. **23**(6).
126. Dace, D.S., et al., *Ocular immune privilege is circumvented by CD4+ T cells, leading to the rejection of intraocular tumors in an IFN-gamma-dependent manner*. J Leukoc Biol, 2007. **81**(2): p. 421-9.
127. Watanabe, H., et al., *Innate immune response in Th1- and Th2-dominant mouse strains*. Shock, 2004. **22**(5): p. 460-6.
128. Noll, K.E., M.T. Ferris, and M.T. Heise, *The Collaborative Cross: A Systems Genetics Resource for Studying Host-Pathogen Interactions*. Cell Host Microbe, 2019. **25**(4): p. 484-498.
129. Threadgill, D.W., et al., *The collaborative cross: a recombinant inbred mouse population for the systems genetic era*. ILAR J, 2011. **52**(1): p. 24-31.
130. Salimova, E., et al., *Variable outcomes of human heart attack recapitulated in genetically diverse mice*. NPJ Regen Med, 2019. **4**: p. 5.
131. Ferguson, B., et al., *Different genetic mechanisms mediate spontaneous versus UVR-induced malignant melanoma*. Elife, 2019. **8**.
132. Ferguson, B., et al., *Melanoma susceptibility as a complex trait: genetic variation controls all stages of tumor progression*. Oncogene, 2015. **34**(22): p. 2879-86.
133. Wang, P., et al., *Diverse tumour susceptibility in Collaborative Cross mice: identification of a new mouse model for human gastric tumourigenesis*. Gut, 2019. **68**(11): p. 1942-1952.
134. Lore, N.I., et al., *Collaborative Cross Mice Yield Genetic Modifiers for Pseudomonas aeruginosa Infection in Human Lung Disease*. mBio, 2020. **11**(2).
135. Rogala, A.R., et al., *The Collaborative Cross as a resource for modeling human disease: CC011/Unc, a new mouse model for spontaneous colitis*. Mamm Genome, 2014. **25**(3-4): p. 95-108.
136. Yang, C.H., et al., *E2f8 and Dlg2 genes have independent effects on impaired insulin secretion associated with hyperglycaemia*. Diabetologia, 2020. **63**(7): p. 1333-1348.
137. Atamni, H.J., et al., *High-fat-diet induced development of increased fasting glucose levels and impaired response to intraperitoneal glucose challenge in the collaborative cross mouse genetic reference population*. BMC Genet, 2016. **17**: p. 10.
138. Karkar, L., et al., *Assessing the host genetic background effects on type 2 diabetes and obesity development in response to mixed-oral bacteria and high-fat diet using the collaborative cross mouse model*. Animal Model Exp Med, 2020. **3**(2): p. 152-159.
139. Ochiai, K., et al., *Boron toxicity in rice (Oryza sativa L.). I. Quantitative trait locus (QTL) analysis of tolerance to boron toxicity*. Theor Appl Genet, 2008. **117**(1): p. 125-33.
140. Lander, E.S. and D. Botstein, *Mapping mendelian factors underlying quantitative traits using RFLP linkage maps*. Genetics, 1989. **121**(1): p. 185-99.

Supplementary Figures and Tables:

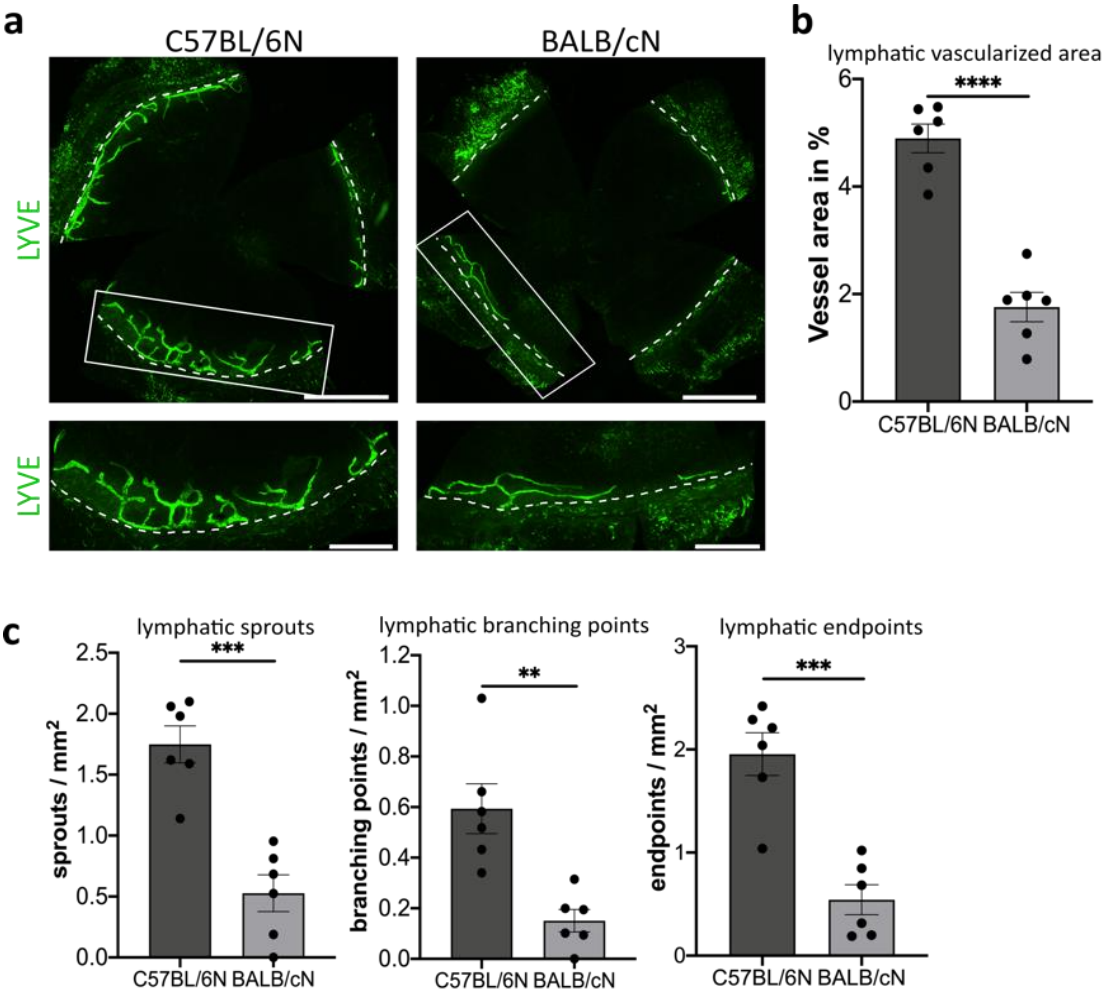

Supplementary Figure 1: Resting limbal lymphatic vasculature in parental strains of low-lymphangiogenic BALB/cN and high-lymphangiogenic C57BL/6N Representative whole mounts of the murine cornea from **(A)** C57BL/6N and BALB/cN stained for LYVE-1. The boxed areas in the top panels are shown in higher magnification in the bottom panels. Dashed lines show the border between the limbus and the cornea. Scale bars: 1 mm top panels and 500 µm bottom panels) **(B)** Quantification of the lymphatic vascularized area of the whole mounts. **(C)** Further characterization of the lymphatic vessel architecture by determination of the number of sprouts, the number of branching points, and the number of end points. Data are expressed as means ± SEM (n=6). Data are presented as means ± SEM. Statistical significance was calculated by two-tailed t-test **p<0.01, ***p<0.001, ****p<0.0001

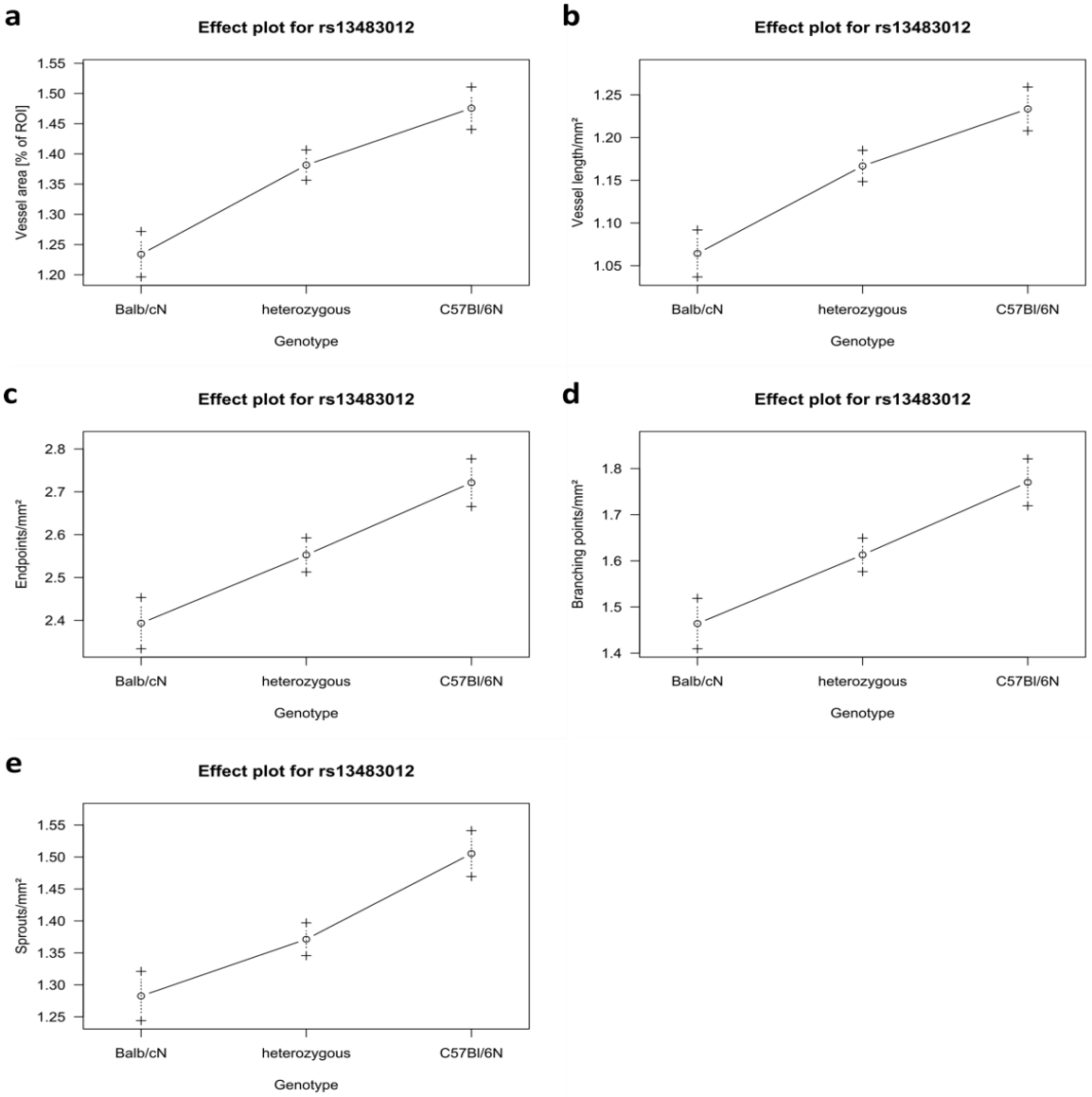

Supplementary Figure 2: Locus effect plots for the reported transformed phenotypes

Marker with the maximum logarithm of the odds (LOD) score on chromosome 17, *rs13483012*, all showing recessive BALB/cN alleles. **A:** Vessel area/mm^2. **B:** Vessel length/mm^2. **C:** End points/mm^2. **D:** Branching points/mm^2. **E:** Sprouts/mm^2.

Supplementary Table 1: Raw counts table of F0 animals

ID	Strain		pairs	Reads pairs and trimming	Read pairs Tophat2	Concordant pair alignment rate to Pseudogenome (Tophat2)	Concordant pair alignment rate to mm10 for comparison	Read pairs counted exonic (Htseq)
175101	Balb/cN	1	90.343.042	79.404.780	70.078.832	85,2%	82,2%	40.283.517
175102	Balb/cN	2	89.083.390	79.928.879	70.688.183	85,9%	82,7%	41.152.725
175106	Balb/cN	3	83.456.407	73.521.405	64.340.105	84,6%	81,4%	38.766.069
175107	Balb/cN	4	79.487.806	69.808.817	61.027.616	84,5%	81,4%	36.706.454
175108	C57Bl/6N	1	85.613.684	75.659.511	59.779.387	76,6%	76,6%	35.838.482
175109	C57Bl/6N	2	85.208.546	75.951.107	61.452.665	78,6%	78,5%	36.980.562
175110	C57Bl/6N	3	82.916.298	73.326.353	52.840.989	70,4%	70,3%	29.682.341
175111	C57Bl/6N	4	87.412.337	78.055.095	62.444.083	77,9%	77,8%	36.313.217

Supplementary Table 2: Differentially expressed genes after filtering overlapping the quantitative trait locus on chr17.

Table

MGI Symbol	log2FoldChange	p-value adjusted (BH)	MGI ID	Ensembl_Gene_IDs
Cbs	-5,16	3,86E-14	MGI:88285	ENSMUSG00000024039
Msln	-4,32	4,13E-03	MGI:1888992	ENSMUSG00000063011
Cdsn	-4,00	3,86E-14	MGI:3505689	ENSMUSG00000039518
H2-DMb1	-2,52	9,10E-03	MGI:95922	ENSMUSG00000079547
Adgrf4	-2,14	3,86E-14	MGI:1925499	ENSMUSG00000023918
Adgrf2	-2,12	6,58E-08	MGI:2182728	ENSMUSG00000057899
Paqr4	-2,01	3,86E-14	MGI:1923748	ENSMUSG00000023909
Hmga1	-2,00	3,86E-14	MGI:96160	ENSMUSG00000046711
Gng13	-1,77	4,57E-03	MGI:1925616	ENSMUSG00000025739
BC051226	-1,68	2,18E-05	MGI:3039585	ENSMUSG00000092564
Dnase1l2	-1,59	9,72E-04	MGI:1913955	ENSMUSG00000024136
Rps2	-1,56	2,53E-07	MGI:105110	ENSMUSG00000044533
Angptl4	-1,11	2,15E-03	MGI:1888999	ENSMUSG00000002289
Acat2	-1,02	5,87E-06	MGI:87871	ENSMUSG00000023832
Atp6v0c	-0,95	3,18E-03	MGI:88116	ENSMUSG00000024121
Ephx3	-0,94	7,00E-06	MGI:1919182	ENSMUSG00000037577
Riok2	-0,91	1,97E-03	MGI:1914295	ENSMUSG00000116564
Amdhd2	-0,87	2,49E-03	MGI:2443978	ENSMUSG00000036820
Slc44a4	-0,82	7,32E-03	MGI:1917379	ENSMUSG00000007034
Wiz	-0,78	2,19E-07	MGI:1332638	ENSMUSG00000024050
Satb1	-0,70	4,51E-03	MGI:105084	ENSMUSG00000023927
Cd2ap	-0,47	1,37E-03	MGI:1330281	ENSMUSG00000061665
Tapbp	0,55	2,69E-04	MGI:1201689	ENSMUSG00000024308
Guca1a	0,56	1,56E-03	MGI:102770	ENSMUSG00000023982
Itpr3	0,56	1,30E-03	MGI:96624	ENSMUSG00000042644
Btbd9	0,56	9,89E-03	MGI:1916625	ENSMUSG00000062202
Mocs1	0,64	2,42E-04	MGI:1928904	ENSMUSG00000064120
H2-T23	0,96	2,45E-04	MGI:95957	ENSMUSG00000067212
Cpne5	1,01	2,84E-04	MGI:2385908	ENSMUSG00000024008
Fgd2	1,01	4,04E-03	MGI:1347084	ENSMUSG00000024013
Ppp1r18	1,02	8,99E-03	MGI:1923698	ENSMUSG00000034595
Glo1	1,08	2,53E-08	MGI:95742	ENSMUSG00000024026
Runx2	1,15	3,52E-06	MGI:99829	ENSMUSG00000039153
Psmb9	1,16	1,02E-03	MGI:1346526	ENSMUSG00000096727
Tap1	1,18	4,62E-09	MGI:98483	ENSMUSG00000037321
Vegfa	1,19	9,43E-04	MGI:103178	ENSMUSG00000023951
Enpp5	1,31	3,86E-14	MGI:1933830	ENSMUSG00000023960
Enpp4	1,33	1,37E-05	MGI:2682634	ENSMUSG00000023961
Clic5	1,44	6,66E-13	MGI:1917912	ENSMUSG00000023959

H2-Q4	1,45	1,09E-13	MGI:95933	ENSMUSG00000035929
A930015D03Rik	1,63	8,83E-04	MGI:1925060	ENSMUSG00000092368
Tmprss3	1,66	2,47E-03	MGI:2155445	ENSMUSG00000024034
Pde9a	2,01	3,86E-14	MGI:1277179	ENSMUSG00000041119
Lst1	2,29	3,45E-11	MGI:1096324	ENSMUSG00000073412
Aif1	2,99	3,86E-14	MGI:1343098	ENSMUSG00000024397
1700031A10Rik	3,94	3,86E-14	MGI:1920536	ENSMUSG00000092239
Apobec2	4,03	4,49E-10	MGI:1343178	ENSMUSG00000040694
Prss41	4,41	9,00E-03	MGI:1918253	ENSMUSG00000024114
H2-T24	4,53	3,86E-14	MGI:95958	ENSMUSG00000053835
Gm11127	8,78	5,10E-06	MGI:3779381	ENSMUSG00000079492